DESIGN AND DEVELOPMENT OF SILK-ELASTINLIKE PROTEIN POLYMER LIQUID EMBOLICS FOR TREATMENT OF HEPATOCELLULAR CARCINOMA

by

Azadeh Poursaid

A dissertation submitted to the faculty of
The University of Utah
in partial fulfillment of the requirements for the degree of

Doctor of Philosophy

Department of Bioengineering

The University of Utah

August 2016

The University of Utah Graduate School

STATEMENT OF DISSERTATION APPROVAL

The dissertation of **Azadeh Poursaid**

has been approved by the following supervisory committee members:

Hamidreza Ghandehari	, Chair	**04.25.16** Date Approved
Joseph Cappello	, Member	**04.25.16** Date Approved
Jindrich Kopecek	, Member	**04.25.16** Date Approved
Eugene Huo	, Member	**04.25.16** Date Approved
Bruce Gale	, Member	**04.25.16** Date Approved

and by **Patrick Tresco**, Chair/Dean of

the Department/College/School of **Bioengineering**

and by David B. Kieda, Dean of The Graduate School.

ABSTRACT

Globally, hepatocellular carcinoma (HCC) of the liver is diagnosed in over 700,000 people annually and trends indicate increasing prevalence. The majority of cases, >80%, are detected at advanced stages where systemic chemotherapies have little efficacy. The primary curative treatment is liver transplant, but if a donor liver is not available, only palliative care such as transarterial chemoembolization (TACE) is possible. TACE targets the tumor blood supply. An embolic containing a chemotherapeutic agent is injected into the tumor's vasculature via an endovascular catheter, subsequently shutting down blood flow while delivering localized chemotherapy. A presently approved product, Lipiodol®, is an oily emulsion mixed with a chemotherapeutic used in conjunction with gelatin particles or synthetic polymer beads that act as emboli. Calibrated spherical drug eluting beads are now gaining favor for this procedure, replacing the multistep oil emulsion system. These beads, however, have shortcomings: aggregation of smaller diameter beads, fracturing of beads while under strain in the catheter, off target embolization particularly in pulmonary circulation, elution of only charged small molecule therapeutics, nondegradability, limited tumor depth penetration, and revascularization induced by a hypoxic state. To address these limitations, a genetically engineered silk-elastinlike protein polymer (SELP) system was developed to create a liquid-to-solid embolic agent capable of retaining and releasing a wider range of therapeutics, controlled degradation into nontoxic amino acids, and soluble until injected into the body where they transition

irreversibly to a solid hydrogel network. This provides potential for ideal injectability as a low viscosity fluid at room temperature followed by optimal embolization by a highly stable hydrogel at body temperature.

The proposed research involved engineering a SELP formulation with suitable viscosity for injection into the tumor vasculature via a microcatheter and a suitable gelation rate and gel strength for stable embolization. The drug release properties of the polymer matrix were determined for small molecule chemotherapeutics such as doxorubicin and anti-angiogenic sorafenib. Preliminary *in vivo* performance of the novel system for TACE was evaluated using a rodent model. Future directions include expansion of *in vivo* studies, particularly in an animal model for HCC and TACE to study therapeutic efficacy and long-term biocompatibility.

I dedicate this thesis to my grandmothers who started addressing me as “doctor” from the advent of my dream of higher education dating to before the new millennium.

TABLE OF CONTENTS

LIST OF FIGURES

LIST OF TABLES

ABBREVIATIONS

2D	2-dimensional
ACN	Acetonitrile
AMPS	2-acrylamido-2-methylpropane sulfonate
ANOVA	Analysis of variance
ATR	Attenuated total reflectance
AVM	Arteriovenous malformation
CCN	Carboxymethyl chitosan
CMC	Carboxymethyl cellulose
CT	Computed tomography
cTACE	Conventional transarterial chemoembolization
DAVF	Dural arteriovenous fistula
DC	Drug capable
DEB	Drug eluting bead
DMEM	Dulbecco's modified eagle medium
DMSO	Dimethyl sulfoxide
DNA	Deoxyribonucleic acid
Dox	Doxorubicin
Dox HCl	Doxorubicin hydrochloride
DSM	Degradable starch microspheres

EDTA	Ethylenediaminetetraacetic acid
EVOH	Ethylene vinyl alcohol
FBS	Fetal bovine serum
FDA	Food and Drug Administration
FSD	Fourier self-deconvolution
FTIR	Fourier transform infrared
GDA	Gastroduodenal artery
H&E	Hematoxylin/eosin
HCC	Hepatocellular carcinoma
HPLC	High performance liquid chromatography
HS	HepaSphere
IACUC	Institutional Animal Care and Use Committee
IHC	Immunochemistry
IR	Infrared
IRI	Irinotecan
LC-MS	Liquid chromatography/tandem mass spectrometry
LCST	Lower critical solution temperature
MA	Methacrylic acid
McT-A	Mercury cadmium telluride
MDO	2-methylene-1,3-dioxepane
MMP	Matrix metalloproteinase
mRECIST	Response evaluation criteria in solid tumors
MRI	Magnetic resonance imaging

MS	Microsphere
NBCA	N-butyl cyanoacrylate
NC	NIPAAM-co-cysteamine
NCHA	NIPAAM-co-hydroxyethylmethacrylate-acrylate
NCVS	NIPAAM-co-cysteamine-vinylsulfone
NIPAAM	Poly(N-isopropylacrylamide-*co*-acrylic acid)
NMR	Nuclear magnetic resonance
OCMC	Oxidized carboxymethyl cellulose
PBS	Phosphate buffered saline
PDGFR	Platelet-derived growth factor receptor
PDMS	Polydimethylsiloxane
PEGMA	Poly(ethylene glycol) methacrylate
PHIL	Precipitating hydrophobic injectable liquid
PPODA	Poly(propylene glycol) diacrylate
PVA	Poly(vinyl alcohol)
QT	Pentaerythritol tetrakis (3-mercaptopropionate)
RAF	Rapidly accelerated fibrosarcoma
RARE	Relaxation enhancement
RPM	Revolutions per minute
RS	Responsive sequence
SD	Sprague Dawley
SD	Standard deviation
SDS	Sodium dodecyl sulfate

SEER	Surveillance, epidemiology, and end Results
SELP	Silk-elastinlike protein
SEM	Scanning electron microscopy
Sol	Solution
Soraf	Sorafenib
Soraf Tos	Sorafenib tosylate
TACE	Transarterial chemoembolization
TAE	Transarterial embolization
TE	Time of echo
TR	Time of repetition
TTP	Time to progression
Tx	Treatment
UAE	Uterine artery embolization
VEGF-A	Vascular endothelial growth factor A
VEGFR-2	Vascular endothelial growth factor receptor-2

ACKNOWLEDGMENTS

My journey to complete a PhD has been metamorphic. Throughout college and into the first years of medical school, I was under the impression I reasoned through situations in a multidimensional manner, pulling on problem solving skills of my "inner" engineer. But to my chagrin, graduate school taught me how much I really did not know and much my scientific thinking needed refinement. These past five years have been filled with a good deal of failing, immense learning, and a couple of successes. But most importantly, it has been centered on personal growth. The connections I have made and the mentorship I have received are priceless. I will cherish them always.

I would like to start by my thanking my advisor, Dr. Hamid Ghandehari. He took a chance on me. The excitement in his presentation of his lab's work got me hooked during our first meet and greet. His patience and commitment to his students have been essential to my progress. Next, I would like to thank my mentor and original mastermind behind my project, Dr. Joseph Cappello. His patience and guidance and calm, eloquent demeanor have been instrumental to my scientific learning. All of my committee members have provided focused guidance throughout my graduate training, essential to developing my project. Dr. Jindrich Kopecek was one of my first graduate school professors, and his teachings in biomaterials and drug delivery created my knowledge base to build upon. Dr. Bruce Gale allowed me to throw in my own side project while taking his microfluidic class, which resulted in a device used for all of my preliminary *in vitro* work. Dr. Eugene Huo provided

expert clinical guidance throughout the entirety of this project and took time out of his busy schedule to catheterize rabbits instead of people, which resulted in the most substantial data, proving our SELP embolic works! My unofficial mentors were just as instrumental as my advising committee. Thank you Drs. Josh Gustafson and Robert Price for putting up with my ignorance and taking time to teach me, even though I hindered your work and messed up a few times.

Now I will start my thank you notes, Jimmy Fallon style:

Thank you Shraddha, Heather, Sarah, Yizhe, Wiebke, Nithya for your friendship. If it wasn't for this lab, I'd never have met you! Thank you Nick, we started off together and fought our way to the finish line, pushing each other along the way. Thank you to my awesome students who kept me going in the lab: Andrea, Erik, Ida, Mitch, Teresa, and Bryant. Thank you Martin for joining SELP; you kept me on track. Thank you Darwin for your calm and sagely advice. Thank you Misti, Lauren, Reesha, Rochelle, Renee, and Jackie of the CMC- my animal studies wouldn't have happened without your assistance and vigilance to help keep my rats healthy. Thank you Janet and my MD-PhD family for always having my back and supporting me. Thank you Ruby, you're awesome. Thank you Dr. Caligiuri for always believing in me and sending Eugene my way. Thank you Dr. Kiser for teaching me to work hard and that hitting a wall in science is normal. Thank you Ashley, Colleen, Giang, and Melissa for supporting me from afar. Thank you to all of my family friends for listening to my whining. Thank you Mom, Dad, and Ahrash for putting up with me and my stress and always having my back. There is no way I would have finished this phase of my education without your unconditional love and support. And thank you to my little Lucy, you got me out of my dark place in the middle of graduate school.

CHAPTER 1

INTRODUCTION

1.1 Introduction

Hepatocellular carcinoma (HCC) remains a substantial clinical burden, rising to the sixth most common cancer worldwide [1]. Surveillance, epidemiology, and end results (SEER) between 2007-2010 showed increased liver cancer mortality rates in the United States [2]. In fact, HCC continues to remain the third major cause of cancer-related death [3]. The standard of care is surgical resection or liver transplantation [4]. However, these methods are effective only for patients with an early disease state and a noncirrhotic liver [3,5]. Underlying cirrhosis is present in approximately 90% of HCC patients, and therefore the majority of cases require other forms of treatment [6]. Treatment must be approached on an individual level taking into account general liver function and tumor stage [7]. Patients who fall into the categories of intermediate or advanced disease are eligible for regional tumor destruction by percutaneous or transarterial techniques to slow disease progression [8]. Transarterial chemoembolization (TACE) is becoming the most commonly employed treatment worldwide because it is the sole palliative therapy whose clinical benefit has been proven statistically significant [6,9]. This procedure consists of catheterizing a patient through the femoral artery, guiding the catheter up the aorta into the hepatic artery, from which branches feeding the tumor sprout [10]. Following positioning

in the primary feeding vessel, a series of agents are delivered including a chemotherapeutic alone or in an oil emulsion, and an embolic agent to occlude the artery. The goal of embolization is to cut off tumor blood supply and induce necrosis. Local release of chemotherapeutics allows for a high concentration within cancerous tissue, maximizing local response and minimizing systemic effects. TACE prevents significant tumor progression, increasing patient survival from months up to 2 years depending on the patient's underlying liver function and disease stage [10]. Patients treated with TACE often die due to tumor progression because of the revascularization of the surviving tumor. To address this issue, new studies are being conducted to combine TACE with systemic sorafenib, an FDA-approved drug for the treatment of HCC. Sorafenib, a multikinase inhibitor available in oral form results in antiproliferative and antiangiogenic effects [11]. Systemic side effects such as fatigue, alterations in liver enzymes, and dermatologic events are common, which causes noncompliance or dose reduction. Furthermore, the drug has an oral bioavailability at around 38-49% [12]. A phase II trial of sorafenib combined with concurrent TACE using doxorubicin provided preliminary data suggesting a complimentary effect [13]. The combination was safe and most adverse effects were associated with the oral dosing of sorafenib, which were managed by dose adjustment.

In conventional TACE, two steps are involved. First, Lipiodol® (Guerbet, Indiana), an iodized oil, is mixed with a chemotherapeutic such as doxorubicin and injected via microcatheter into the tumor arteries where it permeates deeply within the cancerous tissue, moving out into the portal veins thus strengthening antitumor effects [10]. By itself, its effects are short lived. Therefore a second injection of an embolic material is required. Solid gelatin sponge is often used. The material is cut into small particles, hydrated, and

injected to form a stable, but temporary embolus. The gelatin slurry, however, is difficult to inject and its performance is unpredictable [14]. A new category of embolics gaining favor is microsphere particles, particularly drug eluting beads (DEBs) [15]. These microspheres come in size ranges typically spanning from 100-900 μm corresponding to sizes of vessels accessible by microcatheter [16]. Smaller diameter particles allow better tumor penetration, but with consequence of potential aggregation and off-target embolization. One of these products is the DC Bead® (BTG, UK). The DC Bead system consists of poly(vinyl alcohol) (PVA) microspheres of uniform size that deliver doxorubicin and act as embolic agents simultaneously. DEBs combine three critical functions of the conventional therapy into one system. However, as solids they cannot penetrate as deeply into the tumor as a liquid. These beads also have risk of fracturing under stress in the catheter and they do not uniformly pack so recanalization has been shown to occur over time [16]. With regard to drug compatibility, both Lipiodol® and DEBs are limited to delivering low molecular weight, charged molecules like doxorubicin. An effective embolic agent that is proven applicable for localized delivery of a wide variety of chemotherapeutic agents is a significant need, and one that addresses the shortcomings of current systems.

1.2 Silk-elastinlike protein polymers for localized tumor therapy

Silk-elastinlike protein polymers (SELPs) are genetically engineered polymers composed of repeating amino acid sequences based on silk and elastin, naturally occurring proteins found in the silkworm (silk-like units) and mammalian tissues (elastin-like units) [17]. Combination of these two motifs has allowed development of polymeric systems with

very unique properties that have been extensively characterized for drug and gene delivery applications [17,18]. Recombinant DNA methods allow precise control of the polymer sequence and therefore structure and function. By altering the number and sequence of these polymer motifs, the physicochemical properties and biological functions are modulated as required for specific medical applications. Depending on sequence and composition, this polymer at lower temperatures remains in solution into which low molecular weight drugs and larger biologics may be mixed. Increase in temperature triggers transformation into a physically cross-linked three-dimensional gel network. The physical properties of the network including rate of gelation, gel strength, gel stiffness, and rate of drug release are dictated by the polymer's specific silk:elastin ratio as well as the concentration. Figure 1.1 displays the amino acid sequences and structural representation of SELPs 47K and 815K, whose silk:elastin ratios and sequences allow for the characteristics described above. Upon injection, SELP solutions composed of SELP-47K or SELP-815K with greater than 4% protein concentration form hydrogels, which persist in the tissues for more than 12 weeks delivering therapeutic agents continuously for at least 21 days [19,20]. The localized drug delivery aspect and SELPs' unique property of liquid-to-solid transformation provide the opportunity to investigate these polymers as liquid embolic agents in transarterial chemoembolization.

1.3 Aims and scope of this dissertation

A chemoembolic system that combines the depth penetration of the oil-drug emulsion used in conventional TACE, controlled release of therapeutics like DEBs, but with added advantage of co-delivery of multiple agents, and induction of a stable embolus

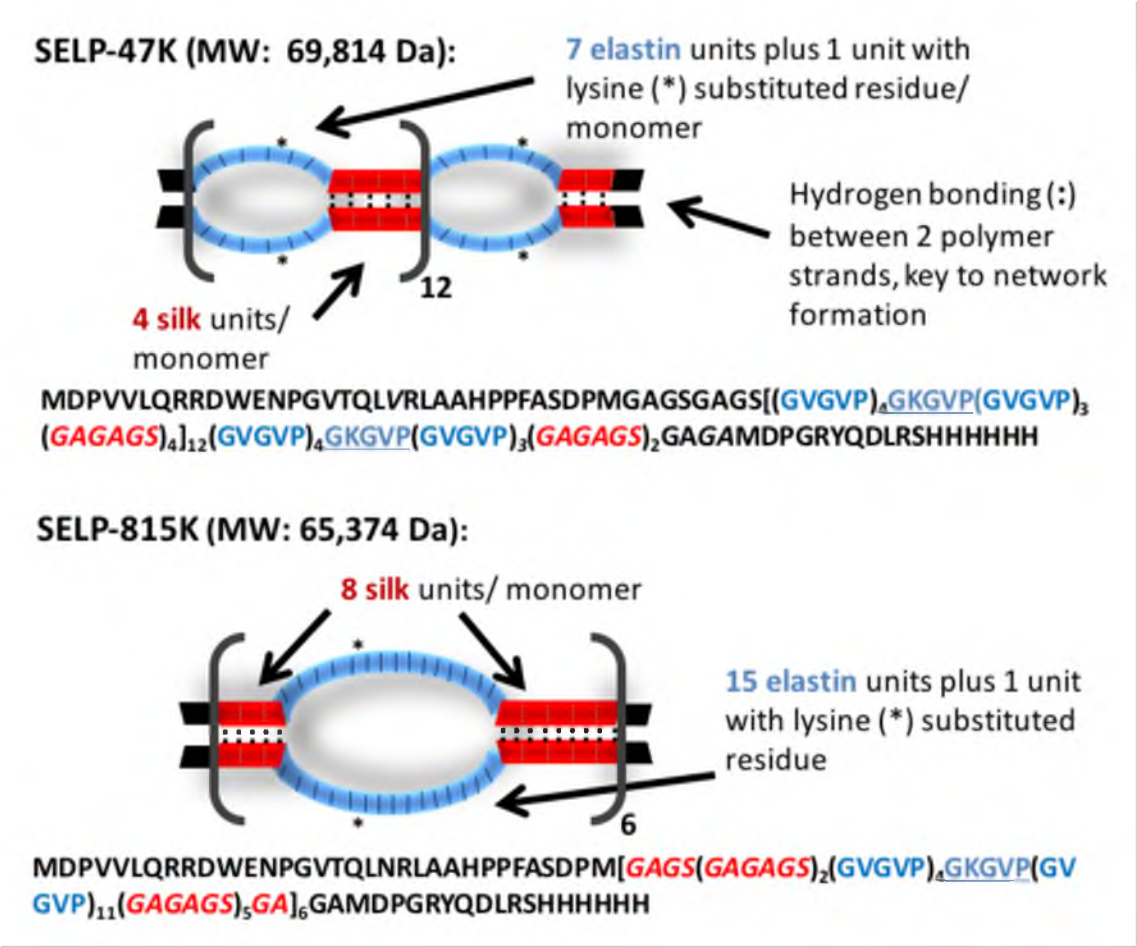

Figure 1.1. Diagram of SELP-47K and SELP-815K protein polymers (single letter amino acid abbreviations are used). The silk-like block, GAGAGS, is represented in red and the elastin-like block, GVGVP, is represented in blue. While the overall content of silk and elastin-like blocks between SELP-47K and SELP-815K are comparable (approximately 1:2), SELP-815K has twice the number of silk and elastin-like blocks per repeat. When in alignment between strands, the silk repeats form beta sheets via hydrogen bonding. Because the silk repeats are twice longer in SELP-815K, they have twice the potential for formation of hydrogen bonds within each repeat. Greater numbers of hydrogen bonds result in stronger network formation and a stronger gel [21].

in one injection is the overarching goal of the work presented herein (Figure 1.2). The central hypothesis of this dissertation is that silk-elastinlike proteins may be used to develop a novel liquid-to-solid polymer embolic capable of co-delivery of multiple chemotherapeutics for use in TACE to treat HCC. To test this hypothesis, three Specific Aims were pursued as outlined in Sections 1.3.1, 1.3.2, and 1.3.3.

1.3.1 Design and characterize an injectable SELP composition

A series of design criteria were established for an injectable liquid embolic addressing maximum viscosity, time of gelation, and final material stiffness. These studies presented in Chapter 3 laid the groundwork for development of an injectable SELP liquid embolic [21]. Using these design criteria, two SELP compositions, SELP-47K and SELP-815K, were selected for evaluation at different concentrations by weight. An elimination process was conducted to narrow down formulations until an adequate material and concentration was determined. Microfluidics devices rendering tumor vasculature were designed and developed for *in vitro* testing of the material candidates. The systematic engineering approach resulted in a SELP formulation consisting of 12% w/w SELP-815K. Established criteria for a successful embolic included injection viscosity of $\leq$ 150 cP, gelation time of $\leq$ 5 minutes, and a storage modulus, G', representative of gel strength $\geq 1 \times 10^5$ Pa by 5 hours. This formulation continued into *in vitro* testing and successful blockage in the microfluidics device under flow was observed. These results warranted an *in vivo* pilot study. Occlusive ability *in vivo* using nontumor bearing rabbits was shown. Histological examination of liver tissue postmortem revealed SELP occluding the arterioles of portal triads, but not central veins. An injectable SELP formulation was

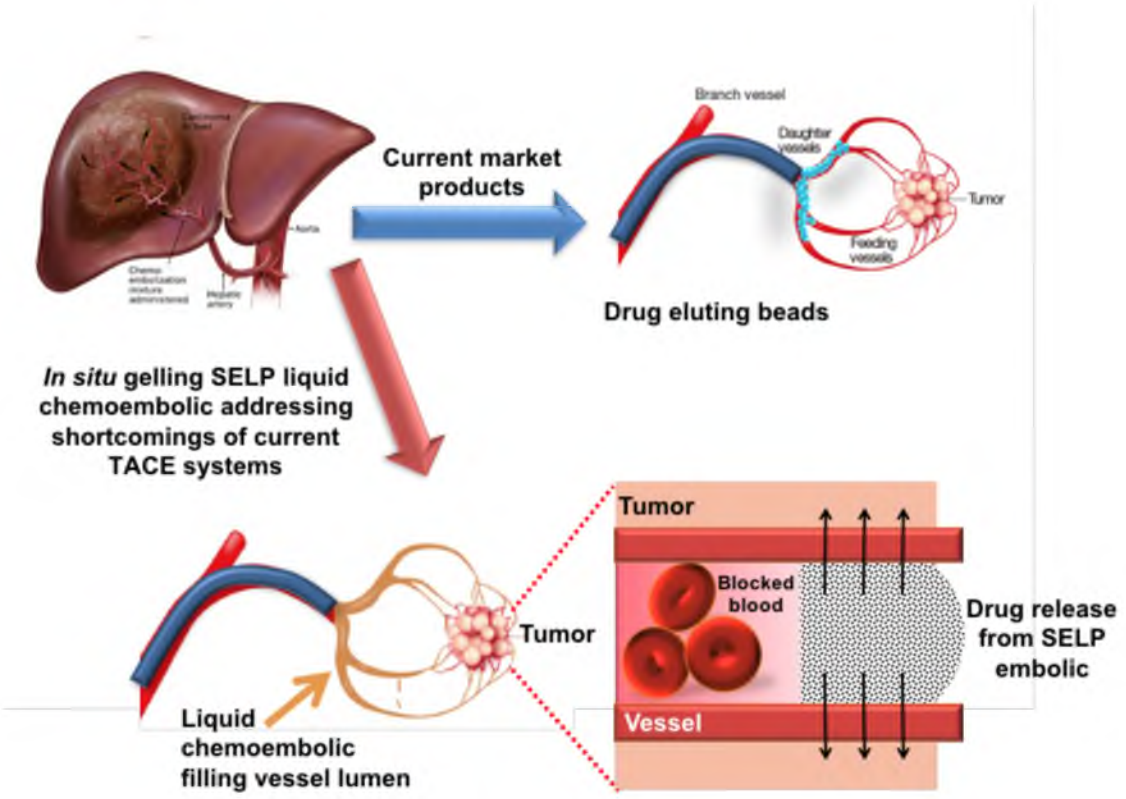

Figure 1.2. Diagrammatic representation of TACE using DEBs to treat HCC as compared to a SELP liquid embolic that is capable of co-delivery of single to multiple drugs. The liquid embolic penetrates deeper into the tumor vasculature and occludes the entire vessel lumen. Figure adapted from Johns Hopkins Medicine [22].

determined that gelled within the arteriole system and remained lodged.

1.3.2 Characterize *in vitro* release of doxorubicin and sorafenib from the SELP-815K matrix and assess physicochemical changes imparted to the gel network as a result of drug incorporation

Clinically, bland embolization of HCC is inferior to chemoembolization treatment [23]. Localized delivery of chemotherapeutics is essential for increased time to progression of the disease. The establishment of an *in situ* gelling SELP-815K liquid embolic naturally paved the way to further develop the bland formulation into a chemoembolic (drug-bearing). Chapter 4 details methods tested to incorporate the drugs doxorubicin and sorafenib individually and in combination. The design criteria set forth by the work in Specific Aim 1 were applied when testing the chemoembolic formulations [24]. The hydrophobic properties of both drugs in addition to the high content of hydrophobic residues in SELP-815K were hypothesized to allow for extended release profiles of each drug individually and concurrently. Direct mix of powder drug in the base form resulted in an injectable drug loaded SELP-815K solution meeting the original design criteria. As predicted by their partition coefficients, higher percentage of doxorubicin was released versus sorafenib. Interestingly, in the dual drug gels, more sorafenib was released in the presence of doxorubicin, without the converse being true. For all groups, *in vitro* drug release achieved therapeutic concentrations for up to 14 days.

1.3.3 Evaluation of drug loaded SELP-815K solutions *in vivo* using a rat model of hepatocellular carcinoma to measure efficacy of localized drug delivery from embolic gel

Culmination of Specific Aims 1 and 2 suggested that SELP-815K may be used as an *in situ* gelling liquid chemoembolic in TACE. The *in vitro* release studies indicated therapeutic concentrations were reached. Therefore, preliminary *in vivo* efficacy studies were performed in hepatic tumors to investigate long-term embolus residence and therapeutic effect from localized release of doxorubicin and sorafenib eluting from the SELP-815K embolic gel. A rodent model using Sprague Dawley (SD) rats for invasive catheterization of the hepatic artery for preclinical investigation of liver-directed therapies was chosen for the remaining studies [25]. A surgical procedure was conducted to determine efficacy from *in vivo* release of the drugs from the SELP-815K matrix, particularly in the presence of both drugs. A small volume of the drug loaded liquid embolic was injected intratumorally. Change in tumor volume over time was monitored via magnetic resonance imaging along with animal health. This preliminary *in vivo* work, which had low animal numbers, resulted in decrease in tumor volume in animals whose tumors were treated with drug loaded SELP. Due to the low numbers, significance cannot be declared at this time, but the results indicate that the drug loaded SELP embolic may reach localized therapeutic drug concentrations.

The following chapters of this dissertation describe the experimental work used to complete the presented aims. A comprehensive literature review of embolics, TACE, and embolics in development is presented in Chapter 2 [26]. Chapters 3 [21] and 4 [24] present the methods, results, and discussions addressing Specific Aims 1-2. Chapter 5 outlines the

conclusions from this dissertation and future directions. Appendix A details methods, results, and discussion for the preliminary *in vivo* work.

1.4 References

[1] Center MM, Jemal A. International trends in liver cancer incidence rates. Cancer Epidemiol Biomarkers Prev 2011;20:2362–8. doi:10.1158/1055-9965.EPI-11-0643.

[2] Altekruse SF, Henley SJ, Cucinelli JE, McGlynn KA. Changing hepatocellular carcinoma incidence and liver cancer mortality rates in the United States. Am J Gastroenterol 2014;109:542–53. doi:10.1038/ajg.2014.11.

[3] Ferri F. Hepatocellular carcinoma. Ferri's Clin Advis 2016. 2nd ed., Elsevier; 2016, p. 605–7.

[4] Brown DB, Nikolic B, Covey AM, Nutting CW, Saad WE a, Salem R, et al. Quality improvement guidelines for transhepatic arterial chemoembolization, embolization, and chemotherapeutic infusion for hepatic malignancy. J Vasc Interv Radiol 2012;23:287–94. doi:10.1016/j.jvir.2011.11.029.

[5] Wörns MA, Galle PR. Future perspectives in hepatocellular carcinoma. Dig Liver Dis 2010;42:302–9. doi:10.1016/S1590-8658(10)60521-X.

[6] Blumgart L. Surgery of the liver, biliary tract, and pancreas. 1. Philadelphia, PA: Saunders, Elsevier; 2007.

[7] Ghassan A-AK, Jarnagin W, Lowery M, D'Angelica M, Brown K, Ludwig E, et al. Liver and bile duct cancer. In: Niederhuber JE, editor. Abeloff's Clin Oncol 5th ed., Churchill Livingstone; 2014, p. 1373–96.

[8] Antoch G, Roelle G, Ladd S, Kuehl H, Heusner T, Sotiropoulos G, et al. Selective and sequential transarterial chemoembolization: survival in patients with hepatocellular carcinoma. Eur J Radiol 2012;81:2290–7. doi:10.1016/j.ejrad.2011.09.010.

[9] Bester L, Meteling B, Boshell D, Chua TC, Morris DL. Transarterial chemoembolisation and radioembolisation for the treatment of primary liver cancer and secondary liver cancer: a review of the literature. J Med Imaging Radiat Oncol 2014;58:341–52. doi:10.1111/1754-9485.12163.

[10] Tam KY, Leung KC-F, Wang Y-XJ. Chemoembolization agents for cancer treatment. Eur J Pharm Sci 2011;44:1–10. doi:10.1016/j.ejps.2011.06.013.

[11] El-Serag HB. Hepatocellular carcinoma. N Engl J Med 2011;365:1118–27.

doi:10.1056/NEJMra1001683.

[12] Ben Mousa A. Sorafenib in the treatment of advanced hepatocellular carcinoma. Saudi J Gastroenterol 2008;14:40–2. doi:10.4103/1319-3767.37808.

[13] Pawlik TM, Reyes DK, Cosgrove D, Kamel IR, Bhagat N, Geschwind JFH. Phase II trial of sorafenib combined with concurrent transarterial chemoembolization with drug-eluting beads for hepatocellular carcinoma. J Clin Oncol 2011;29:3960–7. doi:10.1200/JCO.2011.37.1021.

[14] Ray CE, Lawson MC, Bauer JR. Embolization agents. In: Mauro MA, Murphy KPJ, Thomson KR, Venbrux AC, Morgan RA, editors. Image-Guided Interv. Second, Elsevier Inc.; 2014, p. 87–95.

[15] Lammer J, Malagari K, Vogl T, Pilleul F, Denys A, Watkinson A, et al. Prospective randomized study of doxorubicin-eluting-bead embolization in the treatment of hepatocellular carcinoma: results of the PRECISION V study. Cardiovasc Intervent Radiol 2010;33:41–52. doi:10.1007/s00270-009-9711-7.

[16] Laurent A. Microspheres and nonspherical particles for embolization. Tech Vasc Interv Radiol 2007;10:248–56. doi:10.1053/j.tvir.2008.03.010.

[17] Frandsen JL, Ghandehari H. Recombinant protein-based polymers for advanced drug delivery. Chem Soc Rev 2012;41:2696. doi:10.1039/c2cs15303c.

[18] Gustafson JA, Ghandehari H. Silk-elastinlike protein polymers for matrix-mediated cancer gene therapy. Adv Drug Deliv Rev 2010;62:1509–23. doi:10.1016/j.addr.2010.04.006.

[19] Dandu R, Ghandehari H, Cappello J. Characterization of structurally related adenovirus-laden silk-elastinlike hydrogels. J Bioact Compat Polym 2008;23:5–19. doi:10.1177/0883911507085278.

[20] Gustafson J, Greish K, Frandsen J, Cappello J, Ghandehari H. Silk-elastinlike recombinant polymers for gene therapy of head and neck cancer: from molecular definition to controlled gene expression. J Control Release 2009;140:256–61. doi:10.1016/j.jconrel.2009.05.022.

[21] Poursaid A, Price R, Tiede A, Olson E, Huo E, McGill L, et al. In situ gelling silk-elastinlike protein polymer for transarterial chemoembolization. Biomaterials 2015;57:142–52. doi:10.1016/j.biomaterials.2015.04.015.

[22] Johns Hopkins Medicine. Intra-arterial therapies n.d. http://www.hopkinsmedicine.org/liver_tumor_center/treatments/intraarterial_therapies/.

[23] Lencioni R. Loco-regional treatment of hepatocellular carcinoma. Hepatology

2010;52:762–73. doi:10.1002/hep.23725.

[24] Poursaid A, Jensen MM, Nourbakhsh I, Weisenberger M, Cappello J, Ghandehari H. Silk-elastinlike protein polymer liquid chemoembolic for localized release of doxorubicin and sorafenib. Mol Pharm 2016:Submitted.

[25] Sheu AY, Zhang Z, Omary R a, Larson AC. Invasive catheterization of the hepatic artery for preclinical investigation of liver-directed therapies in rodent models of liver cancer. Am J Transl Res 2013;5:269–78.

[26] Poursaid A, Jensen MM, Huo E, Ghandehari H. Polymeric materials for embolic and chemoembolic applications. J Control Release 2016. doi:10.1016/j.jconrel.2016.02.033.

CHAPTER 2

LITERATURE BACKGROUND

2.1 Introduction

2.1.1 Embolotherapy

The concept of embolization, *i.e.*, deliberate blocking of blood vessels, dates back to the early 1900s. Robert Dawbarn presented "the starvation plan" to treat malignant growths in 1904, discussing how physically stopping blood flow to a tumor via ligation of vessels leads to shrinkage and pain relief for the patient [1]. Attempts to use materials to create a physical obstruction to blood flow dates to the early 1930s by Hamby and Gardener who surgically treated carotid-cavernous fistulas using muscle fragments [2]. Percutaneous embolization as a medical procedure was made possible by the early 1960s' technological development of the fluoroscope, which provided the ability to perform an angiogram by viewing X-rays in real-time. Charles Dotter, considered the "Father of Interventional Radiology," performed the first interventional angiographic procedure in 1964. He invented an automated X-Ray Roll-Film magazine capable of capturing images every 2 seconds, as well as various catheters and the J tipped guidewire [3,4]. Later, he introduced

---

Reprinted *in part and adapted* with permission of Elsevier. Poursaid A, Jensen MM, Huo E, Ghandehari H. Polymeric materials for embolic and chemoembolic applications. J Control Release 2016. doi:10.1016/j.jconrel.2016.02.033.

the concept of percutaneous transluminal angioplasty and the beginnings of diagnostic coronary angiography. He was eventually nominated for the Nobel Prize in medicine in 1978. Building off of these initial developments, interventional radiology soon advanced to treatment of acute gastrointestinal bleeding, occlusion of arteriovenous malformations and fistulas, to more recent advances in interventional oncology, allowing for chemoembolization of highly vascular tumors such as hepatocellular carcinoma.

The earliest embolizations made use of autologous clots, muscle fragments, or stainless steel pellets. By the 1970s, clinical applications began to drive the development of new materials. Gelatin sponges, first developed as hemostatic materials for open surgery, soon transitioned to use as endovascular embolic agents as a response to failures of muscle fragment embolization. Thomas Speakman reported first use of "mashed" gelatin pieces mixed with saline to a consistency of "good porridge" injected into the internal carotid artery to occlude a carotid-cavernous fistula [5]. The occlusion was successful, eliminating signs and symptoms of the fistula without loss of vision or serious complications in the patient postoperatively.

Embolic materials are classified broadly into mechanical embolic agents or flow-directed embolic agents [2]. Mechanical agents such as metal coils and plugs used to treat focal vascular abnormalities are not within the scope of this review. Flow-directed agents can treat diffuse vascular abnormalities and include particulates, polymers, or *in situ* gelling biomaterials delivered via catheters positioned within a target's vascular supply. These materials are subcategorized into permanent or temporary. From a clinical standpoint, the therapeutic goal and intended long-term outcome dictate the choice of materials. Questions typically asked include: "Why is embolization necessary?" and "What

lies downstream of the intended target?" If embolization is required for obstruction of a hemorrhaging vessel, a temporary, fast acting embolic is required. A vascular malformation, on the other hand, often requires a more permanent material and more precise administration. Polymers have been successfully designed for a variety of biomedical applications, including as embolic agents [6]. The ability to tailor the polymer structure-function relationship for a defined need provides a unique materials platform. Both natural and synthetic polymers have been used to develop flow-directed embolics [7].

Gelatin sponge made from purified porcine skin is the first example of a successful naturally derived polymer commonly used as a temporary occlusive material [7,8]. The sponge comes in the form of dry sheets that are manually cut into small sections, then mixed with saline and contrast dye just prior to injection. This material provides a fast, low-cost, transient embolic that is used in multiple clinical applications. However, a severe drawback of this agent is lack of precision in delivery, and unpredictable levels of embolization and recanalization [7]. In response, calibrated microspheres (MSs) have been designed using poly(vinyl alcohol) and derivatives to provide improved control [9]. Although the level and location of occlusion is highly predictable, available MSs are not degradable and result in permanent vessel occlusion. To address these concerns, degradable materials composed of chitosan derivatives, for example, are being designed for synthesis of microspheres with predictable degradation rates [10]. This Chapter highlights these and a series of other embolic materials, first exploring clinical applications followed by material details including physical and mechanical properties, advantages, and disadvantages concluded with a discussion of unresolved issues and future directions in this field. The Chapter discusses both commercially available agents as well as materials

under development.

2.1.2 Clinical applications

2.1.2.1 Vascular malformations and hypervascular tumors

Vascular malformations are often congenital anomalies arising from dysplastic vascular channels. They are characterized by a tangle of thin walled vessels whose abnormal characteristics eventually lead to clinical symptoms requiring treatment. Symptoms vary depending on the category of malformation and location in the body. They are classified as either slow-flow or fast-flow [2,11,12]. Slow-flow vascular malformations consist of capillary, venous, or lymphatic vessels. Symptoms range from externally visible port-wine staining of the skin to painful cyst-like formations. Fast-flow arteriovenous malformations (AVMs) consist of an arteriovenous shunt bypassing the capillary bed [13] resulting in high flow into the venous system. AVMs within the central nervous system may be particularly dangerous and require treatment to prevent risk of hemorrhage, stroke, neurological deficit, or seizure. Cerebrovascular AVMs are graded by the Spetzler-Martin scale that classifies malformations according to size, location relative to functionally eloquent cortex, and type of venous drainage [14]. Microsurgery for low grade AVMs can provide an immediate cure with a relatively low risk of complications, but remains an invasive procedure. Embolization therapy can be used as a sole treatment method or in combination with surgery or radiotherapy to eliminate or stabilize an AVM, decreasing the risk for hemorrhage [15]. Embolic microspheres are approved for the treatment of AVMs. More recently, nonadhesive liquid embolics have been investigated as an improved option [16].

Hypervascular tumors are characterized by tumor induced abnormal vasculature consisting of increased numbers of blood vessels feeding into the tumor. The higher blood flow increases the risk of bleeding during surgical resection. Examples of hypervascular tumors include head and neck tumors like meningiomas and paragangliomas, hepatocellular and colorectal carcinomas, and subsequent metastases. Embolotherapy is often used to block blood flow to the tumor either as a neoadjuvant treatment prior to surgery or as a palliative measure if the tumor is inoperable. This treatment not only decreases the risk of bleeding, but also may lead to shrinkage of the tumor thus improving surgical outcome, quality of life, or both. For hypervascular tumors that are operable, neoadjuvant embolization makes use of microspheres, gelatin sponges, liquid embolics or a combination, depending on the clinician or institutional policy. In the past, the primary goal had been solely to block the blood supply of the tumor. In the case of hepatocellular carcinoma (HCC), endovascular therapy has transitioned into a primary treatment involving the co-delivery of chemotherapeutics and embolics. Liver HCC lesions are unique in that they draw blood from branches off of the hepatic artery while the healthy liver parenchyma primarily receives blood supply from the portal system, allowing embolization of the tumor while preserving the surrounding hepatic tissue [17].

2.1.2.1.1 Transarterial embolization and chemoembolization

Transarterial embolization (TAE) will be explained using treatment of a hepatic tumor as an example. The procedure begins with accessing the arterial system via the femoral artery using the Seldinger technique. Once stable access is established, a guidewire and catheter system is maneuvered to the target location under angiographic guidance. A

diagnostic angiogram is performed to identify the vascular supply to the tumor along with any potential anatomic variants [18]. After diagnostic angiography, a vessel is selected for embolization [19]. The catheter is used to access the target vessel, and location is confirmed by injection of contrast. The selected embolic is delivered next. The primary procedural endpoint is angiographic evidence of stasis [20]. Classically, the term TAE in reference to HCC treatment refers to bland embolization where the goal is to induce ischemic necrosis in the tumor. The embolic agents used to achieve this clinical outcome are highly variable. If a temporary occlusion is desired, gelatin sponge is used. If permanent occlusion is intended, poly(vinyl alcohol) or trisacryl gelatin particles are used. However, clinical data over the past few decades have confirmed bland embolization does not provide the best possible outcome [17,21]. Since TAE, chemoembolization was developed to improve patient morbidity and mortality. It is a procedure similar to TAE, but with the addition of localized delivery of chemotherapeutics via the same catheter, termed transarterial chemoembolization (TACE).

TACE can be divided into conventional TACE (cTACE) and drug-eluting bead TACE (DEB-TACE). Conventional TACE involves sequential delivery of a mixture of chemotherapeutics and ethiodized oil into the tumor vasculature followed by an embolic, whereas the newer DEB-TACE uses a single delivery system of drug loadable microspheres that both occlude the selected vessels and provide controlled drug release [22]. A series of clinical studies in the past decade have shown benefits of DEB-TACE over cTACE. The PRECISION V study, a multicenter randomized trial comparing the short-term outcomes of DEB-TACE and cTACE, demonstrated that DEB-TACE was associated with improved tolerability and significant reduction in liver toxicity and

chemotherapeutic related side effects [23]. The PRECISION ITALIA study randomized patients to cTACE or DEB-TACE, and required a post-TACE follow-up for at least 2 years or until death. This study failed to establish a significant difference between the two groups in terms of overall survival, but did show significantly lower postprocedural pain in the DEB-TACE group [24]. The DEB-TACE group also showed improved objective response, defined as complete or partial response following the modified Response Evaluation Criteria in Solid Tumors (mRECIST) [25].

Finally, the DEB-TACE process provides several more benefits to the clinician and the patient. Handling chemotherapeutics loaded on beads is less complex, and does not require use of ethiodol, which can dissolve certain types of plastic [26]. Lower pain and systemic toxicity postchemoembolization are important benefits to the patient. Some of the current drawbacks of the available DEBs include permanent occlusion, limited selection of drugs that can be loaded onto the beads, and inability to track bead distribution *in vivo*. Development of degradable microspheres may expand treatment options, allowing treatment of organs and tumors that do not have dual blood supplies. New materials that may load more than one drug type will allow for more personalized medicine and combinational chemotherapy.

2.1.2.2 Aneurysms and hemorrhage

Aneurysms are outpouchings or dilatations of weakened vessel walls. As tension on the weakened wall increases, the risk of rupture and hemorrhage increases. They can occur throughout the body, but are more often associated with the aorta, the renal artery, the Circle of Willis, and AVMs. The type of treatment depends on the shape, location, and

cause [9]. Conventional vascular surgery including resection or clipping was the previous standard of care. However, with the development of new tools, endovascular approaches are becoming more common. Before treatment, imaging modalities including multidetector-row CT and Doppler ultrasonography are used to characterize the aneurysm. The liquid embolic Onyx® and liquid glue N-butyl cyanoacrylate (NBCA) are commonly being used to treat smaller aneurysms over metal coils or microspheres [9].

2.1.2.3 Uterine fibroids

Synonymous with uterine leiomyomas or myomas, uterine fibroids are benign tumors of the myometrium [27–29]. They are a major cause of morbidity among women of reproductive age, with an incidence of 20-40% [29,30]. Patient symptoms are highly variable; some patients are asymptomatic whereas others may experience symptoms including abnormal uterine bleeding, chronic pelvic pain, urinary incontinence, ureteral obstruction, and fertility issues. Clinical management of uterine fibroids depends on patient symptoms. An asymptomatic fibroid identified during a pelvic exam will remain under observation whereas symptomatic fibroids may be treated medically or surgically[27].

Uterine artery embolization (UAE) is an organ-preserving treatment alternative originally reported in 1995 [31]. Since the first case reports by Ravina, *et al.,* this procedure has been shown to be safe and effective [2,32]. In UAE studies using permanent microspheres as an embolic, fibroid volume decreased by 53.4 ± 26.9%, 3 months after UAE, by 63.7 ± 28.2% after 6 months, and by 71.8 ± 26.8% after 12 months [33,34].

Uterine fibroids are very sensitive to ischemia. Myomectomy has less of an impact than UAE on overall fertility; therefore women desiring children may choose the more

invasive surgical procedure [29]. However, due to the advantages of minimal access techniques, new degradable materials are being developed for transient embolization. Several clinical case studies have shown that transient occlusion using mechanical compression of the uterine arteries up to 6 hours leads to fibroid volume reduction and menorrhagia symptom relief [35,36]. Development of temporary embolic microspheres (< 6hr) will provide for a similar outcome using the faster UAE while preserving fertility. Table 2.1 summarizes these clinical applications that require embolotherapy.

2.2 Commercially available materials

The number of flow-directed embolic materials is expanding. In this section a series of products with extensive original research and clinical data associated with development and clinical outcome for the indications outlined above will be discussed. Subcategories of flow-directed embolics will be discussed, including temporary and permanent materials. The availability and approved indication of use for the marketed materials discussed vary between countries. Structures and features of these materials are summarized in Table 2.2.

2.2.1 Gelatin sponge

Correll and Wise first introduced the gelatin sponge in 1945 as a new biologic absorbable hemostatic sponge [37]. They tested the new material in high blood flow applications to assess effectiveness of hemostatic properties. In a series of tests, canine livers were cut and saline soaked gelatin sponge was placed over the site of bleeding while applying direct pressure for up to 10 minutes [38]. Complete hemostasis was achieved without any other interventions. Within 1 month, minimal sponge material remained and

Table 2.1. Summary of clinical applications requiring embolotherapy

Clinical Application	Treatment Goal	Polymer Embolic(s) Used	Future Directions	Ref.
Vascular Malformations/Aneurysms	Prevention of hemorrhage; permanent occlusion for symptom control	Liquid embolics: NBCA glue, Onyx® , PHIL™	Nonadhesive liquid embolics with nontoxic diluents	[12-17]
Malignant Hypervascular Tumors	Induction of infarction / local delivery of chemotherapeutics to prompt tumor necrosis	Drug eluting calibrated microspheres, PVA particles, gelatin sponge particles, starch particles	Multi-drug capable MS; "Imageable" MS; degradable MS to allow re-treatment	[18-27]
Uterine Fibroids	Induction of infarction; temporary occlusion to prevent blood loss during surgery	Calibrated microspheres, PVA particles	Degradable MS with predictable degradation rates for transient occlusion	[27-36, 7' 83, 85-86

Table 2.2 Summary of commercially available embolic agents

Material	Polymer Structure	Trade Names	Material Description	Degradable (Y/N)	Drug Incorporation	Ref.
Denatured Collagen	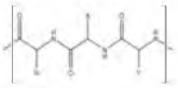	GelFoam® (Pfizer, inc.)	Hemostatic sponge, comprised of a natural protein polymer (Note X and Y represent any amino acid except tryptophan, X is predominantly Proline)	Yes (1 month)	None	[138]
Cross-Linked Starch		Spherex® (Magle Life Sciences) EmboCept® (Pharmacept)	Microsphere, hydroxyl groups can be functionalized	Yes (Minutes to hours)	None	[46]
Poly(n-Butyl-Cyanoacrylate)	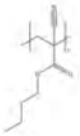	Trufill® (Cordis Neurovascular, Inc.)	Glue	No	None	[51]
Polyvinyl Alcohol-co-Polyethylene	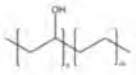	Onyx® (Covidien)	Precipitating Liquid Embolic	No	None	[16]
Poly(N-acryloyl-2-amino-2-hydroxymethylpropane-1,3 diol)-co-Poly(N-methylene-bis-acrylamide)	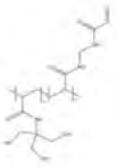	Embosphere® (Merit Medical Systems, Inc.) Embogold® (Merit Medical Systems, Inc.)	Microsphere, Matrix is impregnated with porcine gelatin, and Embogold® has 2% elemental gold incorporated into the sphere	No	None	[90]
Polyvinyl Acetate-co-Polymethylacrylate	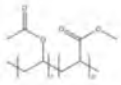	HepaSphere™ (Merit Medical Systems, Inc.) QuadraSphere® (Merit Medical Systems, Inc.)	Microsphere	No	Yes (Doxorubicin)	[99]
Polymethyl methacrylate and Poly (bis[trifluoroethoxy] phosphazene)	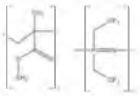	Embozene® (CelNova BioSciences, Inc.) Oncozene™ (CelNova BioSciences, Inc.)	Microsphere	No	Yes	[164] [165]
Polyvinyl Alcohol		Contour™ (Boston Scientific)	Irregular Particles	No	No	[138]
Polyvinyl Alcohol-co-Poly(2-Acrylamido-2-methylpropane sulfonate)	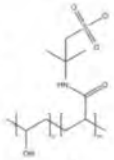	DC Bead® (BTG) LC Bead® (BTG) Bead Block® (BTG)	Microsphere	No	Yes (Doxorubicin, Irinotecan)	[95]
Polyhydroxyethyl methacrylate and Polylactide-co-Polyglycolide with bound Triiodophenol	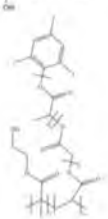	PHIL™ (MicroVention, Inc.)	Precipitating Liquid Embolic	No	No	[72] [74]

the injury had well-differentiated connective tissue covering it. Indications for use expanded and by 1967 the endovascular use of gelatin sponge in two patients was reported by Ishimori, *et al.*, where Gelfoam® was used to endovascularly treat large carotid-cavernous fistula [39]. A polyethylene tube was inserted into the carotid artery and guided to the mouth of the cavernous portion where tightly rolled Gelfoam® with gold film used as an imaging marker was injected until no blood refluxed back through the tube. The level of occlusion was verified postoperatively by radiographic techniques. Complete vessel occlusion was achieved by a combination of mechanical blockage and thrombus formation with the gelatin acting as a physical matrix to promote clot formation [40]. Gelfoam® manufactured by Pfizer is prepared from purified porcine gelatin that is processed with nitrogen resulting in a porous sponge-like material. Similar products are available globally from several other manufacturers, but the principles of preparation and application are similar. The sheet form requires preparation prior to use, including cutting the sheet into small sections followed by mixing with saline and contrast. The mixture is converted into an injectable slurry utilizing two syringes and a three-way stopcock [41]. Another approach is the torpedo method where thin sections are cut into columns and compressed into a "torpedo" that is flushed through a catheter. In addition to the sheet form, gelatin sponge is available in powder format. Gelatin sponge provides quick embolization at a low material cost. The flow reduction is temporary, with most vessels recanalizing between 3 weeks and 4 months [7,42]. Recanalization, however, is unpredictable and may not occur at all. Furthermore, reorganization of the Gelfoam® starts immediately after injection, resulting in resumption of flow. Finally, older case reports have described infection associated with use of these hemostatic sponges, implicating long exposure of the porous

material to contaminated air [43,44]. However, no recent reports within the past decade have confirmed these problems, which may be attributed to general improvements in sterile techniques.

2.2.2 Degradable starch microspheres

Degradable starch microspheres (DSM) developed in the mid 1970s by Pharmacia AB, provide for a highly transient embolic effect [45]. Composed of cross-linked hydrolyzed starch, amilomeres, material half-life is approximately 40 min per the manufacturer (EmboCept® S (PharmaCept) or Spherex® (Magle Life Sciences)) [46]. In practice, the half-life ranges between 25 to 60 min [42,47,48]. The microspheres are degraded *in vivo* by plasma α-amylase into oligosaccharides, maltose, and eventually glucose that enters the normal metabolic cycle. The maximum duration of vessel occlusion is 80 min. Both microspheres average 50 μm in diameter and are intended for temporary embolization of small vessels. DSMs have been used clinically in cTACE in treatment of HCC to provide transient occlusion to reduce blood flow in the tumor bed and increase the amount of time the chemotherapeutic emulsion remains in the cancerous tissue. This material has been used in patients who require multiple chemotherapeutic treatments via cTACE or in patients with decreased hepatic function who cannot tolerate more damage to the surrounding hepatic tissue that may be induced by ischemic necrosis. Pieper, *et al.*, evaluated the embolic properties, time to perfusion, and histologic changes in temporary embolization of healthy swine liver using EmboCept® DSMs [48]. An average of 6 mL of EmboCept® at a concentration of 6 mg/mL was used to embolize an entire hepatic lobe and angiography showed reperfusion in 32 ± 6.1 min. Gross examination of the liver tissue

did not indicate signs of hypoperfusion, and histological examination demonstrated no difference between treated and untreated hepatic parenchyma.

In one animal specimen, however, some previously embolized hepatocytes had signs of apoptosis. This study demonstrated that temporary transarterial embolization with DSMs will not damage healthy hepatic tissue. A potential application for use of these particles based on these results is injecting nontumor-supplying vessels with DSMs immediately before injecting chemoembolic material into the tumor vasculature in order to preserve nondiseased liver parenchyma [48–50].

2.2.3 Liquid embolics and glues

Liquid embolics flow through the vasculature as a fluid, which allows for deep penetration of small diameter target vessels and the ability to conform to the lumen of any vasculature before transitioning into a solid material. Unlike particle systems that have defined diameter ranges for occlusion, liquid embolics can be used to occlude vasculature of a variety of diameters.

2.2.3.1 NBCA

The glue, N-butyl cyanoacrylate (NBCA), emerged as an embolic material in the 1980s and was approved for use by the U.S. FDA in 2000 for the treatment of cerebral AVMs [51,52]. In its monomer form, NBCA is a clear liquid that polymerizes upon activation by contact with any ionic substances (*e.g.,* blood, saline, ionic contrast media, and vascular endothelium) resulting in a rigid matrix [52]. Trufill® marketed by Cordis Neurovascular, Inc., provides physicians with a glue kit consisting of NBCA, ethiodized

oil, and tantalum powder, which are combined on site just prior to use. Recommended concentrations of NBCA range from 25-67% depending on the flow characteristics and anatomy of the occlusion target. Combining NBCA with ethiodized oil slows down the rate of polymerization in static blood from less than 1 second at 67% NBCA to 6 seconds at 25% NBCA [52]. The polymerization of NBCA releases formaldehyde, leading to inflammation of the vessel wall and surrounding tissue, eventually causing a chronic granulomatous inflammation [41,52–54]. Mixtures of NBCA are typically prepared immediately prior to administration, as NBCA will begin polymerization upon exposure to air [41]. Manufacturer recommendations are for only a single injection of NBCA to be administered through a catheter, due to risk of NBCA adhering to the catheter and occluding the lumen. NBCA is commonly used for AVM embolization and off-label for hemoptysis [55], preoperative embolization for partial hepatectomy [56], and acute bleeding in the gastrointestinal tract [57]. While coagulopathies can prevent embolic coils, particles, or Gelfoam® from forming an occlusive thrombus within vessels, the adhesive nature of NBCA allows it to mechanically occupy the intravascular lumen and stop blood flow regardless of blood coagulability [40,41,58].

2.2.3.2 Onyx®

Onyx® (Medtronic plc), first described as a potential embolic agent in 1990 for the embolization of intracranial AVMs, is composed of ethylene vinyl alcohol (EVOH) copolymer dissolved in dimethyl sulfoxide (DMSO) [59]. Onyx® functions by forming a solid EVOH precipitate as the DMSO carrier solvent dissipates within the bloodstream. Unique among liquid embolics, Onyx® solidifies in an "outside-in" fashion. This results in

the almost instantaneous formation of a solid cast around the exterior of the flow, while the interior remains fluid and continues to flow deeper into the lesion. This process is reminiscent of the solidification of a lava flow. Formulations with lower concentrations of EVOH travel more distally from the catheter tip due to lower viscosity, while higher viscosity formulations offer better control in high flow environments. Nevertheless, regardless of the formulation, Onyx® completely solidifies within 5 min of injection [60]. Onyx® forms a permanent occlusion that has been shown to be stable for up to 5.25 years [61]. After being initially approved for use in AVM and intracranial aneurysms, Onyx® has been used to effectively treat peripheral arteriovenous malformations [62], acute hemorrhages in the cardiopulmonary and gastrointestinal systems [63], preoperative embolization of vascular tumors [64], bleeding from ruptured aneurysms [65], and stent graft-related endoleaks [66–68]. Care must be taken when using Onyx® to ensure that it does not contact contrast media or blood prior to exiting the catheter. As such, the use of Onyx® requires that special DMSO compatible catheters be used, and flushing of the catheters with DMSO prior to administration. While Onyx® is nonadhesive, the catheter may still become trapped if the plug formed around the tip during administration becomes too long (>2 cm).

The liquid nature of both Onyx® and NBCA provide an advantage over particulate embolics, allowing passage into smaller vessels. By forming a confluent solid mass, these embolics can completely fill a target aneurysm sac or halt flow within an actively hemorrhaging ruptured aneurysm. Onyx® can occlude vessels down to 5 μm and NBCA vessels 20 μm in diameter [69]. In further comparison of these liquid embolics, NBCA has a very short working time due to rapid polymerization upon contact with ionic fluid (*i.e.*,

blood) and can adhere to any material including vessel walls proximal to the intended target, and even the delivery system itself [70]. This can lead to permanent catheter occlusion requiring replacement of the delivery system and increasing procedure times. Onyx® has a longer working time and is not an adhesive. However, the material is suspended in DMSO that causes vascular inflammation and even angionecrosis if injected rapidly enough to reach high DMSO concentrations at the catheter tip [71]. A study led by Natarajan, *et al.*, analyzing the histopathological changes in resected AVMs after undergoing embolization using Onyx® or NBCA identified evidence of inflammatory damage induced by both materials. Of the 32 patients, Onyx® was used in 22 and NBCA in 10. Perivascular inflammation was evident in 90.9% of the Onyx® tissue samples, and 90% of the NBCA tissue samples. Some inflammation was to be expected as a response to foreign material within the vessel lumen, but chronic foreign-body giant cells were found in 54% of the Onyx® samples and 0% in the NBCA samples. Furthermore, angionecrosis was observed in 60% of the Onyx injected vessels versus 40% in the NBCA injected vessels [69]. Although the sample size was small in this study, it provides insight into complications with these materials that may be addressed by the next generation of liquid embolics in development.

2.2.3.3 PHIL™

Precipitating Hydrophobic Injectable Liquid or PHIL™ (MicroVention, Inc.) is a new injectable liquid embolic that is approved for clinical use in Europe for the embolization of lesions in the peripheral and neurovasculature, including AVMs and hypervascular tumors. Similar to Onyx®, PHIL™ is a nonadhesive embolic suspended in

DMSO, comprised of the copolymer poly(lactide-*co*-glycolide) and poly(hydroxyl ethyl methacrylate) with triiodophenol incorporated into a portion of the monomers via a covalent linkage, providing radiopacity for visualization instead of utilizing tantalum powder as is used with Onyx® [72]. PHIL™ remains suspended in DMSO until it comes into contact with blood or water, at which time the polymer precipitates into a solid and advances into the vasculature as a 'block' instead of forming layers [73]. The covalently bound iodine component is an advantage over the suspended tantalum powder used in Onyx®. Therefore, PHIL™ does not require the 20 min of mixing required for Onyx®. Three concentrations are available: 25%, 30%, and 35% (concentration of polymer by weight). Preliminary clinical data are available for PHIL™ used in treatment of cerebral AVMs and cranial and spinal dural arteriovenous fistulas [73–75]. The study by Kocer, *et al.*, compared AVMs first treated with a liquid embolic followed by resection [74]. Either PHIL™ was used alone or in combination with Onyx®. In this study, the authors noted that PHIL™ compared to Onyx® had better ease of use, faster plug formation, and less CT and MRI artifact at follow-up imaging. However, PHIL™ was more brittle during vessel dissection and less pliable during surgery in comparison to Onyx®. Histopathology showed PHIL™ caused a moderate vascular inflammatory effect and no angionecrosis on same-day resected specimens, while Onyx® had less vascular inflammation. Samaniego, *et al.*, reported on successful use of PHIL™ in treatment of ruptured plexiform AVMs. One major difference of PHIL™ from other liquid embolics was that no microcatheter occlusion occurred during injection. Furthermore, PHIL™ offered less resistance to injection allowing for deeper penetration, but increasing the risk of over penetration and extension into the venous drainage. Finally, Leyon, *et al.*, described the outcome of PHIL™ in treatment of

dural arteriovenous fistulas (DAVFs) with intent to cure. In the case of DAVFs, venous penetration of the embolic material is important; therefore increased penetration of PHIL™ when compared to Onyx® was advantageous as was the retrograde flow that was used to fill fistula feeders.

All three studies showed favorable outcome for PHIL™ as a new liquid embolic and strong competitor to Onyx®. However, the studies had a limited number of patients, fewer than 10 cases each. Larger studies are required to fully evaluate the long-term safety and efficacy of this new product as well as in comparison to the other liquid embolics previously described.

2.2.4 Calibrated microspheres

Poly(vinyl alcohol) particles were developed in the 1970s as a widely used and cost effective permanent embolic. The particles are composed of a water-soluble linear synthetic polymer and synthesized using hydrolysis of poly(vinyl acetate). It was originally marketed as Ivalon® and distributed as a sheet or block material that was subsequently shaved down to irregularly shaped particles prior to use [76]. The polymer material is formulated as foam, which is hardened with formaldehyde then packaged in a dry state. Some of the first case studies using Ivalon® as an embolic were presented by Tadavarthy *et al.,* in 1975, when they embolized the renal artery of dogs and subsequently utilized Ivalon® in patients [77]. This synthetic material proved to be superior to autologous clots in terms of *in vivo* detection and occlusive ability [78]. The PVA material is compressible, but expands back to original size after injection, therefore occluding vessels larger than the internal diameter of the catheter [76]. However, these particles are irregularly shaped with

a large size distribution, leading to clumps that can cause unpredictable behavior during embolization. These clinical disadvantages spurred development of calibrated microspheres composed of synthetic polymers in the 1990s and 2000s. Several microspheres (MSs) are approved for use as embolic agents including: trisacryl gelatin Embosphere® (Merit Medical Systems), and PVA based Contour SE™ (Boston Scientific) and PVA hydrogel Bead Block® (BTG). First, the effect of morphology on clinical outcome will be discussed.

In comparative studies between PVA particles and microspheres, geometry and surface properties proved to be important factors for embolic performance and physiologic outcome [79]. Bendszu, *et al.,* compared the efficacy of Embosphere® to nonspherical PVA in preoperative embolization of meningiomas, measuring devascularization and intraoperative blood loss, along with the inflammatory reaction, the extent of necrotic areas, and the most distal intravascular location of the embolic agent in the resected tissue. Each group had 30 patients and no significant difference existed between groups when comparing devascularization postembolization. However, the mean intraoperative blood loss was significantly higher in the PVA group compared to the MS group. The MSs induced more necrosis, and were found significantly more distally within the tumor vessels compared to the PVA particles. No difference in inflammatory reaction between the groups was observed. These studies corroborate the claims that embolic morphology directly affects performance. Histologic evaluation of the tissues showed that the PVA particles formed aggregates in larger more proximal vessels compared to the Embospheres® that formed chains in smaller vessels located more distally [80]. Similarly, in a prospective study by Chua, *et al.*, 355-500 micron PVA particles and 700-900 micron MSs were

compared in premyomectomy uterine artery embolization for reduction in intraoperative blood loss, with similar results. Under microscopy, nonspherical PVA particles appeared as aggregates of irregularly shaped material, while MSs appeared as isolated or clusters of spherical material with occasional slight deformity. The MSs were found to have penetrated more deeply into smaller caliber tumor vessels, whereas PVA particles were found predominantly in the perifibroid tissues [81].

In an animal study using sheep, the aggregation of the nonspherical PVA particles was demonstrated in embolized ewe uterine arteries. Four size ranges of both PVA particles and trisacryl gelatin MSs were tested [82]. Histological analysis of uterine tissues post-embolization revealed no difference in distribution of the PVA particles regardless of size, compared to the more precise distribution of MSs. All size ranges of PVA particles were located both proximally in aggregates and distally with a wider range of vessels. Furthermore, the mean number of PVA particles in each occluded artery was higher than that of MSs, 12.2 versus 2.2, respectively, and number of particles in occluded arteries varied more with PVA particles [82]. Aggregation may be attributed both to nonuniform shape (more surfaces and total area for particle-particle interaction) and the highly compressible nature of the PVA fostering accretion [79,83]. Although the particles were able to achieve good vessel occlusion, depth of occlusion and distribution could not be controlled, therefore increasing the risk of nontarget embolization and unpredictable level of embolization. These studies provided evidence for a morphological advantage of MSs over PVA, but since the embolic materials tested were different in physical properties, the question remained whether morphology alone could explain the inherent clinical improvements or if the material properties of the polymer itself may have contributed. To

address this, multiple clinical studies comparing PVA MSs to trisacryl gelatin MSs have been conducted. Spies, *et al.*, compared matched particle sizes of spherical PVA MS, Contour SE™, to the trisacryl gelatin Embosphere® for uterine artery embolization treating leiomyomas in 36 patients; there were no differences in the two treatment groups pretreatment and patients were followed for 3 months [84]. A significant number of patients treated with PVA spheres had an incomplete response to treatment, and complete infarction of the lesions was not achieved. Furthermore, the trisacryl gelatin MSs treated patients had superior outcomes in not only level of infarction, but also quality of life score, for short term and long term measures. Similar results were determined in subsequent, larger prospective studies [85–87]. The theory remains that the material properties, high compressibility, of PVA compared with trisacryl gelatin serves to produce early redistribution and recanalization as a result of particle deformation assuming a smaller profile after embolization [84,88], allowing more distal passage when injected, but also partial revascularization of portions of the fibroid tumor tissue [84].

Newer research has been undertaken to identify the effects of material properties on microsphere behavior [83,79,89]. Lewis, *et al.*, conducted an *in vitro* characterization study in 2006 comparing several microspheres including Embosphere®, Contour SE™ and Bead Block®. Evaluation of bead compressibility, a characteristic important for flow-directed embolics, demonstrated that the force required to compress Contour SE™ was substantially lower than both Embosphere® and Bead Block®, 5 kPa versus 27 kPa and 24 kPa respectively, illustrated in Figure 2.1 [83]. Bead passage through a catheter was evaluated using catheters coiled into a figure "8" to emulate vascular tortuosity and measuring ease of injection and level of aggregation. Using the same catheter type and

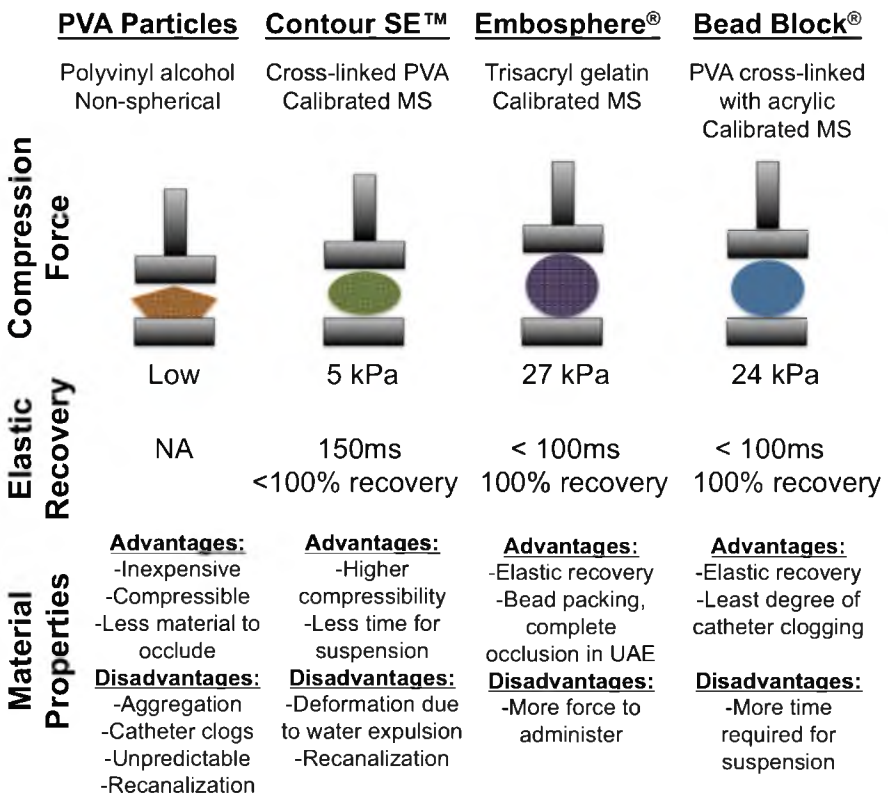

Figure. 2.1. Schematic comparing physical properties of four commercially available embolic microspheres used in bland embolization procedures [79,83,89].

matched microsphere size range, the degree of catheter occlusion was identified as Contour SE™ >> Embosphere® > Bead Block®[83]. Next, the material composition of the presented MSs will be discussed to explain these results.

The trisacryl gelatin MS, Embosphere®(Merit Medical Systems), was originally developed in the early 1990s. It is a copolymer of a N-tris-hydroxymethyl methylacrylamide monomer, a diethylaminoethylacrylamide monomer, and a N,N-methylene-bis-acrylamide monomer [90–92]. The polymerization is followed by a stage of reticulation with gelatin. These microspheres carry an effective cationic charge rendering them hydrophilic and nonaggregating. Suspended in saline and contrast prior to use, they remain uniformly spherical and smooth [93]. Six calibrated size ranges are available, the lowest range being 40-120 μm and highest 900-1200 μm. Contour SE™ (Boston Scientific) microspheres are nonionic materials composed of cross-linked poly(vinyl alcohol) (PVA) synthesized using PVA of molecular weight ≥ 75,000 g/mol, which is reacted by acetalization [94]. Unique among these embolics, PVA MSs are macroporous. The surface region is defined primarily by relatively small pores while the interior region is defined primarily by relatively large pores, and thus pore size progressively increases from the surface to the center of the particle [94]. This structure renders the periphery of the particle more rigid, while the increasing pore size to the center allows for symmetric compressibility. The macroporous structure explains the high compressibility of PVA MSs and supports the theories presented earlier explaining the further penetration and redistribution of these beads as compared to the trisacryl MSs. As for Bead Block® (BTG), these microspheres are composed of a PVA hydrogel cross-linked with acrylic polymer, synthesized following Nelfilcon chemistry that was developed by Ciba-Geigy Corporation

(now Novartis) in 1995 [95]. The PVA is modified into a macromer and co-polymerized with 2-acrylamido-2-methylpropane sulfonate salt (AMPS) in a reverse-suspension polymerization [96]. This sulfonate group imparts hydrophilicity and anionic character to the material, driving hygroscopy. The concentration of AMPS monomers affects physical characteristics of the microspheres. In terms of physical properties, Bead Block® falls in between Embosphere® and Contour SE™ for compressibility but has the lowest degree of catheter clogging. Furthermore, Bead Block® takes more time to reach suspension for injection, but remains suspended twice as long as its competitors [83]. The hygroscopic nature of the Bead Block® may explain the longer suspension time; water molecules surrounding the MS minimize aggregation tendencies. A more comprehensive retrospective study by Abramowitz compared four embolics: nonspherical Contour PVA particles, Contour SE™, Embosphere®, and Bead Block®, for uterine artery embolization using postprocedural magnetic resonance (MR) imaging in 84 patients 6 months post-operatively [97]. Pre- and postprocedural MR imaging results were analyzed for the total number of uterine fibroids present and for the percentage of individual fibroid enhancement. The Embosphere® and Contour PVA particles significantly outperformed Contour SE™ and Bead Block®; mean reduction in enhancement by 83.07% and 76.60%, respectively, compared with mean reductions of 49.78% and 52.53%. Partially infarcted fibroids often continue growing after embolization, increasing a patient's risk for future symptom recurrence [97]. These results corroborate to an extent with the Spies study, with Embospheres® providing the best clinical outcome. The clinical results of the Contour PVA particles in this study may be attributed to the difference in size range. The MSs were all 500-700 μm in diameter while the PVA particles fell into a smaller range of 300-500 μm

in diameter. Unique to the Embosphere® is a gelatin coating. However, most studies surveyed have not specifically investigated how this coating may affect occlusive ability. Since clinical studies often have small patient numbers and individual clinician's techniques differ, a definitive answer has not been identified as to the superiority of one versus other. For uterine fibroids, the Embosphere® may be more advantageous as a bland embolic. Next, MSs used to treat hypervascular tumors requiring chemotherapy will be explored.

The DC Bead® (Drug Capable) also by BTG, has a similar composition as Bead Block®, but synthesized using a higher content of AMPS, which lowers compressibility, therefore are manufactured at lower size ranges [98]. Further, the higher AMPS increases the total number of sulfonate groups, which allow these beads to be loaded with low molecular weight, positively charged drugs via ion-exchange method (Figure 2.2). Drug loading ability establishes another category of embolic agents, namely chemoembolics. Drug loadable microspheres do not have FDA approval in the United States, but are approved by regulatory agencies in many other countries throughout Europe and Asia. Along with the DC Bead®, the HepaSphere™ (Merit Medical Systems) is available for drug loading. Similar to the DC Bead®, the HepaSphere™ can load small, positively charged molecules. HepaSphere™ microspheres are synthesized by a polymerization process of vinyl acetate and methyl acrylate monomers, forming superabsorbent beads that are distributed dry. These beads swell up to 64 times their dry volume following hydration [99,100]. Both of these beads have been tested and approved for loading and release of irinotecan or doxorubicin in TACE treatments in the liver. Multiple comparative studies have been released throughout this past decade addressing the benefits of each drug eluting

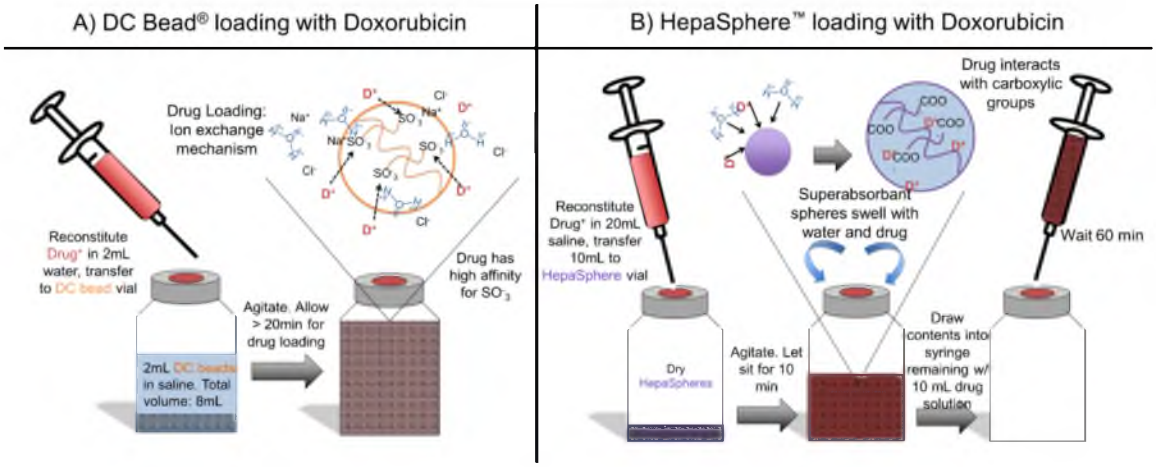

Figure 2.2. Schematics demonstrating loading mechanisms of two commonly used drug eluting microspheres.

microsphere. A 2010 study by Jordan, *et al.*, characterized *in vitro* the loadability, physical properties, and release of irinotecan (IRI) and doxorubicin hydrochloride (Dox HCl) from DC Bead® and HepaSphere™ [101]. Loading mechanisms for each bead depend on the bead material. The DC Bead® utilizes the ionized sulfonate groups on the polymer chain, exchanging a water molecule for the charged drug molecule when submerged in a drug solution. HepaSphere™ uses mechanical loading where rapid absorption of water transports the drug molecules into the matrix and charge interactions between the drug and carboxylic groups maintain the drug inside. DC Bead® requires 2 hrs for drug loading while HepaSphere™ requires 1 hr. Both drugs had similar loading profiles for each bead, however, release kinetics into 0.9% saline media under 5 mL/min flow differed as did the changes imparted to the bead mechanical properties. The total percent of doxorubicin released from the DC Bead® was 27 ± 7 and 18 ± 2 for the HepaSphere™. Time required to reach 75% of the plateau value was 2.2 hrs for both beads. A significant difference between release of doxorubicin from either bead compared to irinotecan has been shown: 102 ± 11 % from the DC Bead® and 95 ± 9% for the HepaSphere™, with $t_{75\%}$ being 1.1 hrs and 0.12 hrs, respectively. This indicates the two drugs interact with the microsphere matrices differently. Although both drugs have similar molecular weights (Dox HCl: 580 Da, IRI: 623 Da) and ionic character, the total partial charge and charge distribution are different. The higher positive charge of the primary amine carried by doxorubicin provides stronger binding kinetics with the sulfonate groups in the DC Bead® and carboxylic groups in the HepaSphere™ compared with the tertiary amine of irinotecan. Differences in release kinetics also affect drug distribution into tissue. Biondi, *et al.*, developed mathematical simulations based on the Langmuir isotherm and the Boyd and

Bhaskar models elucidating transport mechanisms governing doxorubicin and irinotecan release from the DC Bead®, which were confirmed experimentally [102]. In ionic drug loading/releasing systems, mass transport is dictated by the resistance to transport of both the drug and counterion in the liquid film surrounding the carrier. The ion exchange process is much faster than solute diffusion. Therefore drug diffusion within the bulk bead material or across the DEB surface is considered the rate controlling step for release kinetics. Their experimental studies validated the models, showing faster release of irinotecan than doxorubicin. Faster release of irinotecan is dictated by its lower affinity with the DEB, facilitating its removal from the DEB surface making particle diffusion through the bulk the rate controlling step, while the higher doxorubicin affinity for the DEB allows for film diffusion control [102]. These mathematical models may be applied to other systems like the HepaSphere™ as well as other positively charged drugs to estimate release kinetics of a chosen drug prior to clinical application. In terms of mechanical properties and morphology, understanding the effects of drug loading on the microsphere matrices is important for catheter delivery and appropriate vessel occlusion. The Jordan study investigated both change in microsphere size and mechanical properties pre- and postdrug incorporation [101]. Both microspheres prior to drug loading suspended in saline and contrast media were measured microscopically. Postdrug incorporation, either doxorubicin or irinotecan, diameters of both microspheres significantly decreased. DC Bead® diameters dropped by a factor of 0.80 and 0.67 for doxorubicin and irinotecan, respectively, while HepaSphere™ diameters dropped by 0.91 and 0.78. Both drugs are hydrophobic and they displace water to interact with the polymer backbone. In week long release studies using a saline sink, MS diameters began to return to original size. Doxorubicin was noted to have

a slower release profile, particularly in the DC Bead®. These data corroborate with the Biondi mathematical analyses. Finally, change in MS elastic properties was tested. Drug loading increased the elastic moduli. Doxorubicin loaded DC Bead® had a 2.8-fold increase in modulus, while HepaSphere™ increased by a factor of 7.1. Increase by irinotecan was not as high, 1.33 and 1.81, respectively. Increase in rigidity may pose problems clinically since fracturing of particles becomes a risk. In fact, Jordan, *et al.*, observed fractures in the doxorubicin loaded HepaSphere™. Fractured particles may lead to a change in effective size, causing unpredictable embolization patterns. Finally, the variation in drug release profiles is important to consider prior to clinical use. Incomplete drug elution as seen with doxorubicin loaded DC Bead® may lead to reduced therapeutic efficacy and too fast of elution as seen with irinotecan from either MS system may also lead to reduced efficacy over time. However, *in vitro* release studies do not sufficiently model *in vivo* release kinetics.

In vivo studies have been conducted to answer how release kinetics affect tissue concentration of the drug and how this changes efficacy in a tumor model. Namur, *et al.*, investigated doxorubicin release from DC Bead® in a porcine model, evaluating local tissue concentrations post liver embolization [103]. Two size ranges were tested, 100-300 μm and 700-900 μm, loaded with 37.5 mg doxorubicin/mL. Livers were sampled at 28 and 90 days. Infrared microspectroscopy was used to quantify drug amounts within the beads and surrounding tissue. At day 28, the drug content remaining in the beads was 22.5 mg/mL in the smaller diameter spheres and 15 mg/mL in the larger spheres, decreasing to 4 mg/mL and 7 mg/mL, respectively. Tissue changes were also evaluated at these time points. At day 28, the small doxorubicin eluting beads were associated with higher coagulative

necrosis as compared with the larger beads, whereas the larger beads were associated with a higher percentage of fibrosis. By day 90, the necrotic tissue had converted to fibrosis in both test sets. Drug concentration within the tissue corresponded to the state of the tissue. At day 28, small bead group, the doxorubicin concentration was higher in the necrotic tissue, 1.45 μM, than the fibrotic tissue, 0.55 μM. By day 90 these values increased to 2.30 μM and 0.60 μM, respectively. The same trend was observed with the larger beads, 4.80 μM within necrotic tissue, and 1.40 μM within the fibrotic tissue. By day 90, only fibrotic tissue remained surrounding the larger beads, with a mean doxorubicin concentration of 4.80 μM. Doxorubicin levels within normal hepatic parenchyma were below the limit of detection. Based on hepatocellular explant tissue, the IC_{50} of doxorubicin is 0.97 μM, and based on the results from this study, the drug levels were within antiproliferative range. However, microsphere size and location do dictate release kinetics and subsequently tissue drug levels. The larger particles occluded large vessels in proximal portal vessels with high flow adjacent to portal vein branches while the smaller particles travelled more distally into the arterial branches closer to hepatic lobules and sinusoids. A combination of these factors may lead to variable clinical outcome in a tumor model.

In a comparison study of DC Bead® to HepaSphere™ loaded with irinotecan measuring safety and efficacy in a VX2 liver metastases rabbit model, Namur, *et al.*, 2015, showed microsphere material affected drug release rates *in vivo*. This study measured plasma pharmacokinetics of irinotecan and its active metabolite SN38 followed by sacrifice of the test animals 3 days postembolization treatment for tissue assessment [104]. Both spheres at the smallest size range available were used. The median drug loaded HepaSphere™ (HS-I) diameter was 153 μm and 99 μm for the DC Bead® (DC-I). Plasma

concentrations of the drug were twice as high in the HS-I group than DC-I at all measured time points, ranging 5 min to 2 hrs. This trend agrees with the *in vitro* data from the Jordan study [101]. Histologically, both types of drug-loaded microspheres induced significant tumor necrosis as compared with untreated controls. However, HS-I treated animals showed significantly higher rates of tumor necrosis and reduction of surface tumor nodules compared with the DC-I group. This study's use of irinotecan changes the method of drug induced toxicity when compared to doxorubicin. Irinotecan must first be metabolized into its active form, SN38, by hepatic cytochrome P450. Therefore the faster rate of release may not be the only cause of higher necrosis. The HS-I were larger in diameter and less frequently found inside the VX2 tumor nodules than DC-I. This study showed not only the importance of understanding release kinetics from different microspheres, but also understanding the effect of drug loading on microsphere structure and the unique drug mechanism of action. The irinotecan loaded microspheres induced significantly greater necrosis than bland embolization, showing drug efficacy, but the HS-I microspheres were associated with higher necrosis than the DC-I due to faster drug release in normal liver parenchyma (less distal penetration), and ultimately higher conversion to SN38.

These studies comparing the different microspheres show the importance of understanding material differences and how they may affect clinical outcome. Calibrated microspheres have superseded nonspherical PVA particles for bland embolization procedures, providing for more reproducible and complete embolization results. Drug eluting beads have superseded older materials such as Gelfoam® for chemoembolic procedures by providing a combination embolic and drug carrier. Table 2.2 provides a summary of the commercially available embolics.

2.3 Research and development of advanced materials

2.3.1 Degradable/bioresorbable microspheres

Degradable gelatin sponge particles or slurry mixtures composed of porcine proteins have been used since the 1970s. This material, however, does not present the physician enough control with respect to size and therefore vessel selectivity nor rate of degradation. Vessel occlusion depends on aggregation of the particulates followed by thrombus formation. The enzymatic degradation is variable, and rates have been reported on a scale of days to up to 4 months. Furthermore, chronic inflammation is associated with the porcine origin material, along with the formation of foreign body giant cells [105]. The next development in degradable microspheres was the creation of starch MSs. The hydrolyzable starch has a short half-life, minute scale, and the particles have very small diameters, averaging 50 μm, limiting clinical applications. The advancement of degradable embolics has been slower, but several labs are currently developing improved materials [42,106,107]. Treatment of uterine fibroids, for example, requires transient embolization of the uterine artery, particularly in patients who want to remain fertile. Permanent or unpredictably degrading materials lead to chronic inflammation that may lead to consequences for fertility and pregnancy [27,28]. In this application, a resorbable microsphere providing at least 6 hrs of complete occlusion may be well suited [35,36]. In treatment of hepatocellular carcinoma, >90% of patients require retreatment as new vessels sprout to feed the residual tumor. But, current microspheres are permanent and may induce ischemia, resulting in worsening of hepatic function to the point where further embolic treatments may not be tolerated without inducing complete liver failure [108]. Degradable microspheres that occlude and deliver chemotherapeutics over a period of a

few weeks up to 1 month may overcome this problem. Laurent and Moine, *et al.*, have synthesized poly(ethylene glycol) methacrylate (PEGMA) hydrolyzable microspheres for predictable transient embolization that require several hours as compared to minutes to degrade [42,109]. These microspheres were prepared using a suspension polymerization process of poly(lactide-*co*-glycolide)-poly(ethylene glycol) crosslinker and PEGMA monomer. Co-monomers methacrylic acid (MA) and 2-methylene-1,3-dioxepane (MDO) were incorporated to fine tune properties. Minimizing an inflammatory reaction to degradation products was an important factor in design strategy. Materials were chosen that degrade into water-soluble macromolecules post hydrolysis facilitating renal excretion. Microspheres were prepared at sizes ranging from 100 to 1000 μm, similar to commercially available MSs. A series of tests were conducted by Louguet, *et al.*, characterizing these degradable MSs, determining effects of different mole percents (mol %) of MA, and comparing their properties to either Embosphere® or DC Bead®. Evaluations included measuring swelling, injectability, *in vitro* degradation rates, biocompatibility, and doxorubicin loading. Swelling behavior of these MSs was compared to the Embosphere®. Level of swelling was affected by the mol % of MA incorporated into the backbone, conferred by the ionization of this unit. The microspheres were tested for injectability through a microcatheter, evaluating aggregation behavior, compressibility, and elastic recovery. No resistance was detected during injection, suggesting absence of aggregation and sufficient compressibility. Postinjection, the microspheres recovered their original spherical shape. *In vitro* studies resulted in complete degradation within 2 days, and degradation rate correlated to the level of MA in the polymer backbone. Degradation products were tested in contact cytotoxicity studies using L929 cells. No

disruption of cell membranes or change in cell proliferation was observed, indicating good biocompatibility. Next, these microspheres were loaded with doxorubicin and compared to the DC Bead®. Anionic groups along the polymer backbone, carboxylic moieties, provided for electrostatic loading of the drug. Loading efficiency of doxorubicin was >90% in 1 hr, similar to DC Beads®. Finally, *in vivo* degradation and local biocompatibility were examined after implantation into subcutaneous rabbit tissue. Animals were sacrificed at two time points: 2 days and 7 days and 594 different skin sections were examined. By day 2, degradable MSs were detected in 25% of the sections; however, by day 7 there was complete degradation. These degradable microspheres had similar physical characteristics to the marketed Embosphere® and DC Bead®, but with the added advantage of complete degradation within a week of using a hydrolyzable cross-linker. Based on these results, the microspheres' transient uterine artery occlusion was tested in a sheep model and performance was compared to Embosphere®. Six sheep underwent bilateral UAE with either the degradable microspheres or the Embosphere® in the 500-700 μm size range until stasis was reached. Animals underwent angiography at day 7 and then were sacrificed for histological evaluation. All animals embolized with the degradable MSs had normal arterial blood flow in both uterine arteries at day 7, while 50% of the Embosphere® had normal flow and the remaining had reduced flow. Histological analysis revealed the absence of degradable MSs and inflammatory markers, whereas the Embospheres® were found in organized thrombi. In the Embosphere® group, recanalization was characterized by new endothelium, but surrounded by layers of macrophages, neutrophils, and at times foreign body giant cells. Finally, a similar level of degree of uterine necrosis was detected for both groups suggesting the duration of occlusion by the degradable MSs was sufficient

to achieve clinically significant ischemia. Although this was a small study and more comprehensive *in vivo* work remains to be completed, these results are promising, signifying the advantage of a degradable MS for UAE.

The unique properties of natural polymers, like polysaccharides, have been investigated with a recent focus on chitosan derivatives to develop degradable microspheres [10,110,111]. Chitosan is a linear polymer composed of α-1,4-linked 2-amino-2-deoxy-α-D-glucose (N-acetyl-glucosamine), which is derivatized from chitin via deacetylation [10]. Different functionalization methods of chitosan provide for change in water solubility and degradation rates. Weng, *et al.*, recently developed a set of drug capable biodegradable microspheres. Carboxymethyl was introduced into the chitosan chain for water solubility and the resulting structure was cross-linked with oxidized carboxymethyl cellulose (OCMC) with different degrees of oxidation to synthesize microspheres via an inverse emulsion method. The degradation of these microspheres is contingent upon enzymatic action of the glycosidic bonds between the monomer units by enzymes like lysozyme along with hydrolytic cleavage of the cross-linking bonds. The oxidation degree of OCMC defined as the percentage of CMC units oxidized directly affects degradation rates. Three degrees were investigated: OC-I, 9% oxidation degree; OC-II, 17% oxidation degree; and OC-III, 35% oxidation degree. The resulting microspheres ranged in size from 100 to 1000 μm with mean diameters 485 μm, 620 μm, and 689 μm, respectively. The morphology of these MSs after reconstitution from a lyophilized form postproduction revealed round particles with a wrinkled surface. The interior of a fractured MS revealed a highly porous, but nonuniform, internal structure. All three groups were tested *in vitro* measuring degradation rates. At 7 days, the weight

percentages were 44.2, 78.3, and 85.7, respectively. OC-I MSs degraded completely within 15 days while OC-III remained at 55 weight percent after 4 weeks. Swelling experiments determined a higher degree of oxidation correlated with a higher level of cross-linking and a more rigid internal network, therefore lower swelling ratio. Next, these microspheres were loaded with doxorubicin. The polymer network of these MSs include carboxylic moieties, providing an ion exchange mechanism for drug loading similar to the DC Bead®. Release studies were conducted over a period of 24 hrs. Doxorubicin showed linear release from all MS up to 8 hrs, after which release plateaued. Higher release was associated with a lower degree of oxidation: OC-I>OC-II>OC-III. Again, the level of cross-linking affects the release kinetics, offering a level of design control. Finally, the OC-II microspheres were tested *in vivo* in a rabbit renal embolization model to assess embolization and degradation characteristics. During injection, the MSs did not clog the microcatheter and embolization was successful. Three groups of rabbits were followed and sacrificed at days 7, 14, and 73. The embolized and nonembolized kidneys were compared for all gross and histological analyses. At day 7 the embolized kidney grossly matched the nonembolized kidney in size. However, it had demarcated infarction spots as expected. By day 73, the embolized kidney decreased in size by 1/3, a phenomenon seen with permanent embolic MSs. Histologically, the week time point revealed partially degraded microspheres within branches of the renal arteries, designated by "moth-eaten" edges and by day 73, the vessels were patent. Inflammatory cell infiltration was observed at all time points, and sometimes microspheres were found encapsulated within a thrombus but at different stages of degradation and phagocytosis. A more comprehensive animal study was later conducted and rabbits were sacrificed at additional points to sufficiently profile *in vivo* degradation and resultant

inflammatory response [106]. Resorbable MSs, size range 300-500 μm, of oxidation degree 25% were used in these studies (in between OC-II and OC-III). The most significant pathological findings included mild foreign body response at all time points from day 0 to day 30, but increasing neointimal hyperplasia and fibrosis from day 7 to day 30. In a third study, these MSs (group II) and a set with lower oxidation degree, 10% (group I), were compared with Embosphere®, again using a rabbit kidney model. Histological results showed the distribution of group I to be similar to Embosphere® throughout the renal arteries indicating similar physical characteristics including compressibility and deformation. Group II did occlude more proximally (larger vessel diameters) than group I, confirming the physical differences due to higher cross-linking and resultant MS rigidity.

The two degradable microsphere systems reviewed have unique advantages. The PEGMA MSs provide for a more transient embolic that may clinically prove advantageous for uterine artery embolization for the treatment of leiomyomas. These MSs histologically did not demonstrate the same level of inflammatory response and fibrosis as the chitosan based MSs, which is an important characteristic for a true transient embolic to a highly sensitive organ like the uterus. The longer degradation time of the chitosan MSs would prove advantageous in TAE/TACE procedures where retreatment is required after several weeks. Both MSs were loaded with the same chemotherapeutic, doxorubicin, which is currently a widely used drug for the aforementioned treatment of hepatocellular carcinoma. The PEGMA MSs, however, have recently been loaded and tested with two other drugs, sunitinib, an antiangiogenic multikinase tyrosine inhibitor, and bevacizumab, a monoclonal antibody specific to VEGF-A. This provides a unique and very promising advantage over both the chitosan MS and all commercially available MSs [112]. One of the modes of

failure in HCC treatment is initiation of angiogenesis after inducing ischemia. Angiogenesis drives regrowth of vessels to residual tumor nests and ultimately relapse. A degradable MS capable of co-delivering a chemotherapeutic along with an antiangiogenic may address this fundamental issue. Both systems require further testing and analysis in tumor animal models as well as comparison testing to current medical practice to validate their advantages. A weakness in both systems is the release rates. Neither system showed linear release kinetics over an extended period of time. Further modifications of the polymer matrices may improve these rates.

2.3.2 "Imageable" microspheres

As previously described, conventional TACE involves a sequential process of injecting an oily emulsion with a chemotherapeutic drug followed by an occluding material. Typically, the emulsifying agent is an iodinated oil such as Lipiodol® or Ethiodol®. The high iodine content renders the fluid radiopaque. Initially, it was assumed that the opaque oil was an indicative marker for the distribution of the delivered drug. To the contrary, studies have shown ethiodized oil content is a poor marker of local drug concentrations. Gaba, *et al.*, conducted a study in a VX2 liver cancer model in rabbits testing this hypothesis [113]. Rabbits in this study underwent tumor implantation and were subsequently treated via cTACE with doxorubicin during which a series of computed tomography (CT) images were obtained for calculation of iodine content. Posttreatment, with angiographic proof of stasis, the animals were sacrificed and tissue harvested for detection of doxorubicin concentration within the tumor at various locations using liquid chromatography/tandem mass spectrometry (LC-MS/MS). These results found no

significant correlation between calculated iodine content and measured chemotherapy level in the treated tumors, indicating the degree of intratumoral oil deposition is a poor predictor of local drug delivery post-TACE. Design of a drug capable embolic material with an incorporated imageable agent would provide more accurate spatial localization of the embolic and the drug. This combination material would serve both as a research tool to help better understand embolization biology and also provide real-time feedback to the clinician regarding location and level of occlusion [114]. Sharma, *et al.*, began addressing some of these points by loading poly(vinyl alcohol) hydrogel microspheres with Lipiodol® [115]. The LC Bead® (same chemical composition as the DC Bead®) was modified by first lyophilizing the MSs in the presence of an excipient, mannitol, and then mixed with 1 mL of Lipiodol®. These microspheres were analyzed for iodine content and then tested in a saline solution to measure Lipiodol® release and stability. The MSs achieved up to 35.7% iodine by weight versus 38.2% iodine content of pure Lipiodol®. During stability testing over a 27-hr period, the cumulative Lipiodol® release remained below 20% and the radiopacity of these MSs was validated with routine fluoroscopy and CT. Next, visualization of these MSs was characterized *in vivo* in normal swine liver. The MSs were not visible during injection; however, as the MSs began to accumulate within the hepatic artery branches they were visualized via fluoroscopy or CT. Approximately 0.4 mL of radiopaque MSs was required for fluoroscopic visualization while only 0.2 mL was needed for CT. More sensitive CT imaging provided visualization of how single microspheres packed within the vasculature, providing further insight into the mechanics of how the microspheres occlude. In a second study by the same group, the microspheres were loaded with Lipiodol® followed by loading with doxorubicin [114]. A swine model was used, and

either the liver or a kidney underwent chemoembolization. Three-dimensional tissue penetration of the radiopaque microspheres was evaluated *ex vivo* with microCT, and drug permeation and tissue coverage was evaluated with fluorescence microscopy. Two size ranges were tested, 70-150 μm and 100-300 μm. The MSs were visualized forming long columns within the vessels, with the smaller MSs penetrating further into the tissue as expected. Deeper tissue penetration correlated with two-fold greater drug delivery. The highest drug concentration was located immediately surrounding the bead within the first 4 hrs post embolization and declined over hundreds of microns from the bead surface. This study showed that the ability to correlate radiopaque MS location and drug distribution might serve as a useful clinical tool. However, sensitive microCT was required to appropriately visualize these MSs *in vivo*, which is not feasible to use for human patients.

Investigating a different approach to develop a magnetic resonance imaging (MRI) visible, drug capable microsphere using iron-oxide nanoparticles has been evaluated by the Larson group. Poly(lactide-*co*-glycolide) served as the polymer platform for the microspheres co-encapsulated with a ferrofluid of iron-oxide nanoparticles and loaded with the tyrosine kinase inhibitor sorafenib, an FDA approved drug for treatment of hepatocellular carcinoma [116]. These MSs were synthesized using a double emulsion/solvent evaporation method, with both drug and ferrofluid directly incorporated. Characterization of these new embolics described spherical particles with a smooth surface and average diameter of 0.98 μm, a much lower size scale than commercial MSs. The percent of sorafenib by weight was 18.6% and for ferrofluid, 0.54%. These particles were successfully detected via MRI. *In vitro* cytotoxicity studies using a rat HCC cell line demonstrated significant reductions in cell proliferation with increasing doses of the

sorafenib-eluting beads. Based on these results, preliminary animal studies were conducted to assess *in vivo* visibility and therapeutic effectiveness in a rat HCC model. Rats implanted with orthotopic tumors were treated via chemoembolization once the tumors measured 2.5-8.1 mm in diameter visualized using MRI. T_2-weighted images acquired immediately postembolization displayed microspheres deposited within the tumors. Microsphere location was later histologically confirmed using a Prussian blue stain specific to iron and compared with the MRI localization. Animals were sacrificed 3 days postembolization and response to the drug was also assessed by measuring changes in microvessel density, an angiogenic response induced by ischemia. Results indicated no significant difference between the sorafenib treated group and the control group. Although clinical response was not significant, the microspheres accomplished the goal of *in vivo* tracking. The small size of the MSs may have been a contributing factor, carrying less drug than would a 300-500 μm MS.

Another set of MRI visible drug eluting MSs using alginate, an anionic polysaccharide has been developed[117]. Alginate is composed of two uronic acid monomers: (1-4)-linked β-L-guluronic and α-D-mannuronic acids, and the monomers are linked via glycosidic bonds. A cross-linked system is formed with the addition of divalent cations like calcium, leading to a rapid gelation process that allows encapsulation of a drug or imaging moiety [118]. The drug incorporated was amonafide, an investigational cancer drug that is part of the families of topoisomerase inhibitors and DNA intercalators. Magnetic drug clusters were first synthesized, approximately 42 nm in size, using a high temperature hydrolysis reaction. Subsequently, the combination alginate MSs were fabricated using a microfluidic gelation process. Microfluidic chips with channel

dimensions of 130 μm in depth and width were used in a two-step droplet gelation process. The collected MSs were microscopically characterized measuring dimensions and observing morphology. Average diameter was 34 μm with a variation of 8%. The magnetic drug clusters were visualized via confocal microscopy and fluorescent images showed homogenous distribution of clusters throughout the alginate matrix. *In vitro* release studies showed a more linear drug release, with only 47% cumulative release at 24 hrs. These microspheres were used for *in vivo* studies using the rat HCC model to test visibility levels. Immediately postembolization, the animals were moved to the MRI scanner and T_2 weighted images were taken. Microsphere deposition was observed as punctate reductions to the signal intensity. Increasing concentration of total magnetic clusters within the microspheres or increasing the overall size of the microsphere in future directions may increase MR signal intensity and improve visibility. Following a similar path and using the same microfluidics system, the Shen group has developed alginate microspheres with radiopaque barium sulfate nanoparticles for CT imaging [119]. Their microspheres were larger in diameter, but polydisperse, ranging from 149-380 μm. Different weight percentages of barium sulfate content were tested. A minimum of 5% by weight was required for CT visibility and 10% for fluoroscopy. The highest content achieved was 9%. However, these MSs easily ruptured and led to irregularly shaped particles.

Based on the current literature, imageable microspheres require further development before they are ready for use in clinical applications. Their mechanical properties must be verified and compared with approved products. The size ranges capable of being fabricated remain too small to prevent nontarget embolization and associated adverse effects currently seen with the smallest commercially available microspheres, <50

μm [120]. Finally, long term biocompatibility tests and efficacy studies are required to provide insight into their long-term stability and ability to treat intended tumors like liver HCC.

2.3.3 *In situ* gelling liquids

Liquid embolic agents under investigation are primarily targeted towards the treatment of aneurysms, AVMs, and HCC. The administration of currently available liquid embolic polymers, NBCA, Onyx®, and PHIL™ are associated with the introduction of toxic compounds [53,54,69]. Hence, many groups are investigating new *in situ* gelling polymer systems that avoid the use of toxic byproducts or solvents. There are several mechanisms to induce *in situ* gelling, including polymerization, physical gelation, and ionic cross-linking, which are outlined in Figure 2.3. Key parameters for the development of a liquid embolic system are injection viscosity, *in situ* setting time, toxicity, swelling behavior, biocompatibility, biodegradability, mechanical properties, and viscidity.

Liquid embolic polymer systems have been developed using poly(propylene glycol) diacrylate (PPODA) and pentaerythritol tetrakis (3-mercaptopropionate) (QT) [121], as well as poly(N-isopropylacrylamide-*co*-acrylic acid) (NIPAAM) [122]. Both groups of polymers are nondegradable, nonadhesive, and have been considered for use in treating both intracranial aneurysms and AVMs [123,124]. By achieving a higher fill volume in aneurysms, the use of these polymers may prevent recanalization that is observed when using coil embolization. In addition, these material platforms do not

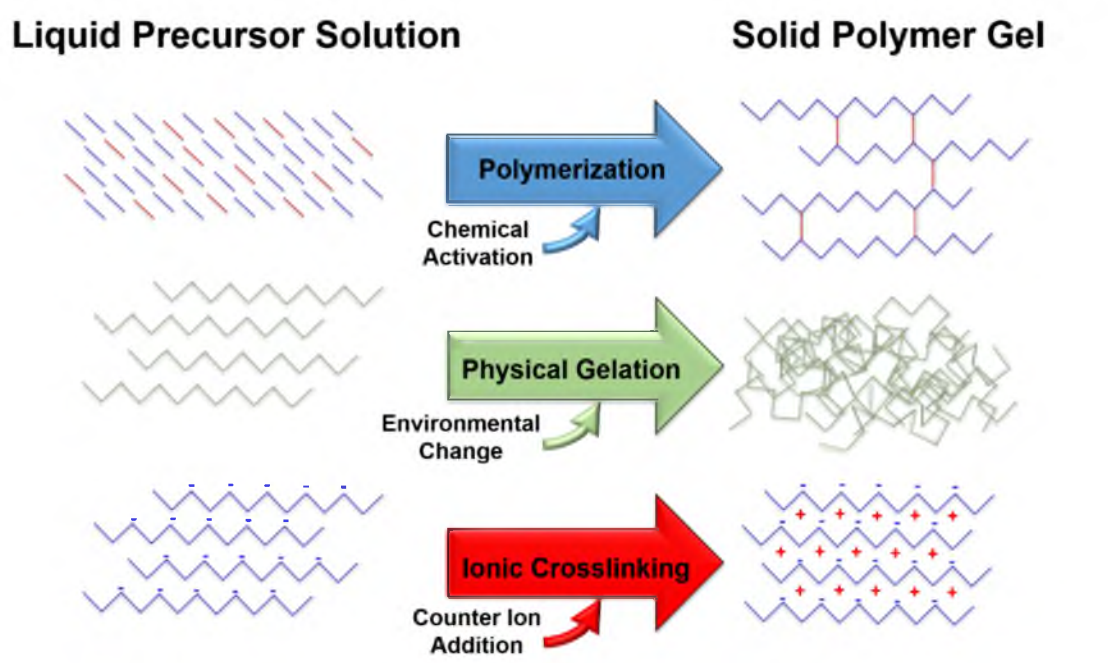

Figure 2.3. Mechanisms of *in situ* gelation for liquid embolics. There are three processes by which liquid embolics transition for a liquid solution to a solid matrix, namely: polymerization, physical gelation, and ionic crosslinking. Polymerization occurs as an activating agent (*e.g.* free radical, anion, enzyme, photon, etc.) induces monomer or pre-polymer units bind to each other forming progressively larger molecules as part of a chain reaction. The resulting matrix is a network of large molecules that are chemically bound (*e.g.* NBCA, PPODA/QT, Fibrin Glue, etc.). Physical gelation occurs as the environment around a preformed polymer changes (*e.g.* temperature, solvent state, etc.) causing the polymer or portions of the polymer to change from a soluble to insoluble state. The polymer thus forms a solid spongy mass composed of entangled polymers that are bound together by intermolecular forces (*e.g.* Onyx® and SELP). Ionic crosslinking occurs with charged polymers as the introduction of multivalent counterions creates bridges between polymer strands via electrostatic interactions (*e.g.* Alginate).

produce toxic byproducts like NBCA or use hazardous organic solvents like DMSO. Both PPODA and QT monomers are liquid at room temperature, but when combined in aqueous environments with nucleophilic activators they chemically react via Michael-type addition to form a hydrogel matrix [123,125]. Proof of concept was confirmed *in vivo* using a canine model with surgically induced aneurysms in the lateral wall of the carotid artery [126]. PPODA and QT were combined in a 2:1 molar ratio to create a hydrophobic monomer solution. Prior to administration, the monomer solution was mixed at a 3:1 ratio with Conray (iothalamate meglumine, Mallinckrodt, Inc.), a high osmolarity ionic contrast dye, at a pH of 11.0 for 2 minutes [125,127]. The addition of the high pH contrast initiated the polymerization, while providing a mechanism for monitoring the administration of the embolic. PPODA-QT had a gel time of 10 min, although this can be reduced via manipulation of PPODA/QT ratio, adjusting the pH, and increasing the mixing time of the monomer and initiating solutions [123,127]. A drawback of this system is the toxicity of the activating solution. Conray, particularly at high pH, is cytotoxic; however, co-administration with a polymer matrix partially ameliorates the toxicity [127]. This study showed that administration of the polymers was feasible for use in aneurysms, but the low number of samples and lack of controls prevented any comparison of efficacy to other polymeric embolic systems. NIPAAM polymers show a low critical solution temperature (LCST) of 32°C in aqueous environments, below which they are soluble and above which they precipitate out of solution [128]. This allows the polymer to be delivered in a liquid form and then be entropically driven out of solution to form a solid hydrogel after injection. NIPAAM based polymers have been functionalized to create degradable [129] and radiopaque embolic versions [130]. A key innovation was the copolymerization of

NIPAAM with other polymers to create a liquid-solid transitioning platform where physical and chemical gelling occur simultaneously under physiological conditions [131,132]. The dual gelling systems combined polymers of NIPAAM-co-cysteamine (NC), which contained a thiol, and either NIPAAM-co-hydroxyethymethacrylate-acrylate (NCHA) or NIPAAM-co-cysteamine-vinylsulfone (NCVS), both of which contain vinyl groups. Mixtures of NC-NCHA or NC-NCVS contain thiol and vinyl groups that undergo Michael-type addition at pH 7.4 to chemically cross link the polymers at body temperature [133]. In an *in vitro* model, the dual gelling system displayed adhesive properties and became loosely affixed to the catheter, which is not ideal for clinical usage due to the potential for entrapment of the delivery system [132]. Live/dead staining and cell proliferation studies with T3T mouse fibroblasts showed that both systems have a high degree of biocompatibility [132,134]. As a proof of concept study, a swine model with a surgically induced aneurysm was successfully treated with the NC-NCHA system. This study validated the ability for the system to be delivered via catheter and solidify within an aneurysm under physiological conditions [132]. However, recanalization of the aneurysm was observed shortly after the procedure. Alginate, derived from polysaccharides extracted from brown seaweed (phaeophycae), is comprised of a copolymer of β-D-Mannuronic acid and α-L-guluronic acid. The absence of toxic monomers, initiators, byproducts, or solvents in alginate's gelation process makes it of interest as a liquid embolic agent [135–137]. Hydrophilic alginate polymers are negatively charged when dissolved in aqueous solutions, but immediately begin forming a nonadhesive hydrogel upon contact with divalent cations, such as calcium [136]. If alginate is combined with calcium prior to injection, it is injectable, but may solidify or form an "alginate coil" within the catheter.

To preclude catheter blockage, specialty double-lumen catheters are used to administer the alginate and calcium solutions separately and have them combine *in situ* [135,138,139]. Alginate gels have been extensively explored for the controlled release of bioactive compounds [140–142], but only bland embolization has been attempted with alginate as a liquid embolic. A solution of alginate lyase and ethylenediaminetetraacetic acid (EDTA) has been communicated by Barnett and Gailloud for being able to selectively remove alginate emboli form occluded vessels *in vivo* [143]. EDTA chelation of calcium ions and enzymatic hydrolysis of the polymer backbone by alginate lyase causes the hydrogel matrix to be rapidly broken down into soluble nontoxic components. The ability to occlude and then selectively reopen vessels is a novel therapeutic treatment modality not available with current commercially available embolic agents.

Algel (Neural Intervention Technologies), an investigational alginate based embolic, was shown to be effective in embolizing aneurysms and AVMs in swine models [144,145]. A high degree of filling ($\geq$ 93%) was achievable using Algel by injecting it into the aneurysm sac while the neck was blocked with a temporary balloon. Follow up angiograms of the study animals (n=8) showed that the parent vessel remained patent while the aneurysm remained occluded after 90 days. Control animals (n=2) whose aneurysms were partially filled survived only 6-8 days [144]. A swine model of AVM was used to demonstrate stability of Algel *in vivo*. Occlusion was stable in all animals at 1 month (n=3) and in 5 of the animals in the 6-month group (n=6) [144]. Histological analysis of tissue samples from both the aneurysm and AVM models showed no significant histological response at either endpoint. Gore and Associates acquired Neural Intervention Technologies and launched a phase 1 clinical trial with the Gore Embolic Liquid (GEL),

previously known as Algel, for the presurgical embolization of AVM in 2006. However, the results of this trial have yet to be reported [137]. Safety concerns with alginate gels include efflux of material from the aneurysm cavity during administration, inadvertent embolization of nontarget vessels, and fracturing of the alginate mass after the reintroduction of flow [146].

Fibrin glue is widely used as a hemostatic in surgery, but has also been explored as an embolic agent. Formed from the catalytic action of thrombin on fibrinogen, fibrin is a protein polymer responsible for the structural formation of hemostatic clots in response to tissue damage [147,148]. Fibrin glue harnesses this natural pathway in order to create a sealant that can be applied selectively during surgery or other procedures to stop bleeding. For use as an embolic, a double barrel syringe is loaded with fibrinogen and aprotinin, an antifibrinolytic agent, in one half, and thrombin, calcium chloride, and visualizing agent in the other. The contents are then mixed in the tip of the syringe as they are injected. The polymerization begins immediately and the solution must be injected rapidly and continuously or the catheter will occlude. Time to occlusion ranges from 55 seconds in a 110 cm 3F catheter to 3 min 10 seconds in a 27cm 5F catheter [149]. Critical to the use of fibrin glue is the injection rate. If injected too slowly the catheter will occlude, and if injected too rapidly the glue will fail to solidify within the target vessel and may pass distally into the lungs, liver, spleen, or heart [149]. The length of the catheter, the rate of injection, and concentration of fibrinogen, thrombin, and Ca^{2+} determine the viscosity of the fibrin glue as it leaves the catheter [150]. Fibrin glue has only been used clinically as an embolic agent in a study for the preoperative embolization of intracranial meningiomas [151]. The final concentration of components in the fibrin embolic system used in this

study was 33.25 mg/ml fibrin (Tissucol Duo S), 3.333 KIU/ml Aprotinin (Trasylol, Beyer), ipromide 139 mg I/ml (Ultravist, Schering), 0.55 mg/ml $CaCl_2$, and 62.5 IU/ml of thrombin. The embolization was successful in all 80 of the study patients. However, every patient developed a headache during the procedure and two patients (2.5%) experienced neurological defects including paresis and hypoethesia from the embolization. The effects of the embolization were mixed. While necrosis was observed within 24 hours of embolization, this was only beneficial if it was within the central mass of the meningioma. In cases where necrosis was observed on the tumor's periphery, the division between the meningioma and surrounding brain tissue became indistinct, increasing risk for compromising healthy perilesional tissue [151]. Unlike other embolics, fibrin glue is derived from human blood and carries a risk of an allergic reaction and transmission of blood borne pathogens [152,153].

Cellulose derivatives have been explored previously as liquid embolics and in the creation of embolic microspheres in part due to their high degree of biocompatibility and biodegradability [154–157]. Whereas previous cellulose based liquid embolics involved the precipitation of cellulose acetate from DMSO similar to Onyx®, the Golzarian group combined oxidized carboxymethyl cellulose (OCMC) and carboxymethyl chitosan (CCN) to form a chemically crosslinking injectable hydrogel [111,158]. Cross-linking occurs via Schiff base formation as an amine on the OCMC acts as a nucleophile and attacks a carbonyl carbon in one of the aldehyde groups on CCN [158]. Gelation at 37 °C in DI water and PBS occurred in 1.53 and 1.30 min, respectively. However, when gelation was evaluated in citrated human plasma, the rate of gelation slowed to 4.28 min, likely due to interactions between the polymer and proteins in the blood. Incorporation of iodine contrast

reagent at 20% by volume bestows radiopacity and only mildly impeded gel formation. A colorimetric live-dead assay showed no significant difference between controls and cells incubated with primary human umbilical vein endothelial cells indicating a lack of cytotoxicity. The polymer gel degraded *in vitro* in the presence of lysozyme due to the enzymatic degradation of chitosan and the hydrolysis of the Schiff base. Only 22.1% of the polymer remained after 21 days in a 10 μg/ml lysozyme solution, indicating that this system is not appropriate if permanent occlusion is desired. Evaluation of the release of doxorubicin and tetracycline from the matrix exhibited peak releases of 31.3% after 50 hours and 65.8% after 24 hours, respectively. *In vivo* comparison of the embolic OCMC/CCN demonstrated deeper penetration into the vasculature of rabbit kidneys than did bioresorbable microspheres (100-300 μm) [111]. This novel embolic shows promise as potential agent for TACE procedures, but may not be appropriate for situations where long-term embolization is desired. These investigational liquid embolics are summarized in Table 2.3.

2.4 Conclusions

In the past 50 years, polymers have been designed, modified, and improved into a variety of embolic agents to address new clinical needs, especially in treatment of vascular malformations and hypervascular tumors such as benign uterine fibroids or malignant hepatocellular carcinomas. The move from irregularly shaped particulate embolics to precisely calibrated microspheres has resulted in improved clinical outcomes by changing the morphology and surface properties of the embolic material. Precise calibration permits reproducible and controllable embolization, while more precise microsphere size ranges

Table 2.3. Investigational liquid embolic materials

Material	Liquid Structure	Gel Structure	Gelation Mechanism	Ref.
Poly(propylene glycol) Diacrylate and pentaerythritol tetrakis (3-mercaptopropionate)	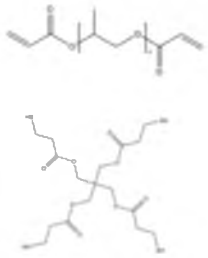	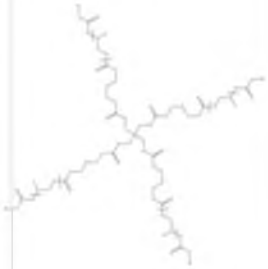	Polymerization	[121]
poly(N-isopropyl acrylamide)-co-cysteamine and poly(N-isopropyl acrylamide)-co-hydroxyethymethacrylate-acrylate	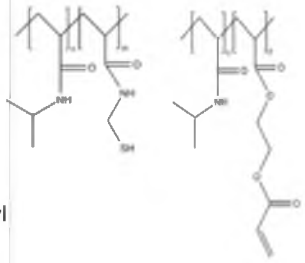	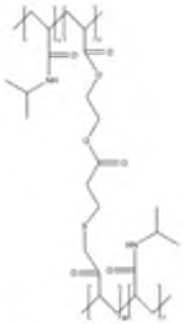	Polymerization and Physical Crosslinking	[122]
Alginate	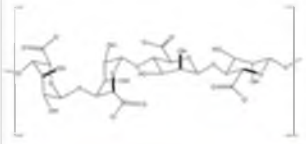	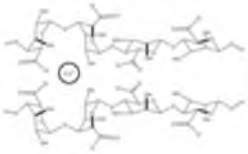	Ionic Crosslinking	[136]
Fibrin Glue	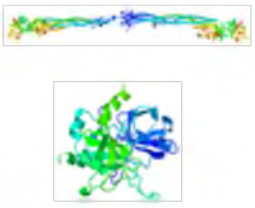	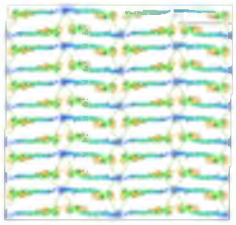	Polymerization	[147] [148]
Oxidized carboxymethyl cellulose and carboxymethyl Chitosan	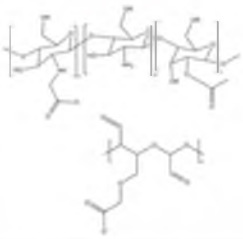	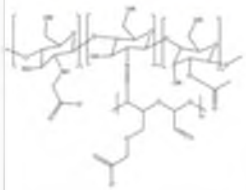	Polymerization	[158]

result in more consistent and predictable levels of obstruction. Following development of microspheres of different polymer compositions, drug delivery became a clinical possibility. A number of calibrated microspheres are now commercially available and beyond those discussed in this Chapter [159,160], *i.e.*, trisacryl gelatin Embosphere® (Merit Medical Systems), and PVA based Contour SE™ (Boston Scientific) and Bead Block® (BTG). In treatment of uterine fibroids, the Embosphere® has increasing clinical evidence for superiority. Its material properties render it more stiff than competitors thus requiring more injection force, but these microspheres deform within the vessels and conform to vessel shape serving as a better embolic to induce complete infarction. Unlike a benign tumor, hepatocellular carcinoma of the liver requires localized injection of a chemotherapeutic. The original method of intraarterial drug infusion, liquid drug infusion followed by particulate embolization, is being replaced by more effective drug eluting microspheres like the DC Bead® or HepaSphere™ in TACE procedures. The archetypical degradable materials like gelatin sponge allow transient vessel occlusion, but similar to permanent particulate PVA, the irregularity in shape and unpredictable degradation rates are less than optimal. Furthermore, conventional TACE does not allow for controlled release of the chemotherapeutic into surrounding tissue. Clinically, the two drug eluting beads discussed have similar clinical outcomes with doxorubicin. However, the differences in their polymer structures affect release kinetics of different drugs as a result of changes to microsphere structure post drug loading. Irinotecan, for example, induced more necrosis in animal models of HCC when delivered via HepaSphere™. Therefore, as new drugs are developed, they must be tested in comparative studies to determine which drug delivery system will be appropriate. In the development arena, degradable/bioresorbable

microspheres are being designed to overcome the disadvantages of gelatin particles by utilizing polymers with consistent degradation rates while maintaining the advantages of calibrated drug eluting microspheres. These technologies are the most evolved and may be commercialized within the next decade. Polymers have been identified based on biocompatibility of degradation products as well as mechanical properties of the primary polymer backbone. Fitting these criteria include poly(ethylene glycol) methacrylate and chitosan derivatives, both of which have been fabricated into degradable microspheres that can be loaded with drugs. Applications for these materials are broader than permanent microspheres since degradation time can be controlled based on polymer backbone additives. With regard to surgical procedures, real-time feedback is a fundamental tool, especially to the practice of interventional radiology. However, injection of contrast does not satisfactorily correlate to the location of the embolic within the vasculature. Though still in the infancy of research and development, imageable microspheres have the potential to provide not only real-time feedback to the clinician by indicating location and distribution of embolic material, but also to show the anticipated drug distribution within cancerous tissues. Finally, liquid embolic materials that solidify *in situ* are increasingly being explored. They are attractive for their ability to deeply penetrate vasculature and completely fill vascular lumen. Fueling future development is the desire for improved efficacy and reduced toxicity. Whereas the first generation of liquid embolics, Onyx® and Trufill®, have toxic byproducts, most of the next generation materials exhibit little to no cytotoxicity. Another area of interest is *in situ* gelling liquids that can be selectively re-solubilized or which degrade passively over time to produce transient occlusive effects. Liquid embolics able to produce predictable transient embolization have the potential to

expand into many novel applications including presurgical embolization in surgical procedures where blood loss is of concern or reduced circulation would be beneficial. Nonetheless, the current investigational liquid embolics presented do not concurrently address the multiple elements for an improved alternative to Onyx® or DEBs. An ideal liquid embolic should be aqueous based, free of cytotoxic solvents or chemical activators for delivery and/or gelation; gel in an appropriate time frame *in vivo* and fill the entire target lumen; incorporate a series of therapeutics for local delivery; and retain high biocompatibility, either as a permanent embolus or as a transient, degradable system. *In situ* gelling silk-elastinlike protein (SELP) polymers provide a recombinant polymer candidate that attests to these characteristics. SELP combines the natural strength of Bombyx mori (silkworm) silk [161] (GAGAGS) and the flexibility of mammalian elastin (GVGVP) [162] via genetic recombination. The silk domains form crystalline structures to provide mechanical strength, and hence a stable embolus. Elastin blocks make the polymer soluble in water and separate the silk complexes to create a porous matrix structure ideal for drug delivery. By varying the number and sequence of silk and elastin monomer blocks, properties such as swelling ratio, gelling rate, drug release profile, and mechanical strength can be controlled with molecular precision [163].

Biosynthetic strategy of SELP recombinant proteins involves a multistep process beginning with the specific design of the amino acid sequence [164]. Recombinant polymers consist of multiple repeats of a given sequence, namely the monomer. The SELP block copolymer has a primary monomer unit that combines silklike and elastinlike blocks at a designated ratio [163]. The DNA oligonucleotides of the monomer unit are synthesized using standard solid phase techniques. The two complementary oligonucleotides are

designed with short overhangs, or sticky ends, recognized by specific restriction enzymes, such as Ban I, to ensure unidirectional assembly [163]. The monomer gene is ligated into a suitable cloning plasmid containing an antibiotic resistance gene for identification and host *Escherichia coli* (*E. coli*) are transformed [165]. The transformed cells are grown and colonies are selected for screening of the monomer gene. Once the DNA sequence of the monomer is verified, the gene is amplified by polymerase chain reaction or with commercially available plasmid amplification kits to begin the construction of the polymer gene [165]. If plasmid amplification kits are used, the monomers are isolated via excision by restriction enzymes followed by agarose electrophoresis and band purification [165]. A suitable expression vector that is temperature inducible is next digested using the same restriction enzyme, Ban I, to create the complementary sticky ends. The amplified monomer stock is combined with the digested expression plasmids and the monomers are multimerized in a random concatemerization process with the aid of DNA ligase [166]. The ligation mixture is used to transform competent *E. coli*, and again colonies are grown and isolated. The carried plasmids are extracted and screened to determine multimer size. The desired plasmid, for example retaining a 6-mer, is amplified and retransformed into the microbial host and protein expression is confirmed using a bench-top, shake flask culture and protein gel electrophoresis [167]. Lab scale fermentation and purification steps ensue to express high quantities of the recombinant protein. Figure 2.4 summarizes this general biosynthetic strategy.

A lab scale, 10 L fermentation bioreactor vessel provides a controlled environment to achieve high bacterial growth required for subsequent protein production. Once appropriate cell density is achieved, the environment temperature is increased to 42° C to

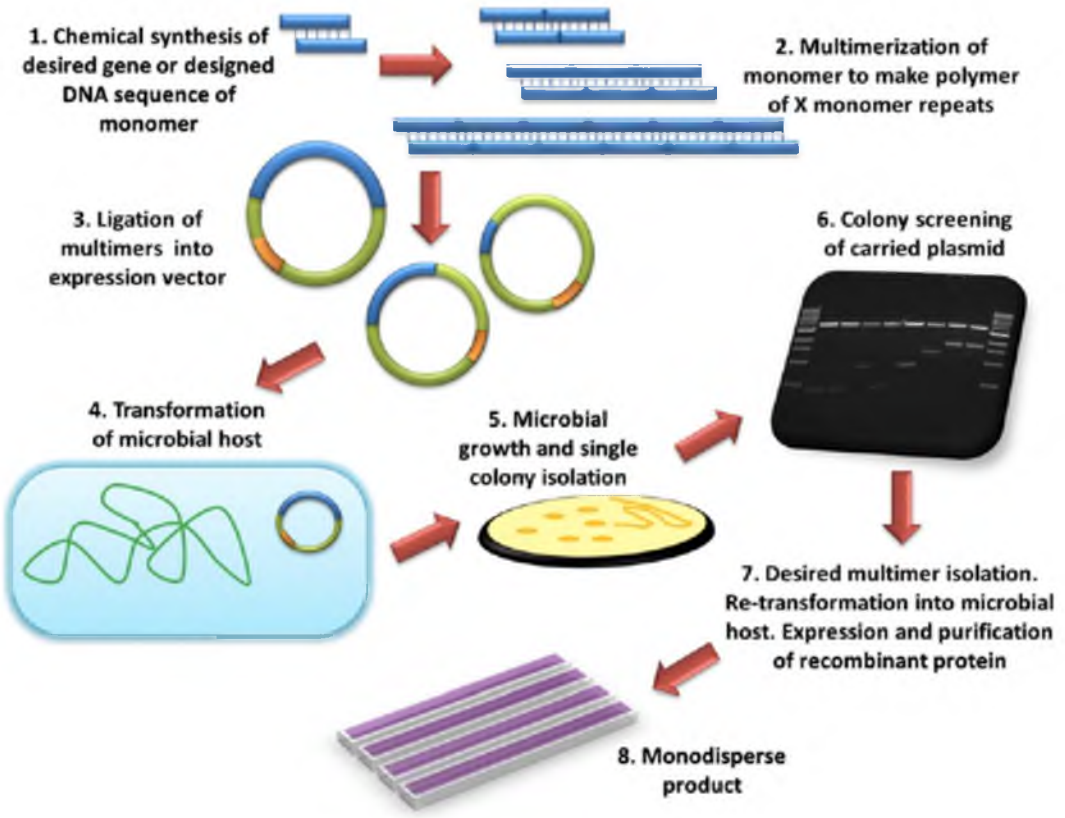

Figure 2.4. General biosynthetic strategy of recombinant polymers [164].

induce transcription and translation of the plasmid followed by a period of protein expression at 40° C. The bacteria are harvested and the SELP protein is purified following a series of ammonium sulfate precipitation and chromatography steps, resulting in several grams of a clean, monodisperse product free of bacterial antigens [164]. The protein is lyophilized or prepared into an aqueous formulation and stored at -80° C until use.

This high degree of control over not only production, but also the protein composition provides an immense advantage over the synthetic polymers currently under investigation for development of improved embolics. To date, a series of SELP compositions have been synthesized and characterized including: 415K, 47K, 815K, 815K-RS1, 815K-RS2, and 815K-RS5. The nomenclature relays the ratios of silklike blocks to elastinlike blocks per monomer, with an additional elastin block substituted with a lysine residue. For example, 415K has 4 silklike blocks, 15 elastinlike blocks, and a 16^{th} elastinlike block retaining the lysine. The RS constructs are analogs of SELP-815K with a matrix metalloproteinase (MMP) responsive sequence (RS) included at specific locations in the polymer backbone [167]. Inclusion of the RS sequence hastens the degradation of these protein polymers *in vivo* in the presence of MMP enzymes, which recognize the RS sequence and catalyze the protein.

All of these polymers have been designed to have similar molecular weight; meaning each polymer gene has a unique number of monomer repeats to achieve a molecular weight of approximately 65-70 kDa. Therefore, direct comparisons between the constructs and their mechanical properties have been studied [166]. In particular, it has been shown the gelation of SELPs is a nonreversible crystallization event dependent on the silk structural motif and the time to gelation is dictated by the overall silk content and

sequence [166]. For example, viscometry studies comparing SELPs 815K and 47K under isothermal conditions at 37 °C and at identical protein concentrations, showed 815K reached the upper maximal limit of the viscometer after approximately 57 min, while SELP-47K took approximately 108 min [166]. The critical gel concentration of each construct also depends on the silk content. The higher the silk content, the lower the weight percent to achieve gelation. Importance of the network formation resultant of the hydrogen bonding between the silk units was clearly illustrated when characterizing the RS constructs. The responsive sequence was placed in specific locations of the 815K monomer: the middle of the silk block (RS5), between the silk block and elastin block (RS1), or within the elastin block (RS2). SELP 815K-RS5 had the most altered mechanical properties, including longest gelation time, lowest mechanical stiffness modulus, and the highest critical gel concentration due to the disruption of the beta sheet formations between the modified silk units [167]. These extensive studies of SELPs have revealed how the physicochemical and material properties of the polymer chains can be precisely tailored [165].

Characterizations have also been geared towards determination of applications for these *in situ* gelling polymers. One avenue extensively studied is use as an injectable biologic delivery system. The ability to mix-in therapeutic agents *ex vivo* followed by direct injection into a target location, such as an externally accessible tumor or via catheter endovascularly, provides a unique delivery platform. Recently, SELPs have been studied in the application of adenovirus-mediated gene-directed enzyme prodrug therapy for treatment of head and neck cancers. The role of SELP was to provide controlled, matrix-mediated release of viral particles to reduce systemic toxicity, prolong gene expression,

and therefore improve therapeutic outcome [168,169].

Furthermore, being composed of amino acids that occur naturally in the body, the degradation products of SELP are bioresorbable. The injectable formulation itself consists of the polymer solubilized in buffered saline, and is nontoxic. When injected into the body, SELP rapidly makes a sol-to-gel transition *in situ* at body temperature with no solvent displacement. The aqueous based system allows for the wide range of therapeutic agents that can be directly incorporated *ex vivo*. Because of these unique and highly tunable attributes, SELPs provide desirable materials for development into an injectable liquid embolic capable of drug delivery. A SELP liquid embolic has many advantages over the available liquid embolics, Onyx® and PHIL™ dissolved in DMSO. These features were all exploited to develop a more superior embolic system, particularly for use in TACE to treat HCC. Chapters 3 through 6 elucidate the development and outcomes of this newly designed SELP liquid embolic.

2.5 References

[1] Dawbarn RHM. The starvation operation for malignancy in the external carotid area: its failures and successes. JAMA 1904;43:792–5. doi:10.1001/jama.1904.92500120002g.

[2] Siskin G, Murray T, Guimaraes M. Brief history and classification of embolic systems. Embolization Ther. Princ. Clin. Appl., Lippincott Williams & Wilkins; 2014, p. 3–9.

[3] Payne MM. Charles Theodore Dotter: The father of intervention. Texas Hear Inst J 2001;28:28–38.

[4] Rösch J, Keller FS, Kaufman JA. The birth, early years, and future of interventional radiology. J Vasc Interv Radiol 2003;14:841–53.

[5] Speakman TJ. Internal occlusion of a carotid-cavernous fistula. J Neurosurg 1964;21:303–5. doi:10.3171/jns.1964.21.4.0303.

[6] Mahapatro A, Kulshrestha AS. Polymers for biomedical applications. American Chemical Society; 2008.

[7] Ray CE, Lawson MC, Bauer JR. Embolization agents. In: Mauro MA, Murphy KPJ, Thomson KR, Venbrux AC, Morgan RA, editors. Image-Guided Interv. Second, Elsevier Inc.; 2014, p. 87–95.

[8] Gavenonis SC, Stravropoulos SW. Embolization techniques and applications. In: Pretorius ES, Solomon JA, editors. Radiol. Secrets Plus. Third, Mosby, Inc.; 2011, p. 241–4.

[9] Thomson KR, Lyon SM, Given MF, Burnes JP. Endovascular treatment of peripheral aneurysms. In: Mauro MA, Murphy KPJ, Thomson KR, Venbrux AC, Morgan RA, editors. Image-Guided Interv. Second, Elsevier Inc.; 2014, p. 256–61.

[10] Weng L, Rostamzadeh P, Nooryshokry N, Le HC, Golzarian J. In vitro and in vivo evaluation of biodegradable embolic microspheres with tunable anticancer drug release. Acta Biomater 2013;9:6823–33. doi:10.1016/j.actbio.2013.02.017.

[11] Neligan PC. Vascular anomalies of the upper extremity. Plast. Surg. Third, 2013, p. 667–93.

[12] Stanley JC, Veith FJ, Wakefield TW. Classification of peripheral arteriovenous and venous malformations. Curr. Ther. Vasc. Endovasc. Surg. Fifth, Saunders; 2014, p. 829–30.

[13] Bolognia JL, Jorizzo JL, Schaffer J V. Vascular malformations. Dermatology, Elsevier Ltd.; 2012, p. 1711–28.

[14] Spetzler RF, Martin NA. A proposed grading system for arteriovenous malformations. J Neurosurg 1986;65:476–83.

[15] van Beijnum J, van der Worp H, Buis DR. Treatment of brain arteriovenous malformations: a systematic review and meta-analysis. JAMA 2011;306:2011–9.

[16] Kolber MK, Shukla PA, Kumar A, Silberzweig JE. Ethylene vinyl alcohol copolymer (Onyx) embolization for acute hemorrhage: a systematic review of peripheral applications. J Vasc Interv Radiol 2015;26:809–15.

[17] Lencioni R. Loco-regional treatment of hepatocellular carcinoma. Hepatology 2010;52:762–73. doi:10.1002/hep.23725.

[18] Hirschl R, Caragine LP. Endovascular techniques for tumor embolization. In: Winn HR, editor. Youmans Neurol. Surg. Sixth, Elsevier Inc.; 2011, p. 1224–8.

[19] Liapi E, Georgiades CC, Hong K, Geschwind JFH. Transcatheter arterial

chemoembolization: current technique and future promise. Tech Vasc Interv Radiol 2007;10:2–11. doi:10.1053/j.tvir.2007.08.008.

[20] Talenfeld AD, Sista AK, Madoff DC. Transarterial therapies for primary liver tumors. Surg Oncol Clin N Am 2014;23:323–51. doi:10.1016/j.soc.2013.11.002.

[21] Lencioni R. Management of hepatocellular carcinoma with transarterial chemoembolization in the era of systemic targeted therapy. Crit Rev Oncol Hematol 2012;83:216–24. doi:10.1016/j.critrevonc.2011.10.008.

[22] Lewis AL, Dreher MR. Locoregional drug delivery using image-guided intra-arterial drug eluting bead therapy. J Control Release 2012;161:338–50. doi:10.1016/j.jconrel.2012.01.018.

[23] Lammer J, Malagari K, Vogl T, Pilleul F, Denys A, Watkinson A, et al. Prospective randomized study of doxorubicin-eluting-bead embolization in the treatment of hepatocellular carcinoma: results of the PRECISION V study. Cardiovasc Intervent Radiol 2010;33:41–52. doi:10.1007/s00270-009-9711-7.

[24] Golfieri R, Giampalma E, Renzulli M, Cioni R, Bargellini I, Bartolozzi C, et al. Randomised controlled trial of doxorubicin-eluting beads vs conventional chemoembolisation for hepatocellular carcinoma. Br J Cancer 2014;111:255–64. doi:10.1038/bjc.2014.199.

[25] Lencioni R, Llovet JM. Modified RECIST (mRECIST) assessment for hepatocellular carcinoma. Semin. Liver Dis., vol. 30, 2010, p. 52–60.

[26] Kirsch M, Zinke A, Kirsch G, Hosten N. Therapy with intra-arterial iodine-131-lipiodol in inoperable hepatocellular carcinoma. Percutaneous Tumor Ablation Med. Radiol., Springer; 2008, p. 89–92.

[27] Ferri FF. Uterine fibroids. Ferri's Clin. Advis. 2016, Elsevier, Inc.; 2016, p. 1271–2.

[28] Walker CL, Stewart EA. Uterine fibroids: the elephant in the room. Science 2005;308:1589–92. doi:10.1126/science.1112063.

[29] Khan AT, Shehmar M, Gupta JK. Uterine fibroids: Current perspectives. Int J Womens Health 2014;6:95–114. doi:10.2147/IJWH.S51083.

[30] Ryan GL, Syrop CH, van Voorhis BJ. Role, epidemiology, and natural history of benign uterine mass lesions. Clin Obstet Gynecol 2005;48.

[31] Kröncke T, David M. Uterine artery embolization (UAE) for fibroid treatment – results of the 5th radiological gynecological expert meeting. Geburtshilfe Frauenheilkd

2015;75:439–41. doi:10.1055/s-0035-1545999.

[32] Ravina JH, Ciraru-Vigneron N, Bouret JM, Herbreteau D, Houdart E, Aymard A, et al. Arterial embolisation to treat uterine myomata. Lancet 1995;346:671–2.

[33] Andersen PE, Lund N, Justesen P, Munk T, Elle B, Floridon C. Uterine artery embolization of symptomatic uterine fibroids. Acta Radiol 2001;42:234–8. doi:10.1034/j.1600-0455.2001.042002234.x.

[34] Pakiz M, But I. Uterine artery embolization for symptomatic uterine fibroids. Int J Gynaecol Obstet 2008;101:81–2. doi:10.1016/j.ijgo.2007.09.025.

[35] Istre O, Hald K, Qvigstad E. Multiple myomas treated with a temporary, noninvasive, Doppler-directed, transvaginal uterine artery clamp. J Am Assoc Gynecol Laparosc 2004;11:273–6.

[36] Vilos GA, Vilos EC, Romano W, Abu-Rafea B. Temporary uterine artery occlusion for treatment of menorrhagia and uterine fibroids using an incisionless Doppler-guided transvaginal clamp: case report. Hum Reprod 2006;21:269–71.

[37] Correll JT, Prentice HR, Wise EC. Biologic investigations of a new absorbable sponge. Surg Gynecol Obstet 1945;81:585–9.

[38] Jenkins HP, Janda R, Clarke J. Clinical and experimental observations on the use of gelatin sponge or foam. Surgery 1946;20:124–32.

[39] Ishimori S, Hattori M, Shibata Y, Shizawa H, Fujinaga R. Treatment of carotid-cavernous fistula by gelfoam embolization. J Neurosurg 1967;27:315–9. doi:10.3171/jns.1967.27.4.0315.

[40] Yonemitsu T, Kawai N, Sato M, Sonomura T, Takasaka I, Nakai M, et al. Comparison of hemostatic durability between N-butyl cyanoacrylate and gelatin sponge particles in transcatheter arterial embolization for acute arterial hemorrhage in a coagulopathic condition in a swine model. Cardiovasc Intervent Radiol 2010;33:1192–7.

[41] Arai Y. Glue. In: Guimaraes M, Lencioni R, Siskin GP, editors. Embolization Ther. Princ. Clin. Appl., Wolters Kluwer Health; 2015, p. 45–9.

[42] Louguet S, Verret V, Bédouet L, Servais E, Pascale F, Wassef M, et al. Poly(ethylene glycol) methacrylate hydrolyzable microspheres for transient vascular embolization. Acta Biomater 2014;10:1194–205. doi:10.1016/j.actbio.2013.11.028.

[43] Lindstrom P. Complications from the use of absorbable hemostatic sponges. AMA Arch Surg 1956;73:133–41.

[44] Siskin GP, Englander M, Stainken BF, Ahn J, Dowling K, Dolen EG. Embolic

agents used for uterine fibroid embolization. Am J Roentgenol 2000;175:767–73. doi:10.2214/ajr.175.3.1750767.

[45] Rothman USE, Lindberg BJ. Agent for intravascular administration 1978.

[46] Malmsjo M, Thordarson E, Apell SP, Fyhr P. Microspheres of hydrolysed starch with endogenous, charged ligands. US20120244198 A1, 2012.

[47] Niessen C, Unterpaintner E, Goessmann H, Schlitt HJ, Mueller-Schilling M, Wohlgemuth WA, et al. Degradable starch microspheres versus ethiodol and doxorubicin in transarterial chemoembolization of hepatocellular Carcinoma. J Vasc Interv Radiol 2014;25:240–7. doi:10.1016/j.jvir.2013.10.007.

[48] Pieper CC, Meyer C, Vollmar B, Hauenstein K, Schild HH, Wilhelm KE. Temporary arterial embolization of liver parenchyma with degradable starch microspheres (EmboCept®S) in a swine model. Cardiovasc Intervent Radiol 2014;38:435–41. doi:10.1007/s00270-014-0966-2.

[49] Murata S, Tajima H, Ichikawa K, Onozawa S, Wang J, Kumita S, et al. Oily chemoembolization combined with degradable starch microspheres for HCC with cirrhosis. Hepatogastroenterology 2007;55:1041–6.

[50] Meyer C, Pieper CC, Ezziddin S, Wilhelm KE, Schild HH, Ahmadzadehfar H. Feasibility of temporary protective embolization of normal liver tissue using degradable starch microspheres during radioembolization of liver tumours. Eur J Nucl Med Mol Imaging 2014;41:231–7.

[51] Kania RE, Sauvaget E, Guichard J-P, Chapot R, Huy PTB, Herman P. Early postoperative CT scanning for juvenile nasopharyngeal angiofibroma: detection of residual disease. AJNR Am J Neuroradiol 2005;26:82–8.

[52] Rosen RJ, Contractor S. The use of cyanoacrylate adhesives in the management of congenital vascular malformations. Semin. Intervent. Radiol., vol. 21, Thieme Medical Publishers; 2004, p. 59.

[53] Brothers MF, Kaufmann JC, Fox AJ, Deveikis JP. n-Butyl 2-cyanoacrylate--substitute for IBCA in interventional neuroradiology: histopathologic and polymerization time studies. Am J Neuroradiol 1989;10:777–86.

[54] Vinters HV, Galil KA, Lundie MJ, Kaufmann JCE. The histotoxicity of cyanoacrylates. Neuroradiology 1985;27:279–91.

[55] Razavi MK, Murphy K. Embolization of bronchial arteries with N-butyl cyanoacrylate for management of massive hemoptysis: a technical review. Tech Vasc Interv Radiol 2007;10:276–82.

[56] Denys A, Lacombe C, Schneider F, Madoff DC, Doenz F, Qanadli SD, et al. Portal vein embolization with N-butyl cyanoacrylate before partial hepatectomy in patients with hepatocellular carcinoma and underlying cirrhosis or advanced fibrosis. J Vasc Interv Radiol 2005;16:1667–74.

[57] Yata S, Ihaya T, Kaminou T, Hashimoto M, Ohuchi Y, Umekita Y, et al. Transcatheter arterial embolization of acute arterial bleeding in the upper and lower gastrointestinal tract with N-butyl-2-cyanoacrylate. J Vasc Interv Radiol 2013;24:422–31.

[58] Yonemitsu T, Kawai N, Sato M, Tanihata H, Takasaka I, Nakai M, et al. Evaluation of transcatheter arterial embolization with gelatin sponge particles, microcoils, and n-butyl cyanoacrylate for acute arterial bleeding in a coagulopathic condition. J Vasc Interv Radiol 2009;20:1176–87.

[59] Taki W, Yonekawa Y, Iwata H, Uno A, Yamashita K, Amemiya H. A new liquid material for embolization of arteriovenous malformations. Am J Neuroradiol 1990;11:163–8.

[60] Yamada R, Uflacker A, Bourgeois A, Adams JD, Guimaraes M. EVOH/DMSO in peripheral application. In: Guimaraes M, Lencioni R, Siskin GP, editors. Embolization Ther. Princ. Clin. Appl., Lippincott Williams & Wilkins; 2014, p. 51–7.

[61] Chandra R V, Leslie-Mazwi TM, Mehta BP, Yoo AJ, Rabinov JD, Pryor JC, et al. Transarterial onyx embolization of cranial dural arteriovenous fistulas: long-term follow-up. Am J Neuroradiol 2014;35:1793–7.

[62] Vanninen RL, Manninen I. Onyx, a new liquid embolic material for peripheral interventions: preliminary experience in aneurysm, pseudoaneurysm, and pulmonary arteriovenous malformation embolization. Cardiovasc Intervent Radiol 2007;30:196–200.

[63] Sadeghi-Azandaryani M, Strube H, Heyn J, Steckmeier B, Reiser MF, Treitl M. Penetrating aortic ulcer in the infrarenal stent-graft landing zone: treatment with coils and the ethylene vinyl alcohol copolymer onyx. J Endovasc Ther 2011;18:123–9.

[64] Gore P, Theodore N, Brasiliense L, Kim LJ, Garrett M, Nakaji P, et al. The utility of onyx for preoperative embolization of cranial and spinal tumors. Neurosurgery 2008;62:1204–12.

[65] Larzon T, Mathisen SR. Internal sealing of acute aortic bleeding with a catheter-delivered liquid to solid embolic agent (Onyx). Vascular 2010;18:106–10.

[66] Eberhardt KM, Sadeghi-Azandaryani M, Worlicek S, Koeppel T, Reiser MF, Treitl M. Treatment of type I endoleaks using transcatheter embolization with Onyx. J Endovasc Ther 2014;21:162–71.

[67] Ling AJ, Pathak R, Garbowski M, Nadkarni S. Treatment of a large type II endoleak via extraperitoneal dissection and embolization of a collateral vessel using ethylene vinyl alcohol copolymer (Onyx). J Vasc Interv Radiol 2007;18:659–62.

[68] Martin ML, Dolmatch BL, Fry PD, Machan LS. Treatment of type II endoleaks with Onyx. J Vasc Interv Radiol 2001;12:629–32.

[69] Natarajan SK, Born D, Ghodke B, Britz GW, Sekhar LN. Histopathological changes in brain arteriovenous malformations after embolization using onyx or n-butyl cyanoacrylate: laboratory investigation. J Neurosurg 2009;111:105–13.

[70] Won Y, Lee SL, Kim Y, Ku YM. Clinical efficacy of transcatheter embolization of visceral artery pseudoaneurysms using N-butyl cyanoacrylate (NBCA). Diagn Interv Imaging 2015;96:563–9. doi:10.1016/j.diii.2015.01.003.

[71] Jahan R, Murayama Y, Gobin YP, Duckwiler GR, Vinters H V, Viñuela F. Embolization of arteriovenous malformations with Onyx: clinicopathological experience in 23 patients. Neurosurgery 2001;48:984–97.

[72] Cruise GM, Constant MJ, Keeley EM, Greene R, Harris C. Polymeric treatment compositions. WO 2014062696 A1, 2014.

[73] Samaniego EA, Kalousek V, Abdo G, Ortega-Gutierrez S. Preliminary experience with Precipitating Hydrophobic Injectable Liquid (PHIL) in treating cerebral AVMs. J Neurointerv Surg 2016:neurintsurg – 2015–012210. doi:10.1136/neurintsurg-2015-012210.

[74] Kocer N, Hanimoglu H, Batur S, Kandemirli SG, Kizilkilic O, Sanus Z, et al. Preliminary experience with precipitating hydrophobic injectable liquid in brain arteriovenous malformations. Diagnostic Interv Radiol 2016. doi:10.5152/dir.2015.15283.

[75] Leyon JJ, Chavda S, Thomas A, Lamin S. Preliminary experience with the liquid embolic material agent PHIL (Precipitating Hydrophobic Injectable Liquid) in treating cranial and spinal dural arteriovenous fistulas: technical note. J Neurointerv Surg 2015:1–8. doi:10.1136/neurintsurg-2015-011684.

[76] Deodhar A, Kaufman JA. Polyvinyl alcohol particles. In: Guimaraes M, Lencioni R, Siskin GP, editors. Embolization Ther. Princ. Clin. Appl., Lippincott Williams & Wilkins; 2014, p. 30–1.

[77] Tadavarthy SM, Moller JH, Amplatz K. Polyvinyl alcohol (Ivalon): a new embolic material 1975;125:609–16.

[78] Tadavarthy SM, Knight L, Ovitt TW, Snyder C, Amplatz K. Therapeutic transcatheter arterial embolization 1. Radiology 1974;112:13–6.

[79] Laurent A. Microspheres and nonspherical particles for embolization. Tech Vasc Interv Radiol 2007;10:248–56. doi:10.1053/j.tvir.2008.03.010.

[80] Bendszus M, Klein R, Burger R, Warmuth-Metz M, Hofmann E, Solymosi L. Efficacy of trisacryl gelatin microspheres versus polyvinyl alcohol particles in the preoperative embolization of meningiomas. Am J Neuroradiol 2000;21:255–61.

[81] Chua GC, Wilsher M, Young MPA, Manyonda I, Morgan R, Belli A-M. Comparison of particle penetration with non-spherical polyvinyl alcohol versus trisacryl gelatin microspheres in women undergoing premyomectomy uterine artery embolization. Clin Radiol 2005;60:116–22.

[82] Pelage J, Laurent A, Wassef M, Germain D, Rymer R, Flaud P, et al. Uterine artery embolization in sheep : comparison of acute effects with polyvinyl alcohol particles and calibrated microspheres. Radiology 2002;224:436–45. doi:10.1148/radiol.2242010847.

[83] Lewis AL, Adams C, Busby W, Jones S a., Wolfenden LC, Leppard SW, et al. Comparative in vitro evaluation of microspherical embolisation agents. J Mater Sci Mater Med 2006;17:1193–204. doi:10.1007/s10856-006-0592-x.

[84] Spies JB, Allison S, Flick P, Cramp M, Bruno J, Jha RC, et al. Spherical polyvinyl alcohol versus tris-acryl gelatin microspheres for uterine artery embolization for leiomyomas: results of a limited randomized comparative study. J Vasc Interv Radiol 2005;16:1431–7.

[85] Siskin GP, Beck A, Schuster M, Mandato K, Englander M, Herr A. Leiomyoma infarction after uterine artery embolization: a prospective randomized study comparing tris-acryl gelatin microspheres versus polyvinyl alcohol microspheres. J Vasc Interv Radiol 2008;19:58–65. doi:10.1016/j.jvir.2007.08.034.

[86] Yu SCH, Lok I, Ho SSY, Tong M, Hui JWY. Comparison of clinical outcomes of tris-acryl microspheres versus polyvinyl alcohol microspheres for uterine artery embolization for leiomyomas: results of a randomized trial. J Vasc Interv Radiol 2011;22:1229–35.

[87] Worthington-Kirsch RL, Siskin GP, Hegener P, Chesnick R. Comparison of the efficacy of the embolic agents acrylamido polyvinyl alcohol microspheres and tris-acryl gelatin microspheres for uterine artery embolization for leiomyomas: a prospective randomized controlled trial. Cardiovasc Intervent Radiol 2011;34:493–501.

[88] Siskin GP, Dowling K, Virmani R, Jones R, Todd D. Pathologic evaluation of a spherical polyvinyl alcohol embolic agent in a porcine renal model. J Vasc Interv Radiol 2003;14:89–98.

[89] Hidaka K, Moine L, Collin G, Labarre D, Louis Grossiord J, Huang N, et al.

Elasticity and viscoelasticity of embolization microspheres. J Mech Behav Biomed Mater 2011;4:2161–7. doi:10.1016/j.jmbbm.2011.08.001.

[90] Laurent A, Beaujeux R, Wassef M, Rüfenacht D, Boschetti E, Merland JJ. Trisacryl gelatin microspheres for therapeutic embolization, I: development and in vitro evaluation. AJNR Am J Neuroradiol 1996;17:533–40.

[91] Boschetti E, Brouard M, Drouet L, Girot P, Laurent A, Wassef M. Microspheres useful for therapeutic vascular occlusions and injectable solutions containing the same 1997.

[92] Reb P, Marion P, De Gioannis B, Krom J. Microspheres useful for therapeutic vascular embolization 2011.

[93] Derdeyn CP, Graves VB, Salamat MS, Rappe A. Collagen-coated acrylic microspheres for embolotherapy: in vivo and in vitro characteristics. Am J Neuroradiol 1997;18:647–53.

[94] Buiser M, Bellisario M, Knapp D, Mangin S, Lanphere J. Embolization 2009.

[95] Gadaleta CD, Ranieri G. Trans-arterial chemoembolization as a therapy for liver tumours: New clinical developments and suggestions for combination with angiogenesis inhibitors. Crit Rev Oncol Hematol 2011;80:40–53. doi:10.1016/j.critrevonc.2010.10.005.

[96] Loh XJ, Scherman OA. Polymeric and self assembled hydrogels: from fundamental understanding to applications. Royal Society of Chemistry; 2012.

[97] Abramowitz SD, Israel GM, Mccarthy SM, White RI, Tal MG. Comparison of four embolic materials at uterine artery embolization by using postprocedural MR imaging enhancement. Radiology 2009;250.

[98] Lewis AL, Stratford PW, Leppard S, Garcia P, Hall B, Gonzalez MVF. Chemoembolisation. US 7442385 B2, 2008.

[99] Lewis AL, Biocompatibles UK. Embolisation devices from biomedical polymers for intra-arterial occlusion and drug delivery in the treatment of cancer. Biomater Cancer Ther Diagnosis, Prev Ther 2013:207.

[100] Anderson ME, Kalva SP. Drug-eluting beads. In: Guimaraes M, Lencioni R, Siskin GP, editors. Embolization Ther. Princ. Clin. Appl., Lippincott Williams & Wilkins; 2014, p. 38–44.

[101] Jordan O, Denys A, De Baere T, Boulens N, Doelker E. Comparative study of chemoembolization loadable beads: in vitro drug release and physical properties of DC Bead and Hepasphere loaded with doxorubicin and irinotecan. J Vasc Interv Radiol

2010;21:1084–90. doi:10.1016/j.jvir.2010.02.042.

[102] Biondi M, Fusco S, Lewis AL, Netti P a. Investigation of the mechanisms governing doxorubicin and irinotecan release from drug-eluting beads: mathematical modeling and experimental verification. J Mater Sci Mater Med 2013;24:2359–70. doi:10.1007/s10856-013-4992-4.

[103] Namur J, Wassef M, Millot JM, Lewis AL, Manfait M, Laurent A. Drug-eluting beads for liver embolization: concentration of doxorubicin in tissue and in beads in a pig model. J Vasc Interv Radiol 2010;21:259–67. doi:10.1016/j.jvir.2009.10.026.

[104] Namur J, Pascale F, Maeda N, Sterba M, Ghegediban SH, Verret V, et al. Safety and efficacy compared between irinotecan-loaded microspheres HepaSphere and DC Bead in a model of VX2 liver metastases in the rabbit. J Vasc Interv Radiol 2015:1–12. doi:10.1016/j.jvir.2015.03.014.

[105] Oh JS, Lee HG, Chun HJ, Choi BG. Evaluation of arterial impairment after experimental gelatin sponge embolization in a rabbit renal model 2015;16:133–8.

[106] Weng L, Seelig D, Rostamzadeh P, Golzarian J. Calibrated bioresorbable microspheres as an embolic agent: an experimental study in a rabbit renal model. J Vasc Interv Radiol 2015:1–8. doi:10.1016/j.jvir.2015.01.014.

[107] Ohta S, Nitta N, Watanabe S, Tomozawa Y, Sonoda A, Otani H, et al. Gelatin microspheres: correlation between embolic effect/degradability and cross-linkage/particle size. Cardiovasc Intervent Radiol 2013;36:1105–11. doi:10.1007/s00270-012-0531-9.

[108] Sieghart W, Hucke F, Pinter M, Graziadei I, Vogel W, Müller C, et al. The ART of decision making: retreatment with transarterial chemoembolization in patients with hepatocellular carcinoma. Hepatology 2013;57:2261–73.

[109] Verret V, Pelage JP, Wassef M, Louguet S, Servais E, Bédouet L, et al. A novel resorbable embolization microsphere for transient uterine artery occlusion: a comparative study with trisacryl-gelatin microspheres in the sheep model. J Vasc Interv Radiol 2014;25:1759–66. doi:10.1016/j.jvir.2014.06.025.

[110] Zhou X, Kong M, Cheng X, Li J, Li J, Chen X. Investigation of acetylated chitosan microspheres as potential chemoembolic agents. Colloids Surfaces B Biointerfaces 2014;123:387–94. doi:10.1016/j.colsurfb.2014.07.044.

[111] Weng L, Rostambeigi N, Zantek ND, Rostamzadeh P, Bravo M, Carey J, et al. An in situ forming biodegradable hydrogel-based embolic agent for interventional therapies. Acta Biomater 2013;9:8182–91. doi:10.1016/j.actbio.2013.06.020.

[112] Bédouet L, Verret V, Louguet S, Servais E, Pascale F, Beilvert A, et al. Anti-

angiogenic drug delivery from hydrophilic resorbable embolization microspheres: An in vitro study with sunitinib and bevacizumab. Int J Pharm 2015;484:218–27. doi:10.1016/j.ijpharm.2015.02.039.

[113] Gaba RC, Yap FY, Martinex EM, Li Y, Guzman G, Parvinian A, et al. Transarterial sorafenib chembolization: preliminary study of technical feasibilty in a rabbit model. J Vasc Interv Radiol 2013;24:744–50. doi:10.1016/j/jvir.2013.01.488.

[114] Dreher MR, Sharma K V, Woods DL, Reddy G, Tang Y, Pritchard WF, et al. Radiopaque drug-eluting beads for transcatheter embolotherapy: experimental study of drug penetration and coverage in swine. J Vasc Interv Radiol 2012;23:257–64.

[115] Sharma K V, Dreher MR, Tang Y, Pritchard W, Chiesa OA, Karanian J, et al. Development of "imageable" beads for transcatheter embolotherapy. J Vasc Interv Radiol 2010;21:865–76. doi:10.1016/j.jvir.2010.02.031.

[116] Chen J, White SB, Harris KR, Lewandowski RJ, Shea L, Larson a. C. Poly(lactide-co-glycolide) microspheres for MRI-monitored sorafenib transarterial chemoembolization in a rabbit VX2 model. J Vasc Interv Radiol 2015;26:S81. doi:10.1016/j.jvir.2014.12.224.

[117] Kim DH, Chen J, Omary RA, Larson AC. MRI visible drug eluting magnetic microspheres for transcatheter intra-arterial delivery to liver tumors. Theranostics 2015;5:477–88. doi:10.7150/thno.10823.

[118] Thu B, Bruheim P, Espevik T, Smidsrød O, Soon-Shiong P, Skjåk-Bræk G. Alginate polycation microcapsules: I. Interaction between alginate and polycation. Biomaterials 1996;17:1031–40.

[119] Wang Q, Qian K, Liu S, Yang Y, Liang B, Zheng C, et al. X-ray visible and uniform alginate microspheres loaded with in situ synthesized BaSO 4 nanoparticles for in vivo transcatheter arterial embolization. Biomacromolecules 2015;16:1240–6. doi:10.1021/acs.biomac.5b00027.

[120] Brown KT. Fatal pulmonary complications after arterial embolization with 40–120-μm tris-acryl gelatin microspheres. J Vasc Interv Radiol 2004;15:197–200.

[121] Vernon B, Birdno M, Preul M. In situ gelling self-reactive materials for embolization. US 20060263301 A1, 2006.

[122] Vernon B, Martinez A. Gel strength and solution viscosity of temperature-sensitive, in-situ-gelling polymers for endovascular embolization. J Biomater Sci Polym Ed 2005;16:1153–66.

[123] Riley CM, McLemore R, Preul MC, Vernon BL. Gelling process differences in reverse emulsion, in situ gelling polymeric materials for intracranial aneurysm

embolization, formulated with injectable contrast agents. J Biomed Mater Res - Part B Appl Biomater 2011;96 B:47–56. doi:10.1002/jbm.b.31729.

[124] Cheng V, Lee BH, Pauken C, Vernon BL. Poly (N-isopropylacrylamide-co-poly (ethylene glycol))-acrylate simultaneously physically and chemically gelling polymer systems. J Appl Polym Sci 2007;106:1201–7.

[125] Brennecka CR, Preul MC, Bichard WD, Vernon BL. In vivo experimental aneurysm embolization in a swine model with a liquid-to-solid gelling polymer system: initial biocompatibility and delivery strategy analysis. World Neurosurg 2012;78:469–80. doi:10.1016/j.wneu.2011.10.029.

[126] Brennecka CR, Preul MC, Becker TA, Vernon BL. In vivo embolization of lateral wall aneurysms in canines using the liquid-to-solid gelling PPODA-QT polymer system: 6-month pilot study. J Neurosurg 2013;119:228–38. doi:10.3171/2013.3.JNS121865.

[127] Brennecka CR, Preul MC, Vernon BL. In vitro delivery, cytotoxicity, swelling, and degradation behavior of a liquid-to-solid gelling polymer system for cerebral aneurysm embolization. J Biomed Mater Res - Part B Appl Biomater 2012;100 B:1298–309. doi:10.1002/jbm.b.32696.

[128] Jeong B, Kim SW, Bae YH. Thermosensitive sol–gel reversible hydrogels. Adv Drug Deliv Rev 2002;54:37–51.

[129] Cui Z, Lee BH, Pauken C, Vernon BL. Degradation, cytotoxicity, and biocompatibility of NIPAAm-based thermosensitive, injectable, and bioresorbable polymer hydrogels. J Biomed Mater Res Part A 2011;98:159–66.

[130] Lee BH, Leon C, McLemore R, Macias JV, Vernon BL. Synthesis and characterization of thermo-sensitive radio-opaque poly (N-isopropylacrylamide-co-PEG-2-iodobenzoate). J Biomater Sci Polym Ed 2011;22:2357–67.

[131] Bearat HH, Lee BH, Valdez J, Vernon BL. Synthesis, characterization and properties of a physically and chemically gelling polymer system using poly (NIPAAm-co-HEMA-acrylate) and poly (NIPAAm-co-cysteamine). J Biomater Sci Polym Ed 2011;22:1299–318.

[132] Bearat HH, Preul MC, Vernon BL. Cytotoxicity, in vitro models and preliminary in vivo study of dual physical and chemical gels for endovascular embolization of cerebral aneurysms. J Biomed Mater Res - Part A 2013;101 A:2515–25. doi:10.1002/jbm.a.34554.

[133] Bearat HH, Lee BH, Vernon BL. Comparison of properties between NIPAAm-based simultaneously physically and chemically gelling polymer systems for use in vivo. Acta Biomater 2012;8:3629–42. doi:10.1016/j.actbio.2012.06.012.

[134] Lee BH, Beart HH, Cheng V, McLemore R, Robb SA, Cui Z, et al. In vitro and in vivo demonstration of physically and chemically in situ gelling NIPAAm-based copolymer system. J Biomater Sci Polym Ed 2013;24:1575–88.

[135] Jordan O, Doelker E, Rüfenacht DA. Biomaterials used in injectable implants (liquid embolics) for percutaneous filling of vascular spaces. Cardiovasc Intervent Radiol 2005;28:561–9. doi:10.1007/s00270-004-0238-7.

[136] Becker TA, Kipke DR, Brandon T. Calcium alginate gel: a biocompatible and mechanically stable polymer for endovascular embolization. J Biomed Mater Res 2001;54:76–86. doi:10.1002/1097-4636(200101)54:1<76::AID-JBM9>3.0.CO;2-V.

[137] Barnett BP, Hughes AH, Lin S, Arepally A, Gailloud PH. In vitro assessment of EmboGel and UltraGel radiopaque hydrogels for the endovascular treatment of aneurysms. J Vasc Interv Radiol 2009;20:507–12. doi:10.1016/j.jvir.2009.01.005.

[138] Vaidya S, Tozer KR, Chen J. An overview of embolic agents. Semin Intervent Radiol 2008;25:204–15. doi:10.1055/s-0028-1085930.

[139] Becker TA, Kipke DR. Flow properties of liquid calcium alginate polymer injected through medical microcatheters for endovascular embolization. J Biomed Mater Res 2002;61:533–40. doi:10.1002/jbm.10202.

[140] Gombotz WR, Wee SF. Protein release from alginate matrices. Adv Drug Deliv Rev 2012;64:194–205.

[141] Pawar SN, Edgar KJ. Alginate derivatization: a review of chemistry, properties and applications. Biomaterials 2012;33:3279–305.

[142] Tønnesen HH, Karlsen J. Alginate in drug delivery systems. Drug Dev Ind Pharm 2002;28:621–30. doi:10.1081/DDC-120003853.

[143] Barnett BP, Gailloud P. Assessment of EmboGel--a selectively dissolvable radiopaque hydrogel for embolic applications. J Vasc Interv Radiol 2011;22:203–11. doi:10.1016/j.jvir.2010.10.010.

[144] Becker TA, Preul MC, Bichard WD, Kipke DR, McDougall CG. Calcium alginate gel as a biocompatible material for endovascular arteriovenous malformation embolization: six-month results in an animal model. Neurosurgery 2005;56:793–801.

[145] Becker TA, Preul MC, Bichard WD, Kipke DR, McDougall CG. Preliminary investigation of calcium alginate gel as a biocompatible material for endovascular aneurysm embolization in vivo. Neurosurgery 2007;60:1119–28.

[146] Raymond J, Metcalfe A, Desfaits A-C, Ribourtout E, Salazkin I, Gilmartin K, et al.

Alginate for endovascular treatment of aneurysms and local growth factor delivery. AJNR Am J Neuroradiol 2003;24:1214–21.

[147] Kollman JM, Pandi L, Sawaya MR, Riley M, Doolittle RF. Crystal structure of human fibrinogen. Biochemistry 2009;48:3877–86. doi:19296670.

[148] Malkowski MG, Martin PD, Guzik JC, Edwards BF. The co-crystal structure of unliganded bovine alpha-thrombin and prethrombin-2: movement of the Tyr-Pro-Pro-Trp segment and active site residues upon ligand binding. Protein Sci 1997;6:1438–48. doi:9232645.

[149] Richling B. Homologous controlled-viscosity fibrin for endovascular embolization. Part II: catheterization technique, animal experiments. Acta Neurochir (Wien) 1982;64:109–24.

[150] Richling B. Homologous controlled-viscosity fibrin for endovascular embolization. Part I. Experimental development of the medium. Acta Neurochir (Wien) 1982;62:159–70.

[151] Probst EN, Grzyska U, Westphal M, Zeumer H. Preoperative embolization of intracranial meningiomas with a fibrin glue preparation. AJNR Am J Neuroradiol 1999;20:1695–702.

[152] Berguer R, Staerkel RL, Moore EE, Moore FA, Galloway WB, Mockus MB. Fatal reaction to the use of fibrin glue in deep hepatic wounds: case reports. J Trauma 1991;31:408–11.

[153] Duarte AP, Coelho JF, Bordado JC, Cidade MT, Gil MH. Surgical adhesives: systematic review of the main types and development forecast. Prog Polym Sci 2012;37:1031–50.

[154] Wright KC, Greff RJ, Price RE. Experimental evaluation of cellulose acetate NF and ethylene-vinyl alcohol copolymer for selective arterial embolization. J Vasc Interv Radiol 1999;10:1207–18.

[155] Kinugasa K, Mandai S, Terai Y, Kamata I, Sugiu K, Ohmoto T, et al. Direct thrombosis of aneurysms with cellulose acetate polymer, part II: preliminary clinical experience. J Neurosurg 1992;77:501–7. doi:10.3171/jns.1992.77.4.0501.

[156] Mandai S, Kinugasa K, Ohmoto T. Direct thrombosis of aneurysms with cellulose acetate polymer. Part I: Results of thrombosis in experimental aneurysms. J Neurosurg 1992;77:497–500. doi:10.3171/jns.1992.77.4.0497.

[157] Sugiu K, Meguro T, Nakashiama H, Ohmoto T. Successful embolization of a spinal perimedullary arteriovenous fistula with cellulose acetate polymer solution: technical case report. Neurosurgery 2001;49:1257–60; discussion 1260–1.

[158] Golzarian J, Weng L. Liquid embolic material including carboxymethyl chitosan crosslinked with carboxymethyl cellulose. US 8936795 B2, 2015.

[159] Stampfl S, Bellemann N, Stampfl U, Radeleff B, Lopez-Benitez R, Sommer C-M, et al. Inflammation and recanalization of four different spherical embolization agents in the porcine kidney model. J Vasc Interv Radiol 2008;19:577–86.

[160] Stampfl S, Bellemann N, Stampfl U, Sommer CM, Thierjung H, Lopez-Benitez R, et al. Arterial distribution characteristics of Embozene particles and comparison with other spherical embolic agents in the porcine acute embolization model. J Vasc Interv Radiol 2009;20:1597–607.

[161] Lucas F, Shaw JTB, Smith SG. Amino-acid sequence in a fraction of Bombyx silk fibroin. Nature 1956;178. doi:10.1038/178861a0.

[162] Sandberg LB, Soskel NT, Leslie JG. Elastin structure, biosynthesis, and relation to disease states. N Engl J Med 1981;304:566–79.

[163] Haider M, Leung V, Ferrari F, Crissman J, Powell J, Cappello J, et al. Molecular engineering of silk-elastinlike polymers for matrix-mediated gene delivery: biosynthesis and characterization. Mol Pharm 2005;2:139–50. doi:10.1021/mp049906s.

[164] Price R, Poursaid A, Ghandehari H. Controlled release from recombinant polymers. J Control Release 2014;190:304–13.

[165] Megeed Z, Cappello J, Ghandehari H. Genetically engineered silk-elastinlike protein polymers for controlled drug delivery. Adv Drug Deliv Rev 2002;54:1075–91. doi:10.1016/S0169-409X(02)00063-7.

[166] Gustafson JA, Ghandehari H. Silk-elastinlike protein polymers for matrix-mediated cancer gene therapy. Adv Drug Deliv Rev 2010;62:1509–23. doi:10.1016/j.addr.2010.04.006.

[167] Price R, Poursaid A, Cappello J, Ghandehari H. Effect of shear on physicochemical properties of matrix metalloproteinase responsive silk-elastinlike hydrogels. J Control Release 2014.

[168] Gustafson JA, Price RA, Greish K, Cappello J, Ghandehari H. Silk-elastin-like hydrogel improves the safety of adenovirus-mediated gene-directed enzyme-'prodrug therapy. Mol Pharm 2010;7:1050–6. doi:10.1021/mp100161u.

[169] Gustafson J, Greish K, Frandsen J, Cappello J, Ghandehari H. Silk-elastinlike recombinant polymers for gene therapy of head and neck cancer: from molecular definition to controlled gene expression. J Control Release 2009;140:256–61. doi:10.1016/j.jconrel.2009.05.022.

CHAPTER 3

IN SITU GELLING SILK-ELASTINLIKE PROTEIN POLYMER FOR TRANSARTERIAL CHEMOEMBOLIZATION

3.1 Introduction

Embolic agents are frequently used in interventional radiology procedures, and particularly in transarterial embolization treatments of hypervascular tumors. Primary hepatocellular carcinoma (HCC) is one such malignancy, with an annual world-wide incidence of over half a million cases [1]. Despite advances in treatment, HCC remains the third leading cause of cancer-related deaths [2-9]. Treatment selection is directed by the stage of cancer and availability of expertise [2]. Surgical resection in early stage disease with well-preserved liver function may be curative. Less than 30% of the patients fall into this category, and the surgical therapies achieve a 5-year survival ranging 50-75% [6, 9-11]. For the remaining patients, noncurative palliative care or bridge-to-transplant treatments are implemented to improve survival. These include transarterial embolization, and more specifically transarterial chemoembolization (TACE). TACE involves selective access of hepatic arteries supplying the tumor, and administration of a combination of

---

Reprinted with permission of Elsevier. Poursaid A, Price R, Tiede A, Olson E, Huo E, McGill L, et al. In situ gelling silk-elastinlike protein polymer for transarterial chemoembolization. Biomaterials 2015;57:142–52.

chemotherapeutic and embolic agent to reduce tumoral blood supply and induce necrosis [12, 13]. This ability to selectively deliver chemotherapeutic agents allows for a reduction in side effects and preservation of healthy surrounding tissue, while maintaining treatment efficacy.

Biomaterials used in these procedures widely vary region-to-region on a global scale [14, 15]. A presently approved product, Lipiodol®, is a radiopaque ethiodized oil mixed with a chemotherapeutic creating an emulsion often used in conjunction with gelatin particles or synthetic polymer beads, which act as embolics [7, 13, 16]. The oily emulsion penetrates the vasculature, with higher retention levels in HCC as compared to healthy hepatic tissue [13]. The liquid nature allows permeation down to the capillary level, affording more extensive drug exposure. However, the duration of drug release is short (days), and follow-up treatments are not optimal due to the vessel occlusion from the first treatment. Drug eluting beads (DEBs) are now gaining favor for this procedure, replacing the multistep oil emulsion system. These beads provide localized sustained drug release up to 30 days while reducing arterial blood inflow and reducing washout of the chemotherapeutic. However, they too have shortcomings, i.e., aggregation of smaller diameter beads, off target embolization particularly in pulmonary circulation and in the kidneys, elution of only charged small molecule therapeutics, nondegradability, and limited tumor depth penetration [15, 17].

To address limitations of both systems, recombinant silk-elastinlike protein polymer (SELP) formulations that are injectable as a liquid at room temperature, therefore capable of accessing smaller caliber vessels like Lipiodol®, then transitioning into a solid hydrogel at 37°C capable of occlusion and drug delivery like the DEBs, were investigated.

Recombinant polymers offer versatile material platforms in which function can be achieved through precise design of sequence and length. SELPs are a family of genetically engineered protein polymers capable of broad range drug release and tunable physicochemical properties and degradability [18-21]. SELPs are block copolymers consisting of silk-like and elastin-like units. Two compositions, SELP-47K and SELP-815K (Figure 1.1) were chosen for this evaluation based on previous work showing appropriate solubility, solution stability, injectability, gelation rate, and gel strength [18, 19, 22]. Both of these polymers remain soluble in aqueous solution at room temperature and begin to gel as the temperature is raised to 37°C. At this temperature, gelation can occur within minutes. The rate of gelation is dependent on the concentration of the SELP and the level of shear processing the protein experiences prior to use [23]. SELP-47K and SELP-815K have similar molecular weights and silk to elastin compositional ratio (1:2), but lengths of the silk and elastin blocks per repeat are doubled in SELP-815K compared to SELP-47K. The use of multiple SELPs allows examination of the dependency of TACE performance on sequence and compositional difference of the selected polymers.

The SELP embolic was qualified on the basis of two primary performance criteria. The SELP composition had to be injectable through a commercially available microcatheter and had to occlude an *in vitro* model tumor of an arterio-capillary bed under simulated blood flow conditions. Following *in vitro* testing, the formulation showing highest efficacy was then tested *in vivo*, using a rabbit model.

3.2 Materials and methods

3.2.1 Materials

SELP-47K and SELP-815K were synthesized and characterized as previously described [18, 19, 22]. C5 Emulsilex was purchased from Avestin (Ottawa, ON) and modified using high pressure valves and fittings from Autoclave Engineers (Erie, PA). Merit Maestro® Microcatheters, guide wire torque devices, and arterial access kits were donated by Merit Medical Systems (South Jordan, UT). 0.018" Nitinol Mandrel Wire guidewires from GALT Medical (Garland, TX) were used.

3.2.2 Design and fabrication of model microfluidics device

A biomimetic vasculature design was made using AutoCAD software based on the Murray-Hess law of minimal work [24-26]. Size of the arterio-capillary bed was based on the average tumor size in patients with intermediate HCC, a diameter of 4-6 cm. Lithography techniques were used to create a silicon wafer mold for fabrication of devices out of polydimethylsiloxane (PDMS) (Sylgard 184, Dow Corning). PDMS was prepared at a ratio of 10:1 PDMS to curing agent (part of Sylgard kit), and the mixture poured over the mold and into a petri dish for the device backing. The molds were cured in an oven at 65°C for an hour. Inlet and outlet ports were cored out of the backing side of the device sandwich using a 1.5 mm biopsy punch. Next, the PDMS piece retaining the channels design and the flat PDMS backing were corona plasma treated, oxidizing the surface and sandwiched together to create the final device. The seal was tested by injecting a dye solution at a series of pressures.

3.2.3 Formulation development

SELP formulations were made up in 1X phosphate buffered saline (PBS) and concentrations were calculated based on weight. Lyophilized protein for a predetermined concentration was weighed and slowly added to chilled PBS in a 1.7 mL snapseal graduated microtube (GeneMate), while vortexing. The sample was transferred to ice every 30 seconds to maintain low temperatures. Once fully reconstituted, the sample was flash frozen in liquid nitrogen and stored at -80°C until use. Samples prepared for *in vivo* testing were made using sterile, pyrogen-free PBS (Life Technologies) and using aseptic technique. The *in vivo* formulations were stored in capped sterile 1 mL syringes (BD Medical) or CryoFreeze cell culture tubes (GeneMate).

3.2.4 Rheological characterization

Rheological testing was carried out with an AR 550 stress-controlled rheometer from TA Instruments (New Castle, DE) using a steel 20 mm diameter, 4 degree cone-and-plate configuration. Characterization consisted of viscosity testing, carried out using an oscillation procedure with a temperature ramp from 18°C to 37°C at an angular frequency of 6.283 rad/s, followed by an oscillatory time sweep of 5 hrs at 37°C, angular frequency of 6.283 rad/s, and 0.1% strain measuring dynamic viscoelastic moduli G' and G", the storage and loss moduli, respectively. Individual samples previously prepared and stored frozen were thawed just before use in 18-23°C water and centrifuged at 14,000 rpm in a Centrifuge 5417C (Eppendorf) for 45 seconds to remove bubbles. Immediately 150μL was transferred to the Peltier plate, at 18°C. Measurements were conducted in triplicate.

3.2.5 Shearing and contrast incorporation

Shear processing was performed using an Avestin C5 Emulsiflex homogenizer custom modified with a high pressure needle valve fitted with a 3-way Luer-Lok stopcock. Stainless steel parts contacting the sample were depyrogenated prior to use with 0.5 M sodium hydroxide and rinsed with depyrogenated water and PBS. Samples were prepared just prior to processing via reconstitution of lyophilized protein at a predetermined concentration in 1X chilled PBS as previously described. To maintain low temperatures, the homogenizer was submerged in an ice bath. After transferring the polymer sample into the sample cylinder, nitrogen gas was used to pressurize the chamber to 80psi. Slowly opening the homogenizing valve, the sample flowed into the pump body chamber where the motor pump generated 17,000 psi sending the sample through the needle valve and collected into sterile 1 mL syringes (BD Medical). Collected samples were either aliquoted into 1.8 mL CryoFreeze tubes (GeneMate) or the syringes were capped and immediately flash frozen in liquid nitrogen and stored at -80°C. For *in vivo* studies, iso-osmolar contrast dye, Visipaque™ 320 (GE Healthcare), was added during the reconstitution step to 20% by weight and the formulation was sheared as described above.

3.2.6 *In vitro* testing of polymer candidate

To mimic the low blood pressure of the hepatic system, the *in vitro* setup consisted of a syringe pump delivering warmed PBS at 3.4 mL/min via silicone tubing into three fabricated microfluidic devices linked in parallel and partially submerged in a water bath set to 37°C. A pressure gauge monitored the overall pressure, and a temperature probe monitored the internal temperature of the device. During flow, the pressure was maintained

below 1 psi. The device chosen for occlusion testing had a second port for the microcatheter. The microcatheter was submerged in the water bath to equilibrate to temperature. 1 mL of the SELP candidate formulation was manually injected using a 1 mL syringe (BD Medical) over 30 seconds.

3.2.7 *In vivo* feasibility testing of polymer candidate

Hepatic embolization was conducted in male New Zealand white rabbits (4-4.5 kg body weight) to verify the occlusive ability of the candidate SELP formulation *in vivo*. The procedural protocol was approved by IACUC and conducted in accordance with all applicable regulations. The surgical procedure consisted of anesthetizing the animal and exposing the right femoral artery via a surgical cutdown. Arterial access was obtained with a radial artery line kit. 2% lidocaine (Vetone) was dripped onto the vessel to prevent spasm during needle and sheath insertion. The microcatheter was advanced under fluoroscopic guidance using a OEC/GE Series 9800 Mobile C-arm (GE Healthcare, Little Chalfont, UK) up the femoral artery and aorta into the celiac trunk. Depending on the size of vessels and the anatomical variation, the catheter was maneuvered up the common hepatic artery, into the proper hepatic artery, and if vessel diameter permitted, either the left or right hepatic artery. Visipaque™ 320 contrast dye was used to visualize the vessels. Following identification of the vessel, a 1 mL syringe of the sheared 12% w/w SELP-815K containing 20% w/w Visipaque™ 320 was thawed, centrifuged (Forma 400 ML GP Centrifuge, Thermo Electron Corp.) for 45 seconds to remove bubbles, and manually injected under fluoroscopic visualization. Following injection, a volume of sterile saline equivalent to the holdup volume of the catheter (0.6 mL) was injected to expel the SELP from the catheter.

Five minutes was allotted for gel formation, after which contrast dye was injected to determine the level of occlusion. Another 5-minutes was allotted, followed by a second contrast injection, to ensure the SELP embolus remained lodged. Following imaging, the animal was euthanized. For a histological control, one animal underwent the entire procedure except it was injected with saline only. Each of the three test animals had a preinjection contrast angiogram showing flow, thus acting as a control prior to SELP injection. The procedures were conducted by an interventional radiologist who specializes in TACE procedures.

3.2.8 Histological analysis

Liver and lungs of each animal were immediately fixed in 10% buffered formalin for 48 hrs and then transferred to 70% ethanol. Sections from each liver lobe and each lung lobe were cut in 5 μm slices and analyzed. Tissue samples were stained using both hematoxylin and eosin (H&E) stain and an immunohistochemistry (IHC) stain specific for SELP using an antibody for poly-Histidine (anti-6X His tag®, Abcam, Cambridge, MA; 1:3000 dilution), which is found in the carboxyl-terminal sequence of the SELP polymer strand. A chromogenic detection was used, IView diaminobenzidine research detection kit (Ventana Medical Systems) and hematoxylin counterstain (Ventana Medical Systems) in the IHC procedure. A piece of pregelled SELP was fixed, sliced, mounted onto a slide, and stained as a positive control using both stains. Slides were imaged using a Nikon DXM 1200C Digital Camera affixed to an Olympus BH2 microscope and analyzed in ACT-1C for DXM1200C software.

3.2.9 Statistical analysis

All experiments were conducted in triplicate and data are presented as the mean ± standard error of the mean unless specified otherwise. For the rheological traces of the moduli, the raw data were processed using a rolling average of 10 points to minimize noise, particularly in the slower gelling formulations. Significance between multiple groups was determined using a one-way analysis of variance (ANOVA) with a Tukey's posttest, and a two-tailed Student's t-test was used for comparing pairs of data. Significance was reported as $p<0.05$, highly significant when $p<0.01$, and very highly significant when $p<0.001$.

3.3 Results

3.3.1 Design and fabrication of model microfluidics device

The goal of the model design was to mimic the microcirculation of vessels feeding a hepatic tumor, particularly arterioles, which range in size from 10-100 μm. Using the Murray-Hess law as a guideline for calculating the channel widths of daughter branches, the entry branch was 1000 μm in width, branching down consecutively until reaching central channels 50 μm in width (Figure 3.1). Size and geometry of the channels were limited by the loft lithography technique used to create the device mold. Channel height was 100 μm throughout the entire length of the device. The *in vitro* microfluidics device provided a method to create a system where overall pressure drops as the total area increases with each branch point. This idea was verified when multiple devices were connected in a parallel circuit, representing acini in a liver lobe, and the overall pressure dropped from an average of 5.6 ± 0.7 (SD) psi when a single device was attached to 4 psi when two were connected and then down to 0 psi when three were connected in parallel.

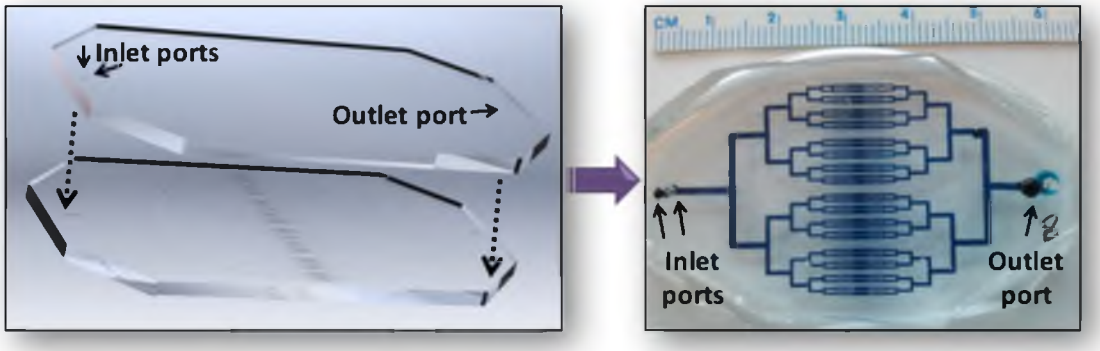

Figure 3.1. Three-dimensional model of the microfluidics device designed and fabricated to represent the vasculature of a hepatic tumor. The entry channel is 1000 μm in width and each branch divides into two daughter branches until reaching 50 μm, representing small arterioles, then increasing in size back to 1000 μm. The height of the channels is 100 μm throughout the device. Soft lithography techniques were used to fabricate the device mold, and the devices were constructed of polydimethylsiloxane (PDMS).

Sensitivity of the pressure gauge was not high enough to determine pressures between 0 and 1 psi. Fabricated devices were all checked with dye colored water for any potential leaks prior to use in the *in vitro* experiments.

3.3.2 Formulation development

The viscosity, gelation time, and mechanical properties of SELPs not only depend on the composition of the polymer sequence, but also on the concentration of the polymer solution and its shear processing. Target specifications for the maximum viscosity, the maximum gelation time and the minimum gel stiffness were defined either experimentally or empirically. The maximum viscosity able to be injected through a commercial microcatheter was determined to be 150 cP, using silicone oil standards (Brookfield). The maximum gelation time was set at 5-minutes to allow enough time for injection, but short enough for the gel to set prior to venous washout. A minimum gel stiffness at 5 hr of 1E5 Pa was set based on empirical evidence. Testing of formulations began with 16% w/w (weight percent) of SELP-47K and -815K, the maximum solubility for each polymer. The lyophilized polymers were reconstituted in PBS and immediately underwent rheological testing. Evaluations continued with polymer concentrations of 14 and 12% w/w. Shearing was evaluated for its effect in improving gelation time and final gel stiffness. In this case, sheared formulations were processed and frozen in liquid nitrogen prior to thawing and testing.

3.3.3 Rheological characterization and finalization of candidate formulation

Each rheological run consisted of a viscosity measurement followed by a 5-hr oscillatory trace of the polymer sample to measure the viscoelastic moduli, G' and G". Formulations were evaluated by comparing the sol/gel transition point (the crossover point of G' and G") and the gel stiffness at 5 hr (G' plateau). A viscosity specification was set based on the injectability of silicone oil standards through tubing of inner diameters similar to clinical microcatheters. In the injection temperature window of 18-25 °C, the maximum injectable viscosity was 150 cP. As a reference, Lipiodol® viscosity at 20°C is 34-70 cP. The first formulations tested were 16% w/w SELP-47K and SELP-815K (both with no shear processing). Viscosity of the formulations remained well below the specified value (Figure 3.2A). However, the oscillatory traces (Figure 3.3A and B) demonstrated insufficient gel time and mechanical properties. Nonsheared 16% w/w SELP-47K required over 100-minutes to reach its gel point, G'>G", and the final gel stiffness at 5 hr (5.9E1 Pa) was orders of magnitude less than the specified value (1E5 Pa). Compared to SELP-47K, the nonsheared 16% w/w SELP-815K reached its gel point faster (3.5-minutes) and achieved a greater gel stiffness at 5 hr (3.7E4 Pa); however, the gel stiffness did not meet the specified value either.

With these results, the SELP-815K formulation underwent shear processing. As expected, shearing caused a dramatic increase in gelation. Shearing of the 16% w/w SELP-815K caused the material to immediately gel. At 14% w/w, SELP-815K still gelled at room temperature prior to freezing and storage and the viscosity was nearly 700cP at the outset and rose with increasing temperature (Figure 3.2B). The SELP-815K concentration was

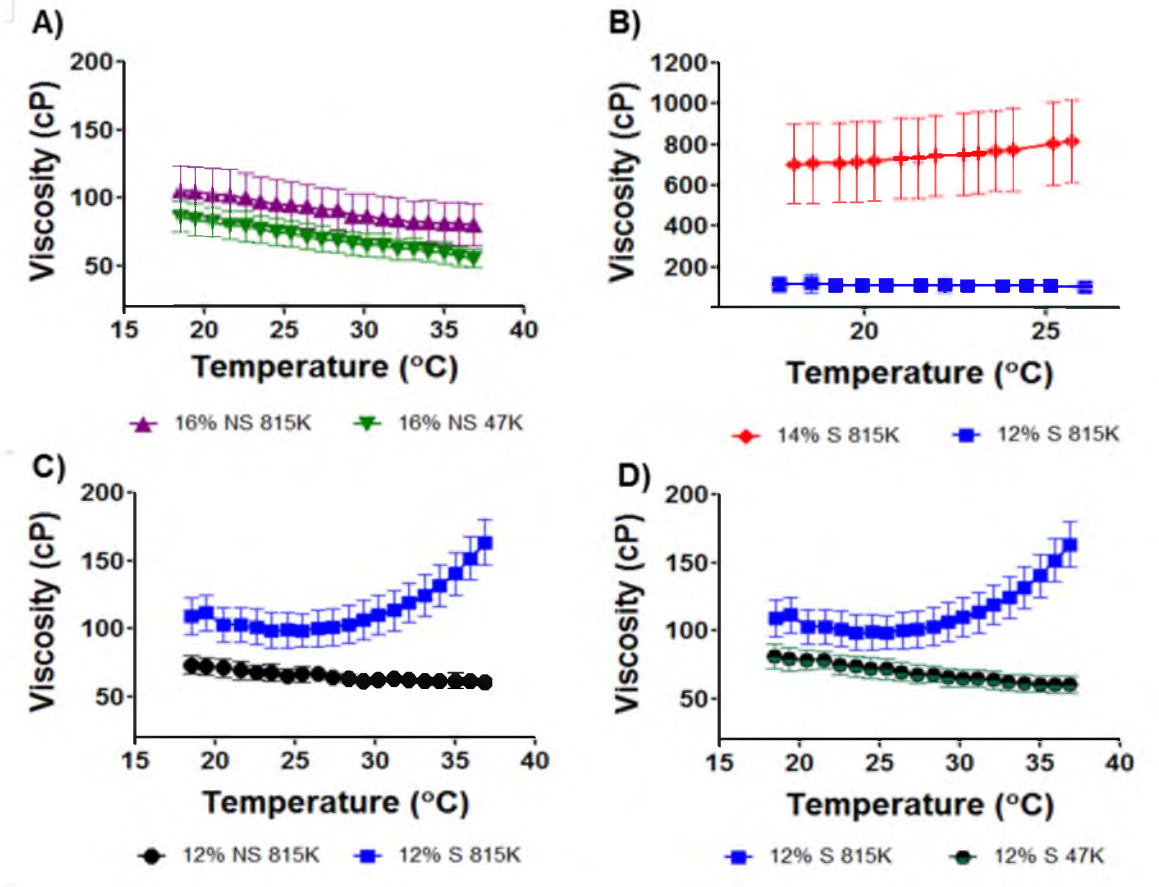

Figure 3.2. Viscosity traces of candidate polymer compositions. The maximum viscosity target of 150 centipoise (cP) was specified to permit a formulation to be injectable through a commercially available 2.8F microcatheter. Viscosities were measured between 18 and 37°C, representing the injecting temperature range. A) 16% w/w formulations of reconstituted lyophilized polymer nonsheared (NS) of both SELP-47K (47K) and SELP-815K (815K) remained below 150cP. B) 14% w/w sheared SELP-815K began to gel upon thawing the sample and the viscosity was above the specification. Reduction to 12% w/w sheared SELP-815K provided appropriate viscosity. C) Comparison of nonsheared and sheared 12% w/w SELP-815K. 12% sheared (S) SELP-815K showed increasing viscosity as a result of network formation but the viscosity remained in the injectable range. D) Comparison of 12% w/w sheared SELP-815K and SELP-47K. The lack of increasing viscosity with increasing temperature by 12% w/w sheared SELP-47K indicated slower network formation. For all traces N=3 ± SEM.

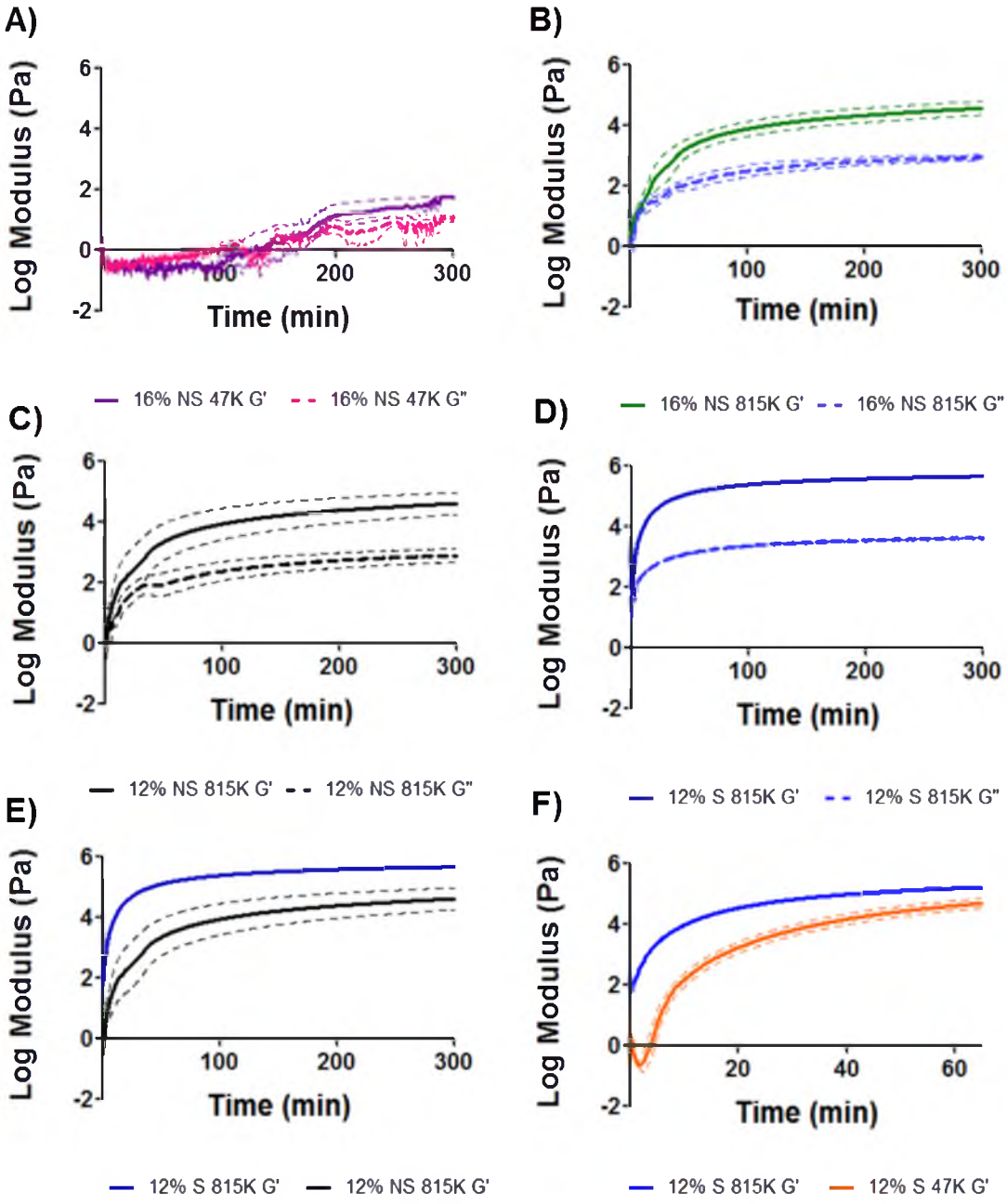

Figure 3.3. Rheological characterization of candidate polymer compositions. The shear storage modulus, G', and the shear loss modulus, G", were measured and used to assess time to gel formation and final gel stiffness over 5 hr. Panels A-D provide G'/G" traces of candidate compositions. Panel E compares G' of sheared and nonsheared 12% w/w SELP-815K, showing the effect of shear processing on final gel stiffness. Panel F shows the difference in rate of gelation between 12% w/w sheared SELP-815K and 12% w/w sheared SELP-47K; the faster gelation by 12% w/w sheared SELP-815K finalized the selection of this candidate to move into *in vitro* testing. All traces N=3 ± SEM.

reduced further to 12% w/w and the formulation was tested and compared both with nonsheared and sheared. While shearing increased the viscosity of the formulation, it remained less than the specified 150 cP until reaching close to body temperature (Figure 3.2B). The mechanical differences between nonsheared and sheared 12% w/w SELP-815K were evident in the oscillatory traces (Figure 3.3C-E). The 5 hr stiffness of sheared 12% w/w SELP-815K (4.4E5 Pa) was significantly greater than nonsheared 12% w/w SELP-815K (4.2E4 Pa) (Figure 3.4A). Additionally, shearing reduced the sample-to-sample variability as evident by the decrease in average standard error of the mean from 0.020 to 0.012 for nonsheared and sheared 12% w/w SELP-815K, respectively.

Lastly, 12% w/w SELP-47K was sheared and compared to sheared 12% w/w SELP-815K. Viscosity of 12% w/w SELP-47K remained less than 150 cP (Figure 3.2D) and no statistically significant difference in 5-hr stiffness was observed compared to sheared 12% w/w SELP-815K (Figure 3.4A). However, the gel stiffness at 5-minutes of the 12% w/w SELP-47K was significantly less than SELP-815K (Figure 3.4B), possibly indicating that SELP-47K might be less resistant to venous washout. Based on these results, the sheared 12% w/w SELP-815K met the property specifications of viscosity <150 cP, gelation time <5 min, and final gel stiffness >1E5 Pa, therefore proceeded to further testing. The 12% w/w SELP-47K was eliminated because of its inferior gel stiffness at 5-minutes.

3.3.4 *In vitro* testing of polymer candidate

Having met the rheological properties specifications, sheared 12% w/w SELP-815K was tested in an *in vitro* vessel occlusion model designed to simulate a TACE procedure (Figure 3.5). A single microfluidic device under a flow rate of 3.4 mL/min produced an overall systemic pressure of 6 psi (310 mmHg). Hepatic sinusoids have

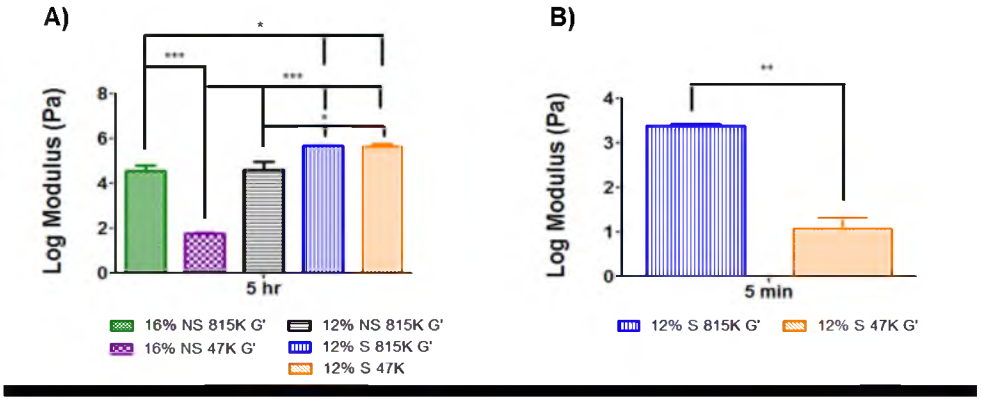

C) Systematic elimination of formulation candidates (mean ± SEM)

Polymer composition	*Weight percent (%)*	*Non-sheared/ sheared*	*Viscosity at 25°C (cP)*	*Log 5 min gel stiffness (Pa)*	*Log 5 hour gel stiffness (Pa)*	*Outcome*
SELP-47K	16	NS	73.89 ± 9.38	-0.41 ± 0.12	1.77 ± 0.05	Reject
SELP-815K	16	NS	94.66 ± 17.06	1.10 ± 0.17	4.57 ± 0.22	Reject
SELP-815K	14	S	806.10 ± 203.55	NA	NA	Reject
SELP-815K	12	NS	66.62 ± 5.63	1.07 ± 0.46	4.62 ± 0.36	Reject
SELP-47K	12	S	71.90 ± 7.58	0.76 ± 0.42	5.64 ± 0.15	Reject
SELP-815K	12	S	98.72 ± 12.38	2.48 ± 0.07	5.67 ± 0.02	**Accept**
SELP-815K + Contrast	12	S	107.95 ± 18.22	3.38 ± 0.04	5.65 ± 0.07	**Accept**

(n = 3)

Figure 3.4. Comparison of the rheological characteristics between candidates. Panel A presents a comprehensive comparison of the 5 hr stiffness of the formulations. Statistical significance is evident between all groups except 12% w/w sheared SELP-815K and 12% w/w sheared SELP-47K. Panel B compares the 5-minute modulus between 12% w/w sheared SELP-815K and 12% w/w sheared SELP-47K, showing that the SELP-815K formulation gels significantly faster. Panel C presents a summary of the key parameters and their results used to identify the suitable candidate for an embolic, 12% w/w sheared SELP-815K. *p<0.05, **p<.01, ***p<.001.

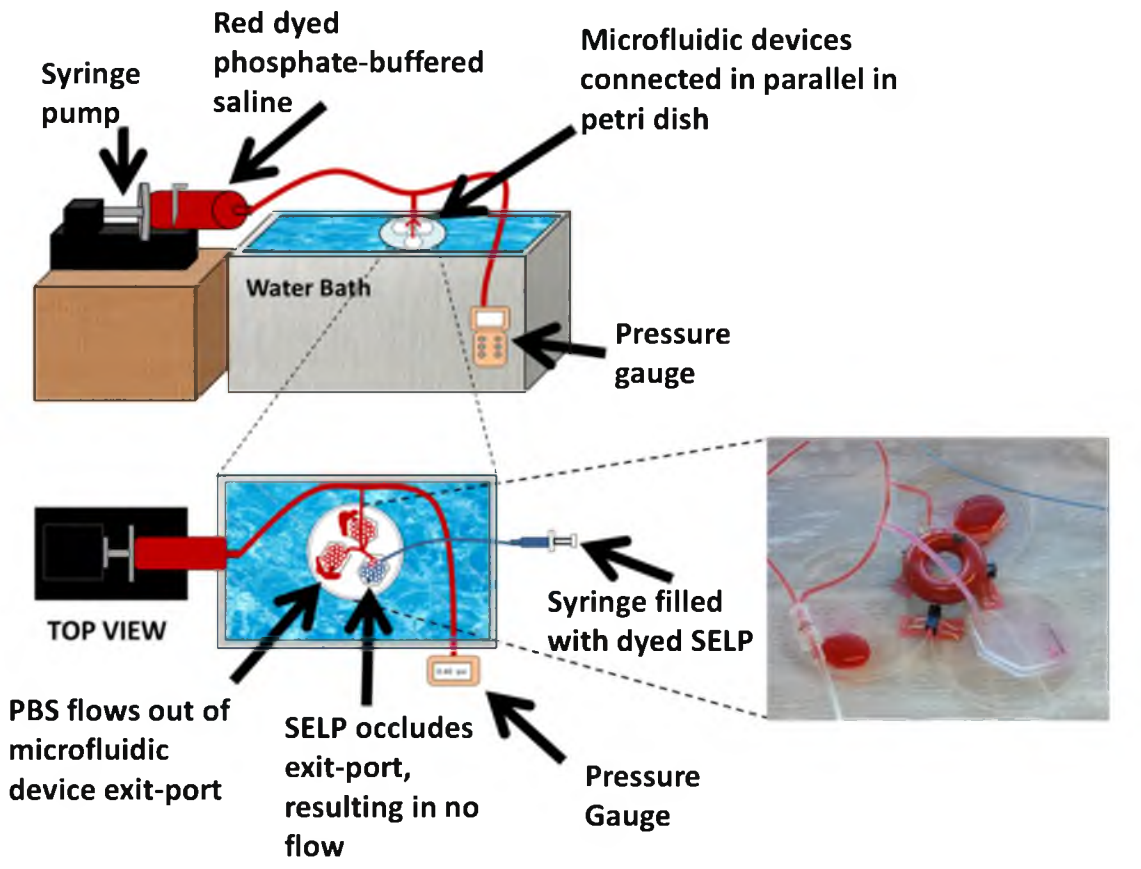

Figure 3.5. Schematic of the *in vitro* test setup. Setup used to evaluate the occlusive ability of the candidate formulation under flow conditions. The image shows occlusion of the microfluidics device by 12% w/w sheared SELP-815K.

blood pressure dropping below 10 mmHg [27]. Therefore, multiple microfluidic devices were linked in parallel in order to increase the overall cross sectional area of the fluid path, thus decreasing the overall systemic pressure at this flow rate. Linking 3 microfluidic devices in parallel yielded an overall systemic pressure <1 psi (<52 mmHg), comparable to physiological pressure in liver sinusoids, and this configuration was used for all occlusion tests. Furthermore, the cross sectional area of a single center channel in the microfluidics device equates to the same cross sectional area of a 12 μm diameter vessel (size of a small terminal arteriole). The flow rate of 3.4 mL/min translates to 20 mm/s velocity within the central channels, which is similar to the mean physiological velocity of erythrocytes in arterioles up to 60 μm diameters (from 1.0-31.7 mm/s) [28]. While not perfect, the microfluidic device was considered sufficient for screening of the SELP embolic candidate for preliminary occlusion before advancing to *in vivo* testing.

Three microfluidic devices were connected in parallel and allowed to equilibrate to 37°C submerged in a water bath. Warm PBS was circulated through all three devices at 3.4 mL/min using one of the two inlet ports of each device. A 150 cm 2.8 F microcatheter was flushed with warm PBS, connected to a 1 mL syringe filled with sheared 12% w/w SELP-815K, and inserted into the second inlet port of one of the devices. The formulation was injected over 30 seconds. The injected material visibly filled the channels of the device, with approximately 100-150 μL flowing out before occlusion occurred. Occlusion was evident by the absence of forward flow and the reflux of the inflow PBS (see inset photograph in Figure 3.5). Consequently, the systemic pressure spiked to 4 psi (207 mmHg), also consistent with occlusion of the injected device. The test was repeated 3 times, and in each trial sheared 12% w/w SELP-815K showed similar blockage, reflux,

and pressure spikes indicative of an effective embolic. Thus, the sheared 12% w/w SELP-815K formulation moved forward to *in vivo* testing.

3.3.5 *In vivo* feasibility testing of polymer candidate

Sheared 12% w/w SELP-815K was tested for vascular occlusion *in vivo* using male New Zealand white rabbits. Male rabbits were selected because their arterial blood vessels were large enough for endovascular access of the liver using human microcatheters. Contrast dye was included in the 12% w/w SELP-815K formulation at 20% by weight to aid in visualization during injection. The formulation with contrast dye was characterized to verify that no substantive changes occurred in mechanical properties, gelation, or injection properties (Figure 3.4C).

While the rabbits were under general anesthesia, a 2.8 F microcatheter was maneuvered to the proper hepatic artery; however, the right or left hepatic arteries could not be effectively discriminated. A control animal was injected with saline only, equivalent to the volume of the SELP formulation, and the animal was euthanized. The saline control animal served for tissue comparisons postsurgery. SELP-815K was injected into three animals. Pre-injection angiograms showed contrast filling the liver blood vessels confirming full patency of blood flow (Figure 3.6A). Each rabbit was injected with 0.8-0.9 mL of sheared 12% w/w SELP-815K in a 1 mL syringe, followed by 0.6mL of saline to flush the polymer from the catheter. Following a 5-minute gelling period, the catheter was pulled back approximately 2-5 millimeters and contrast was injected to assess the level of stasis. Stasis was indicated by the increased pressure required to administer the contrast and visually by the absence of forward flow of contrast (Figure 3.6B). While the addition

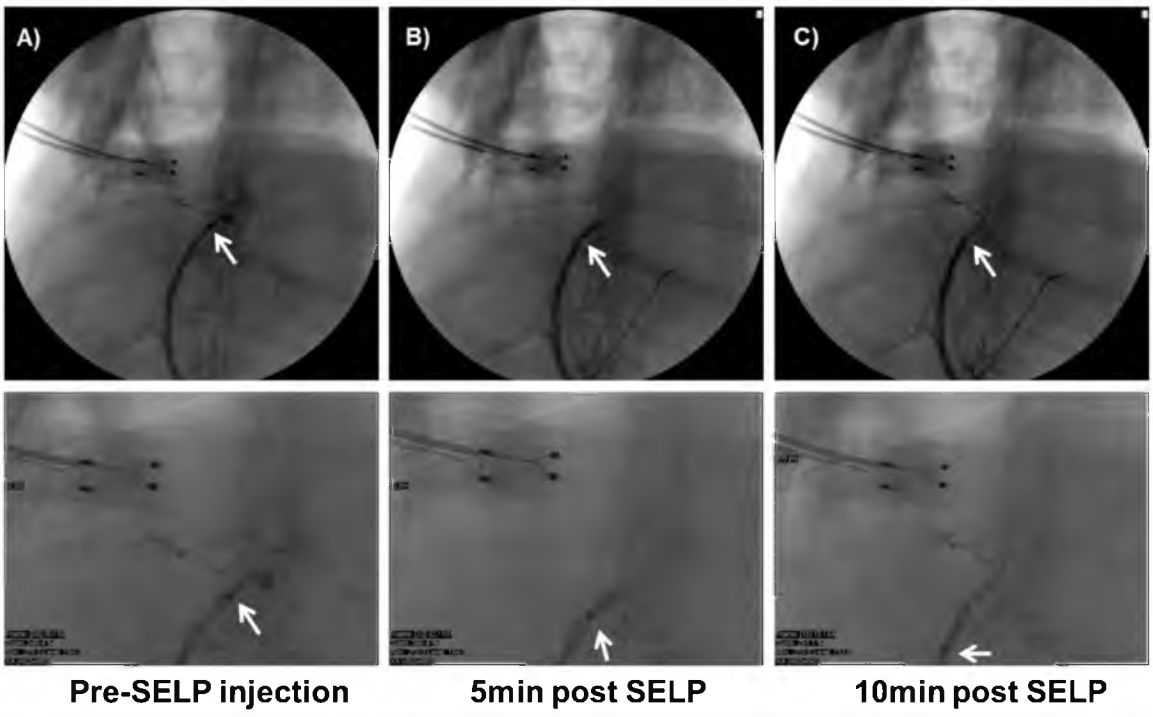

Figure 3.6. 12% w/w sheared SELP-815K tested *in vivo* in male New Zealand White rabbits. A) Contrast observed filling the hepatic arterial supply, with catheter tip in proper hepatic artery. B) Contrast angiography at 5-minutes post SELP injection shows hard stasis, no flow into hepatic branches. C) Contrast angiography at 10-minutes post SELP injection shows continued stasis. Below each panel, higher magnification of the image is shown for clarity.

of contrast dye to the SELP-815K formulation aided in visualizing the injected polymer in the major artery at the point of injection, it was not sufficient to visualize the polymer in the smaller vessels nor did it interfere with postinjection angiographic assessment. At 10-minutes postinjection, contrast was readministered as the catheter was pulled back a few more millimeters. Persistence of the embolus and resistance to contrast injection verified clinically-termed hard stasis (Figure 3.6C). The animal was then euthanized and organs were harvested for histological analysis.

3.3.6 Histological analysis

The liver and lungs were immediately harvested for fixation in 10% buffered formalin. Sections from each lobe of the liver were analyzed. Anatomically, the hepatic artery branches down to terminal arterioles that are an element of the portal triad, consisting of a bile duct, arteriole, and venule [29]. These terminal arterioles transition into an arteriosinusoidal branch that continues and becomes the hepatic sinusoids, which empty into the central vein. Lymphatic vessels communicate with these branching vessels of the portal triads as well. In analysis of the liver sections, these anatomical markers were used to identify the path of the injected SELP. The histological images (shown in Figure 3.7A-B) provide a direct comparison of the control saline injected animal to a SELP-815K injected animal, focusing on a portal triad, the arterioles (indicated by arrows) and the terminal branches of the portal vein (indicated by arrowheads) The histological sections of the control animals showed arterioles, clearly demarcated by a ring of smooth muscle, filled with red blood cells, indicative of patency. The H&E stained histological sections of SELP-815K-injected animals, showed arterioles filled with an amorphous pink substance.

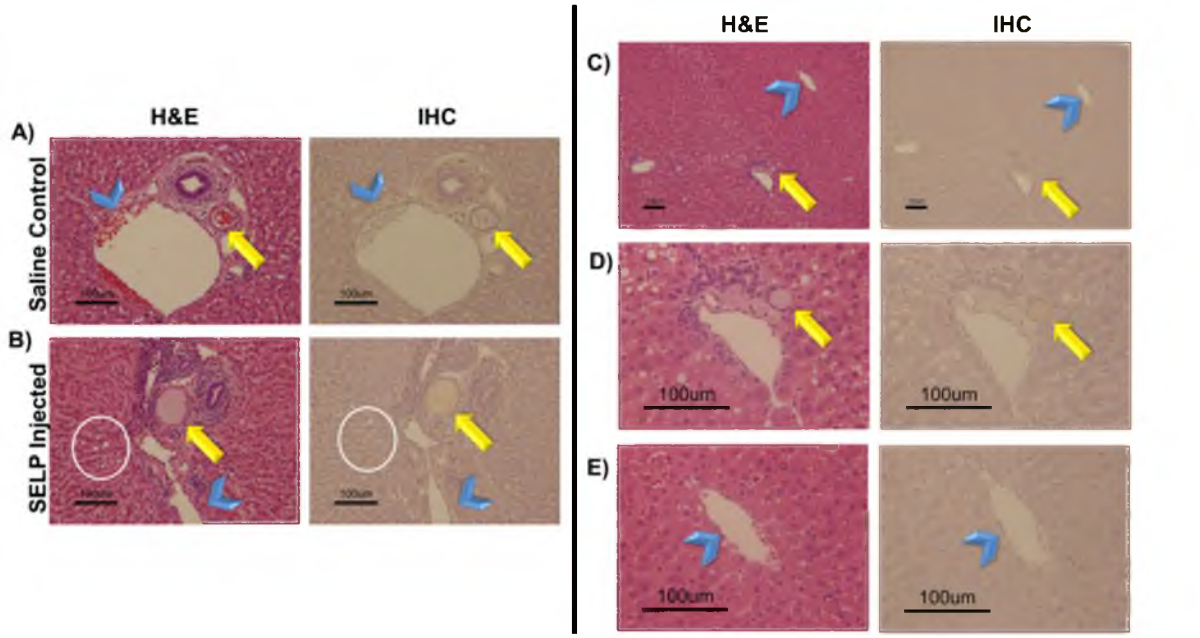

Figure 3.7. Histological analysis of hepatic tissue locating embolic material. Rows A) and B) provide histological comparison of control and test animal hepatic tissues showing evidence of SELP filling the hepatic arteriole. Both hematoxylin and eosin (H&E) stain and an immunohistochemistry (IHC) stain specific for SELP were used for visualization. The arrow indicates arterioles and the arrowheads indicate the portal venules, for reference. The presence of vacuolization in the hepatocytes of the test animal (encircled) provides more evidence of hypoxic damage induced by occlusion of the hepatic arterial vessels upstream. Images taken at 152X total magnification. Rows C-E) show evidence of SELP within hepatic arterial supply (indicated by the arrows) and no evidence of flow through into the venous drainage via the hepatic central veins (indicated by the arrowheads). Row C, images taken at 30X total magnification, showing a portal triad and its draining central vein. Rows D and E show the portal triad and central vein individually at 152X total magnification. SELP is evident in row D within the arteriole indicated by the arrow. SELP is not evident tracking to or entering the draining central vein in row E.

Previous work in our lab has identified SELP-815K histologically by H&E after intratumoral injection as an amorphous pink substance [30]. To confirm its presence, an IHC staining technique using antibodies against SELP-815K identified the polymer signal by correlation with positive control samples of fixed and sectioned SELP-815K gels. In addition to the physical presence of the SELP-815K in the arterioles, a functional attribute of embolization was also evident. Hepatocytes in the histological sections of the SELP injected animals (Figure 3.7B**,** encircled in white) showed a high degree of vacuolization, which is a physiologic response to hypoxia. All sections were examined for SELP-815K in draining veins. SELP was visible periodically in hepatic sinusoids, which anastomose with the hepatic arterioles, but there was no evidence of SELP in the draining central veins (indicated by arrowheads in Figure 3.7). A series of panels tracking SELP in a portal triad arteriole (arrow) to the draining central vein with increasing magnification are shown in Figure 3.7C-E. Row 3.7D shows the portal triad. Again, SELP is seen filling the entirety of the arteriole. At this magnification, vacuolization is also very apparent in adjacent hepatocytes. Row 3.7E shows the central vein. No SELP was identified and the amount of red blood cells both within the vein and the venules draining into the vein is less than seen in the control tissues, consistent with upstream blockage. Both lungs were also sectioned and examined for off target embolization (Figure 3.8). Multiple sections from each lobe were examined both by H&E and IHC and no evidence of SELP was identified.

3.4 Discussion

Hepatocellular carcinoma has recently emerged as the third leading cause of cancer-related death worldwide [2-9]. The World Health Organization reported 745,000 deaths in

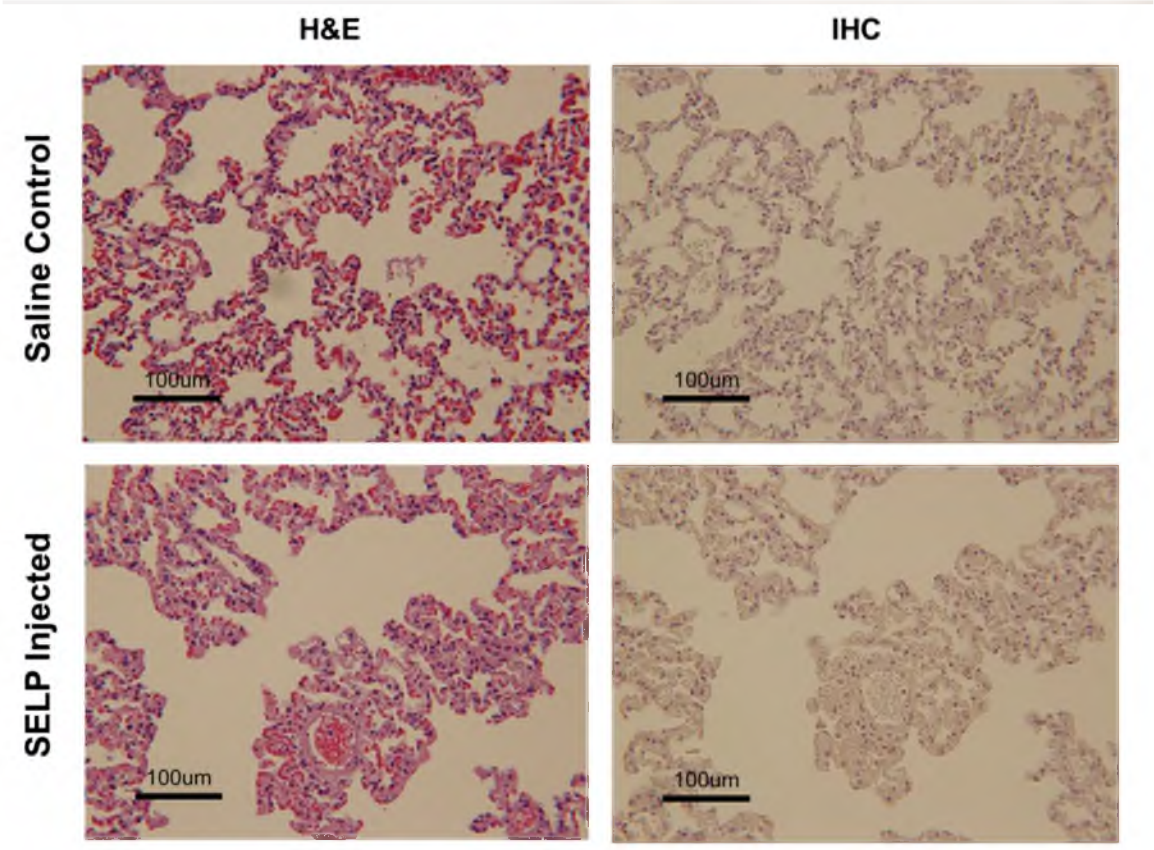

Figure 3.8. Histological sections of rabbit lungs. Panels A and B are sections from a saline control animal. Panels C and D are sections from an SELP injected animal. No evidence of SELP in the lungs of test animals was found. Lungs did not show signs of vascular occlusion. Images taken at 76X total magnification.

2012. Transarterial chemoembolization, although not curative, has proven to be an effective therapy for intermediate stage disease [9, 10]. However, the materials used in this treatment are highly variable and no global standard exists. The two leading systems include Lipiodol® emulsion with a chemotherapeutic agent that must be followed by particulate embolization with Gelfoam® and drug eluting beads, such as DC Bead®. The attributes of each system were considered and used in the design of a novel embolic using the *in situ* gelling SELP biomaterial. The goal of this work was to formulate an injectable, aqueous-based material using silk-elastinlike protein polymers capable of transitioning into a physical hydrogel network *in vivo* without solvent displacement. The system would serve a dual purpose: vessel occlusion and drug delivery. The advantage of the liquid Lipiodol® drug emulsion over the drug eluting beads (DEBs) is its deep permeation into the tumor vasculature, increasing the total diffusive area of the co-administered drug. A liquid SELP formulation would retain this characteristic. The advantage of the solid DEBs is their immediate occlusion of blood vessels upon injection. A SELP that rapidly transitions to a solid hydrogel would achieve this characteristic as well. Therefore, a SELP embolic encompassing the occlusive properties of DEBs and the vasculature permeation of Lipiodol® could provide a single embolizing agent capable of localized release of a variety of therapeutic drugs. The aim of this work was to produce an injectable SELP formulation that undergoes sol-to-gel transition at body temperature, lodges at the arteriole level and induces hemostasis. Importantly, injectability through commercially available microcatheters commonly used in TACE procedures was required. The maximum injectable viscosity of 150 cP eliminated several candidates. A balance between mechanical properties comprising rapid gelation, robust gel stiffness and injectable

viscosity had to be achieved. Because several requirements had to converge, a panel of formulations including two polymers, SELP-47K and SELP-815K, were tested. Formulations of reconstituted lyophilized polymer with no shear processing were initially characterized and while meeting the viscosity specification, they lacked sufficient gelation speed and mechanical stiffness.

Based on previous experience [23], shear processing of the polymer formulations was used to improve the mechanical properties. The effect of shear was clearly shown in both viscosity and gelation. It is hypothesized that the shearing breaks weak intramolecular bonds and allows the polymer strands to align, making stronger long range hydrogen bonds intermolecularly between silk units, which are the chief networking component in SELP hydrogels [23]. While the shearing of high concentration SELP formulations (16% w/w and 14% w/w) resulted in too rapid gelation and excessive viscosity, sheared 12% w/w SELP-47K and SELP-815K both resulted in acceptable viscosity (<150 cP), gelation (<5-minutes), and gel stiffness (>1E5 Pa at 5 hr). The two formulations, however, were distinguished by their gel stiffness at 5-minutes, which if maximized was considered a potential benefit in rapid vascular occlusion. Sheared 12% w/w SELP-815K achieved 10-fold greater gel stiffness at 5-minutes than sheared 12% w/w SELP-47K. The difference was attributed to SELP-815K's increase in the number of silk and elastin units per polymer repeat (2X) compared to SELP-47K. Thus, sheared 12% w/w SELP-815K was the selected formulation.

Following formulation identification, *in vitro* studies were conducted to determine if the sheared 12% w/w SELP-815K composition would occlude a microfluidics device representative of a vasculature system under flow conditions. The design of the device

provided a simulated environment in which pressure drops occurred with each set of daughter branches to mimic the low pressure environment of hepatic microcirculation. The average blood pressure entering the hepatic artery is 90 mmHg, which quickly drops to <10 mmHg at the arteriosinusiods. By connecting several devices in parallel, representing the hepatic lobules, a low pressure environment was created (<52 mmHg). Injection of sheared 12% SELP-815K under flow conditions successfully and consistently occluded the device. To verify the effect of concentration and shearing on the gelation kinetics, non-sheared samples of both SELP-47K and SELP-815K at 12% and 14% were tested in the *in vitro* setup, and as the rheological data predicted, the injected polymer solutions flushed straight through the devices under flow conditions. Sheared 12% SELP-47K also did not perform as a successful embolic; more than 50% of the injected volume flushed through and only parts of the tested devices were occluded. Therefore, in this *in vitro* setup, the performance of the sheared 12% SELP-815K was optimal, particularly in comparison to all other candidates.

Occlusion in the *in vitro* test warranted *in vivo* investigation. New Zealand white rabbits were chosen in order to enable the use of commercially available microcatheters. While the proper hepatic artery of the rabbit was accessed with the 2.8F microcatheter under fluoroscopic imaging, the right and left hepatic arteries were too small. Therefore, SELP-815K was injected proximally to the branch point of the vessel. Angiography, before and after SELP injection, visibly verified hard stasis in the hepatic vasculature. Flourographic images clearly demarcated the point of stasis (Figure 3.6). No forward flow of contrast was identified. Additionally, injection of contrast following SELP embolization required increased injection pressure. This resistance indicated clinically described hard

stasis. Furthermore, the second injection of contrast 10-minutes postembolization showed a stable embolus that did not reorganize or move, a phenomenon observed with gelatin particles used with Lipiodol. Injection of the SELP formulation also required less force than the commercial products and required less material to achieve the same level of stasis. Only 0.8-0.9 mL of SELP was used to embolize the vessels as compared to the 2-4 mL of microspheres (total volume of beads) typically used in a TACE procedure [31]. The SELP formulation did not require multiple injections to achieve occlusion, contrary to microspheres in clinical practice.

Histological analysis of the hepatic tissue complemented the observations during the procedures. SELP-815K was identified within the hepatic arterioles that make up part of the portal triad. SELP was also identified in associated lymphatic vessels, as expected because they intimately interact with the arterioles as well as the sinusoids as they empty into the central veins. The portal venules, also part of the portal triad, anastomose with the hepatic arterioles and provide an avenue for SELP to enter. However, SELP was observed within these venules only in two instances. The portal venules also dump into the sinusoids, which channel blood flow into the central veins, and continue to form the hepatic veins and subsequently the vena cava. There was no evidence of SELP in any of the draining veins indicating that the SELP embolic gelled within the arterial branches with no evident venous washout. Furthermore, the hepatic tissue of the SELP injected animals showed high degrees of vacuolization in the hepatocytes. Hepatocytes are highly metabolically active and small changes in blood supply induce damage evident by vacuolization. Decreased amount of red blood cells throughout the capillaries was another confirmation of upstream occlusion as compared to the saline control samples. Finally, as another assessment of

venous washout, the lungs were examined for any off target embolization. No evidence of SELP was present in the lungs of the SELP injected animals. The lung ultrastructure was similar between the saline control and SELP injected animals. Embolization with microspheres has been associated with migration of particles to the lungs [32, 33]. Although these *in vivo* tests were a feasibility study, the results provide clear indication that the sheared 12% w/w SELP-815K formulation formed a solid gel network within the catheterized arteries of the liver and remained lodged in the hepatic tissue. No off target embolization indicates that the SELP formulation entered the microcirculation of the liver and gelled before venous washout, satisfying the final specification and validation of our hypothesis. Further investigation of *in vivo* performance and safety of SELP-815K over longer periods of time to determine intravascular stability, both in tumor and nontumor bearing animals, is warranted. Moreover, a drug delivery component must be added to develop a therapeutically effective chemoembolic to treat hepatocellular carcinoma.

3.5 Conclusion

Based on specified design parameters, sheared 12% w/w SELP-815K formulation was developed as an injectable embolic candidate. *In vivo* evaluation provided further evidence that this material occluded the targeted hepatic arterial blood supply in the rabbit liver. Histological examination of the injected tissue showed SELP occluding at the arterial level without drainage into the venous system via the central veins to systemic circulation. These data suggest that SELP-815K may be used as an *in situ* gelling liquid embolic in TACE and warrants further investigation to determine long term residence and therapeutic efficacy in hepatic tumors. The next phase of this work requires investigation of drug

loading levels of the gel followed by chemotherapeutic effects.

3.6 References

[1] Center MM, Jemal A. International Trends in Liver Cancer Incidence Rates. Cancer Epidemiology Biomarkers & Prevention. 2011;20:2362-8.

[2] El-Serag HB. Hepatocellular Carcinoma. New England Journal of Medicine. 2011;365:1118-27.

[3] Montella L, Addeo R, Caraglia M, Del Prete S. Latest Developments in Targeted Therapy for Hepatocellular Carcinoma. Expert Review of Anticancer Therapy. 2010;10:1635-46.

[4] Brown DB, Nikolic B, Covey AM, Nutting CW, Saad WE, Salem R, et al. Quality Improvement Guidelines for Transhepatic Arterial Chemoembolization, Embolization, and Chemotherapeutic Infusion for Hepatic Malignancy. Journal of Vascular and Interventional Radiology. 2012;23:287-94.

[5] Forner A, Llovet JM, Bruix J. Hepatocellular Carcinoma. Lancet. 2012;379:1245-55.

[6] SEER Cancer Statistics Review, 1975-2009 (Vintage 2009 Populations). National Cancer Institute. Bethesda, MD, 2011. Available from URL http://seer.cancer.gov/csr/1975_2009_pops09/.

[7] Bruix J, Sherman M. Management of Hepatocellular Carcinoma. Hepatology. 2005;42:1208-36.

[8] Hernandez-Gea V, Toffanin S, Friedman SL, Llovet JM. Role of the Microenvironment in the Pathogenesis and Treatment of Hepatocellular Carcinoma. Gastroenterology. 2013;144:512-27.

[9] Llovet JM, Bruix J. Systematic Review of Randomized Trials for Unresectable Hepatocellular Carcinoma: Chemoembolization Improves Survival. Hepatology. 2003;37:429-42.

[10] Dufour JF, Bargellini I, De Maria N, De Simone P, Goulis I, Marinho RT. Intermediate Hepatocellular Carcinoma: Current Treatments and Future Perspectives. Annals of Oncology. 2013;24;24-9.

[11] Altekruse SF, McGlynn KA, Reichman ME. Hepatocellular Carcinoma Incidence, Mortality, and Survival Trends in the United States from 1975 to 2005. Journal of Clinical Oncology. 2009;27:1485-91.

[12] Lewis AL, Dreher MR. Locoregional Drug Delivery Using Image-Guided Intra-Arterial Drug Eluting Bead Therapy. Journal of Controlled Release. 2012;161:338-50.
[13] Tam KY, Leung KC, Wang YX. Chemoembolization Agents for Cancer Treatment. European Journal of Pharmaceutical Sciences. 2011;44:1-10.

[14] Barkey NM, Tafreshi NK, Josan JS, De Silva CR, Sill KN, Hruby VJ, et al. Development of Melanoma-Targeted Polymer Micelles by Conjugation of a Melanocortin 1 Receptor (MC1R) Specific Ligand. Journal of Medicinal Chemistry. 2011;54:8078-84.

[15] Bruix J, Sherman M. Management of Hepatocellular Carcinoma: An Update. Hepatology. 2011;53:1020-2.

[16] Bruix J, Llovet JM. Two Decades of Advances in Hepatocellular Carcinoma Research. Seminars in Liver Disease. 2010;30:1-2.

[17] Laurent A. Microspheres and Nonspherical Particles for Embolization. Techniques in Vascular and Interventional Radiology. 2007;10:248-56.

[18] Cappello J, Crissman J, Dorman M, Mikolajczak M, Textor G, Marquet M, et al. Genetic Engineering of Structural Protein Polymers. Biotechnology Progress. 1990;6:198-202.

[19] Cappello J, Crissman JW, Crissman M, Ferrari FA, Textor G, Wallis O, et al. In-Situ Self-Assembling Protein Polymer Gel Systems for Administration, Delivery, and Release of Drugs. Journal of Controlled Release. 1998;53:105-17.

[20] Cappello J, Ghandehari H. Engineered Protein Polymers for Drug Delivery and Biomedical Applications. Advanced Drug Delivery Reviews. 2002;54:1053-5.

[21] Ghandehari H. Recombinant Biomaterials for Pharmaceutical and Biomedical Applications. Pharmaceutical Research. 2008;25:672-3.

[22] Dandu R, Cresce AV, Briber R, Dowell P, Cappello J, Ghandehari H. Silk–Elastinlike Protein Polymer Hydrogels: Influence of Monomer Sequence on Physicochemical Properties. Polymer. 2009;50:366-74.

[23] Price R, Poursaid A, Cappello J, Ghandehari H. Effect of Shear on Physicochemical Properties of Matrix Metalloproteinase Responsive Silk-Elastinlike Hydrogels. Journal of Controlled Release. 2014;195:92-8.

[24] Barber RW, Emerson DR. Biomimetic Design of Artificial Micro-Vasculatures for Tissue Engineering. Alternatives to Laboratory Animals. 2010;38 Suppl 1:67-79.

[25] Emerson DR, Cieslicki K, Gu X, Barber RW. Biomimetic Design of Microfluidic Manifolds Based on a Generalised Murray's Law. Lab on a Chip. 2006;6:447-54.

[26] Murray CD. The Physiological Principle of Minimum Work. I. The Vascular System and the Cost of Blood Volume. Proceedings of the National Academy of Sciences. 1926:207-14.
[27] Rhoades RA, Bell DR. Medical Physiology: Principles for Clinical Medicine: Lippincott Williams & Wilkins; 2012.

[28] Gaehtgens P, Meiselman HJ, Wayland H. Erythrocyte Flow Velocities in Mesenteric Microvessels of the Cat. Microvascular Research. 1970;2:151-62.

[29] Blumgart LH. Surgery of the Liver, Biliary Tract, and Pancreas. 1. Philadelphia, PA: Saunders, Elsevier; 2007.

[30] Price R, Gustafson J, Greish K, Cappello J, McGill L, Ghandehari H. Comparison of Silk-Elastinlike Protein Polymer Hydrogel and Poloxamer in Matrix-Mediated Gene Delivery. International Journal of Pharmaceutics. 2012;427:97-104.

[31] Lencioni R, de Baere T, Burrel M, Caridi JG, Lammer J, Malagari K, et al. Transcatheter Treatment of Hepatocellular Carcinoma with Doxorubicin-Loaded DC Bead (DEBDOX): Technical Recommendations. Cardiovascular and Interventional Radiology. 2012;35:980-5.

[32] Clark TW. Complications of Hepatic Chemoembolization. Seminars in Interventional Radiology: Thieme Medical Publishers; 2006. p. 119.

[33] Brown KT. Fatal Pulmonary Complications after Arterial Embolization with 40–120-μm Tris-acryl Gelatin Microspheres. Journal of Vascular and Interventional Radiology.15:197-200.

CHAPTER 4

SILK-ELASTINLIKE PROTEIN POLYMER LIQUID CHEMOEMBOLIC FOR LOCALIZED RELEASE OF DOXORUBICIN AND SORAFENIB

4.1 Introduction

The need for improved cancer therapies is becoming more evident as the number of cases refractory to standard of care treatments increases. The incidence of hepatocellular carcinoma (HCC) of the liver has nearly tripled since the early 1980s in the United States and this disease affects over half a million patients worldwide each year [1, 2]. Treatment is dictated by staging level and the patient's overall liver function. Patients with intermediate stage HCC are candidates for loco-regional therapy including transarterial chemoembolization (TACE) [3]. TACE involves angiographic identification of the vessels feeding into the tumor followed by embolization to induce necrosis and locally deposit a high concentration of chemotherapeutic. The success of TACE is due to the dual blood supply of the liver. Cancerous tissue draws blood from branches of the hepatic artery, while healthy parenchyma receives over 75% of its blood supply from the portal vein [4].

Manuscript submitted to Molecular Pharmaceutics. Poursaid A, Jensen MM, Nourbakhsh I, Weisenberger M, Hellgeth J, Sampath S, Cappello J, Ghandehari H. Silk-elastinlike protein polymer liquid chemoembolic for localized release of doxorubicin and sorafenib. Mol Pharm 2016:Submitted.

Occlusion of the hepatic artery branches preserves liver function while thwarting tumor progression. Clinically, inclusion of locally delivered chemotherapeutic time to disease progression when compared to embolization alone [5].

Doxorubicin is a commonly used chemotherapeutic dosed intravenously or locally. It intercalates DNA as well as inhibits topoisomerase II, preventing DNA replication [6]. Additionally, this drug forms oxygen free radicals resulting in cytotoxicity [7]. Sorafenib is approved for treatment of HCC by oral administration. This drug targets growth signaling by blocking the enzyme RAF kinase and inhibits the VEGFR-2/PDGFR signaling cascade to block tumor angiogenesis [8]. Because of their complimentary mechanisms of action, there is interest in combination treatments with both drugs. In a phase II clinical trial of advanced HCC, the two drugs were administered systemically and the combination therapy was associated with significantly longer time to tumor progression (TTP), 6.4 versus 2.8 months, and median overall survival, 13.7 versus 6.5 months, than doxorubicin alone [9]. A recent phase III trial in Japan concluded that oral sorafenib following TACE increases the TTP, albeit not significantly. The lack of significance was attributed to 73% of patients requiring dose reduction or treatment lag due to toxic side effects. Delay in sorafenib administration post-TACE likely contributed to the lack of significance. Local hypoxia resulting from TACE induces angiogenesis by increasing serum concentrations of VEGF, suggesting that sorafenib may exert optimal anti-angiogenic effects when administered immediately after or during TACE [10]. In other clinical trials investigating addition of systemic sorafenib to doxorubicin delivered via TACE, adverse events attributed to sorafenib resulted in dose reduction or premature treatment termination [11-13]. Therefore, co-localized delivery of sorafenib may provide

a more convenient and effective approach.

Drug eluting beads (DEBs) are a widely used embolic system for localized delivery in TACE [14]. However, the mechanism of drug incorporation limits the drugs that may be used. Leading microspheres use either an ion exchange method or a swelling process followed by interaction of the drug with ionized side chains [15]. In both methods, only charged low molecular weight drugs may be incorporated. Most commonly, the positively charged salt forms of doxorubicin or irinotecan have been incorporated into clinically available DEBs [16]. A further limitation of these nondegradable DEBs is their finite size and inability to penetrate down to the arterio-capillary level of the vessels feeding into the tumor, decreasing penetration and reducing the total tumor volume that may be exposed to drug. DEB drug delivery relies on the concentration gradient within the spheres followed by either diffusive or matrix swelling mechanisms for nondegradable polymer matrices [17]. There are two liquid embolics on the market, Onyx® and PHIL™. Onyx®, composed of ethylene vinyl alcohol (EVOH) copolymer, and PHIL™, which is comprised of a copolymer poly(lactide-*co*-glycolide) and poly(hydroxyl ethyl methacrylate), both dissolved in the organic solvent dimethyl sulfoxide (DMSO) [15]. As these embolics are solvated in DMSO, their use is associated with vascular inflammation and angionecrosis [15]. Neither Onyx® nor PHIL™ can be used to deliver drugs as the dissipation of DMSO during administration would cause a burst release of the entire therapeutic payload, resulting in acute local toxicity and transient therapeutic effects. To address these limitations, aqueous formulated silk-elastinlike protein polymers (SELPs) have been in development as a drug loadable, *in situ* gelling liquid embolic. In the first stage of development, a SELP formulation was determined complying with design criteria of an

injectable embolic outlined in Table 4.1 [18]. SELPs are genetically engineered materials that exhibit an irreversible sol-gel transition at physiological temperature [19, 20]. Gelation occurs without the need for chemical-induced cross-linking. Rather, this phase transition occurs spontaneously at 37°C as the elastinlike units thermodynamically collapse, aligning the silk-like units, which form hydrogen bonded beta sheets resulting in a physically cross-linked matrix [19, 21]. The liquid nature of the embolic composition is ideal for microcatheter intrarterial administration and distal target vessel penetration. The material is also opportune for direct drug incorporation immediately prior to use, thereby allowing for tailored drug selections. In this work, we investigated the direct incorporation of doxorubicin and sorafenib, individually and jointly, in the SELP-815K formulation previously described [18]. Both drugs have low water solubility, with experimental partition coefficients (logP) of 1.3 and 4.1, respectively [6, 22]. Previous investigation of the release of hydrophilic low molecular weight molecules incorporated into a variety of SELP compositions showed rapid release on the time scale of hours [23]. The high lipophilicity of doxorubicin and sorafenib and the high content of hydrophobic residues in the SELP-815K backbone, which comprises 6 repeats of 8 silk motifs (GAGAGS) and 15 elastinlike motifs (GVGVP), with one lysine substituted elastinlike motif (GKGVP) (189 valine, 105 alanine, and 102 proline residues/molecule [24]), was expected to extend release kinetics [24].

Herein, we evaluated the incorporation and release of both drugs, doxorubicin and sorafenib, from SELP-815K hydrogel, individually and in combination in both the salt forms and base forms, and with or without dimethyl sulfoxide (DMSO) to predissolve the drug(s). The viscosity and gelation kinetics of the drug-loaded SELP-815K, required for

Table 4.1. Criteria previously established for injectable SELP-815K liquid embolic [18]

Design Criterion	***Specification Parameter Targets and Rationale***
Injectability	Viscosity $\leq$ 150 cP required for injection through clinical microcatheters.
Gelation kinetics	Sol-gel transition time $\leq$ 5 minutes required for gel retention in arterial vessel with minimal venous washout.
Embolic effect	Final gel stiffness, storage modulus G' $\geq$ $1x10^5$ Pa required for stable maintenance of gel embolus against hepatic blood pressure.

an injectable liquid chemoembolic, were analyzed. Release rates of the drugs individually and together from the gelled SELP-815K matrices were determined *in vitro,* with the target of continuous release for no less than 14 days as available from DEBs. Morphology and protein secondary structure formation in the gels with and without loaded drugs were evaluated using scanning electron microscopy (SEM) and Fourier Transform Infrared Spectroscopy (FTIR), respectively.

4.2 Experimental section

4.2.1 Materials

SELP-815K was synthesized and characterized as previously described [18-20, 24]. Sorafenib tosylate, sorafenib base, and doxorubicin HCl were purchased from LC Laboratories and doxorubicin base was purchased from MedKoo Biosciences. Chemicals and salts used included acetonitrile (Fisher Scientific), ammonium acetate (Fisher Scientific), sodium dodecyl sulfate (SDS) (Sigma), and phosphate buffered saline tablets (Amresco).

4.2.2 Single agent *in vitro* cytotoxicity

Growth inhibition by the base drugs used in this study was evaluated on three different hepatoma cell lines, two human HCC lines and one rat cell line, using a 2-(2-methoxy-4-nitrophenyl)-3-(4-nitrophenyl)-5-(2,4-disulfophenyl)-2H-tetrazoliummono-sodium salt (WST-8) cell viability assay (Dojindo Molecular Technologies, Inc., Rockville, MD). Human cell lines Hep3B and HepG2 were obtained from ATCC (Manassas, VA) and cultured in EMEM cell culture medium (ATCC) supplemented with

10% fetal bovine serum (FBS). The rat hepatoma line, McA-RH7777, was generously donated by the Larson Lab (Northwestern University, IL). This line was cultured in DMEM cell culture medium (ATCC) supplemented with 10% FBS. All lines were grown at 37° C in a humidified atmosphere of 5% CO_2. To prevent precipitation of the drugs, media containing 0.5% DMSO was used throughout all the studies. Doubling time of the cell lines was similar. Therefore, cells were plated at the same density of 7,000 cells per well in 96-well plates for 24 hrs. Media was removed, cells were washed with PBS, and treatment was applied. Drug concentrations were varied to include data points ranging from nontoxic to highly toxic. Following 72 hrs of incubation, the media was removed and cell viability was quantified using the WST-8 assay with a SpectraMax M2 spectrophotometer (Molecular Devices, Sunnyvale, CA). Each experiment was performed with N=6, assessing viability at 10 different drug concentrations. Relative cell viability was calculated by normalizing against the UV absorbance of untreated cells. GraphPad Prism was used to plot relative cell viability as a function of log drug concentration with a nonlinear least-squares regression analysis and calculation of IC_{50} values presented in Table 4.2.

4.2.3 Formulation development and drug incorporation

As previously described, SELP-815K formulations were prepared at 12% w/w in 1X phosphate buffered saline (PBS) [18]. Powder drugs were milled for 12 hrs to reduce crystal size and variability using a custom built ball mill. Milled samples were inspected microscopically to verify homogeneity. Two methods of drug incorporation were investigated. First, drugs were dissolved in dimethyl sulfoxide (DMSO) at a concentration of 100 mg/mL and 50 μL of the drug solution was spiked into 150 μL of liquid 12% SELP-

Table 4.2. Results from single drug cytotoxicity

IC_{50} Values of Each Drug per HCC Cell Line (μM)		
	Sorafenib	**Doxorubicin**
Hep3B	3.47 ± 0.2	0.29 ± 0.04
HepG2	1.72 ± 0.70	0.62 ± 0.41
McA-RH7777 (rat hepatoma)	6.88 ± 0.83	0.48 ± 0.32

815K followed by 10 seconds of manual mixing, resulting in a 9% w/w SELP concentration and a 25 mg/mL drug loading. Drug loading concentration was chosen based on manufacturer specified loading of doxorubicin in DEBs [25]. The same loading was used for sorafenib. Second, milled powder drug was incorporated directly into 150 μL of liquid 12% w/w SELP-815K and 50 μL saline was added to dilute the SELP to 9% w/w (equivalent to the samples with drug dissolved in DMSO) followed by mechanical mixing using a custom built overhead mixer equipped with a 1/16" diameter spiral impeller for 10 seconds at 5400 RPM, resulting in a 25 mg/mL drug loading. For dual drugs, drug loading was 12.5 mg/mL for each drug, for a total drug loading of 25 mg/mL. Samples were chilled on ice until tested. Samples incorporating powder drug in 12% w/w SELP-815K were prepared without dilution, however the volume addition of the powdered drug was not considered in the calculation of the SELP concentration. Samples with powdered drug were tested at 25 and 50 mg/mL for single drug loaded samples and 25 mg/mL per drug for dual drug loaded samples.

4.2.4 Rheological characterization

An AR 550 stress-controlled rheometer from TA Instruments (New Castle, DE) was used for rheological testing. A cone-and-plate configuration equipped with a stainless steel 20 mm diameter, 4 degree geometry was used. An oscillation procedure with a temperature ramp from 18°C to 37°C (5.76 °C/min) at an angular frequency of 6.283 rad/s was run to measure viscosity, followed by an oscillatory time sweep of 3 hrs held at 37°C, using angular frequency of 6.283 rad/s, and 0.1% strain to measure the dynamic storage modulus G'. Individual samples previously prepared and stored frozen were thawed just

before testing at 18-23°C and centrifuged at 14,000 rpm (Centrifuge 5417C, Eppendorf) for 30 seconds. Drug was incorporated as described in Section 4.2.3 immediately before testing. A 150μL of test solution was immediately transferred to the Peltier plate, which was pre-chilled to 18°C. Measurements were conducted in triplicate.

4.2.5 SEM analysis of drug loaded gels

Gel samples were examined by scanning electron microscopy (SEM) using an FEI Quanta 600F for qualitative analyses. Samples were prepared with drugs as described in Section 4.2.3, drawn into 0.5cc insulin syringes and sealed with paraffin film to prevent evaporation. The syringes were incubated overnight at 37°C to allow curing. The resulting gels were extruded from the syringe barrel (after cutting off the needle), sliced into 20 μL disks and weighed. Gel samples were flash frozen in liquid nitrogen and lyophilized for 24 hrs. The disks were mounted on carbon tape and coated with a 6 nm layer of gold palladium (Gatan 682 Precision Etching Coating System) for imaging. Secondary electron images were taken with beam parameters of 3.0 spot size and 10.00 kV voltage. Images were also taken postdrug release by the same method.

4.2.6 *In vitro* drug release

The drug loaded SELP solutions were drawn into 0.5 cc insulin syringes and incubated overnight at 37°C followed by cutting into gel disks as previously described. Weights were measured and recorded. Individual gels were placed into 8-dram glass vials to which 25 mL of release media consisting of 1X PBS, 1% SDS was added. The elution volume was chosen to ensure sink conditions and complete dissolution of both drugs, if all

drug eluted immediately. At predetermined time points, 1 hr, 3 hrs, 6 hrs, 12 hrs, 1 day, 3 days, 5 days, 7 days, 10 days, 14 days (and 20 and 30 days for extended release studies) a sample volume was removed for analysis and replaced with fresh media. Vials were sealed and maintained in a shaking incubator at 37°C, 120 RPM. The 9% SELP-815K gels underwent release testing for 14 days. The 12% SELP-815K gels were tested for 30 days. Drug content in the release media was detected by reverse phase high performance liquid chromatography (HPLC) (Agilent Technologies, Santa Clara, CA) using a reverse phase C18 (4.6 × 250 mm, 5 μm) X-Terra column (Waters, Milford, MA) and a guard column of the same packing material. The elution gradient at time zero began with mobile phase of 40% 20mM ammonium acetate and 60% acetonitrile (ACN) which increased to 72% ACN over 9 minutes at a flow rate of 1 mL/min [26]. Percent cumulative release was calculated using the experimental drug loading per disk based on the prerelease weight.

4.2.7 Gel-swelling ratio

The swelling ratio was measured for the 9% gels 14 days postrelease. Gel disks were removed from the release media, blotted dry with lint free wipes, and weighed. Samples were then snap frozen in liquid nitrogen and lyophilized for 24 hrs. The swelling ratio was calculated as $q = \frac{Wet\ Weight}{Dry\ Weight}$.

4.2.8 ATR-FTIR analysis of SELP drug-loaded gels

FTIR analysis was performed on a Nicolet 6700 spectrometer (Thermo Scientific) equipped with a mercury cadmium telluride (McT-A) detector and a SmartiTX attenuated total reflectance (ATR) accessory fitted with a single element diamond crystal. Individual

spectra were acquired with 512 co-added scans ratioed to a background of 512 scans from the diamond itself. Scans were performed over the range of 850 to 4000 cm^{-1} with a resolution of 4 cm^{-1}. Hydrated 9% SELP-815K gels fully loaded with drug incorporated as a DMSO solution or milled powder were tested. Absorbance spectra of powdered drug, PBS, and DMSO were measured as references. Data were analyzed with OMNIC 9.2 software loaded with Proteus Protein Analysis Kit from Thermo Scientific. The background spectrum of the buffer was subtracted, as was DMSO, if applicable, and the baseline was corrected. The amide I region (1700 cm^{-1} to 1600 cm^{-1}) was deconvoluted using Gaussian curves by the Voigt model. The second derivative of spectra was used to identify locations of the secondary structure peaks. The percentages of secondary structures in each sample were calculated from peak integration.

4.2.9 Statistical analysis

All rheological and drug release experiments were conducted in triplicate and data are presented as the mean ± standard deviation (SD) unless otherwise specified. Significance between multiple groups was determined using a one-way analysis of variance (ANOVA) with a Tukey's posttest, and a two-tailed Student's t-test for comparing pairs of data. Statistical significance was reported as $p<0.05$, highly significant when $p<0.01$, and very highly significant when $p<0.001$.

4.3 Results

4.3.1 Rheological characterization of drug loaded liquid SELP-815K

SELP solution was loaded with doxorubicin, sorafenib or both drugs in various chemical and physical forms and evaluated first to qualify the various formulations with respect to the targeted physical and mechanical requirements of an injectable liquid chemoembolic described in Table 4.1. The salt forms of the drugs, doxorubicin hydrochloride (Dox HCl) and sorafenib tosylate (Soraf Tos), which are the more soluble forms of the drugs used clinically, were tested first. Dox HCl was mixed into the SELP solution either directly as a powder or as a solution dissolved in DMSO. All experiments with both drugs were conducted at a consistent drug loading level based on the clinically specified loading level of doxorubicin with drug-eluting beads, 25 mg/mL.

Immediately, the addition of Dox HCl to the SELP solution caused a noticeable increase in viscosity. The viscosity of the SELP solution with Dox HCl, incorporated as either a drug powder and more so as a DMSO solution, was more than 2-fold greater than the SELP control with no drug (Figure 4.1A). Additionally, the viscosity of the SELP-Dox HCl DMSO showed a temperature effect, unusual for SELP-815K solutions. The initial average viscosity at 18 °C of 394 ± 149 cP decreased with increasing temperature to 123 ± 44 cP at 37 °C. This temperature thinning effect was not seen with the Dox HCl powder, which averaged 250 ± 114 cP throughout the temperature ramp.

Sorafenib tosylate was mixed into SELP solution either dissolved in DMSO or in powder form and similarly tested. The same trends as for Dox HCl were observed, though the magnitude of the changes was less (Figure 4.1B). As observed with Dox HCl, SELP with Soraf Tos in DMSO had greater viscosity than the SELP control and displayed

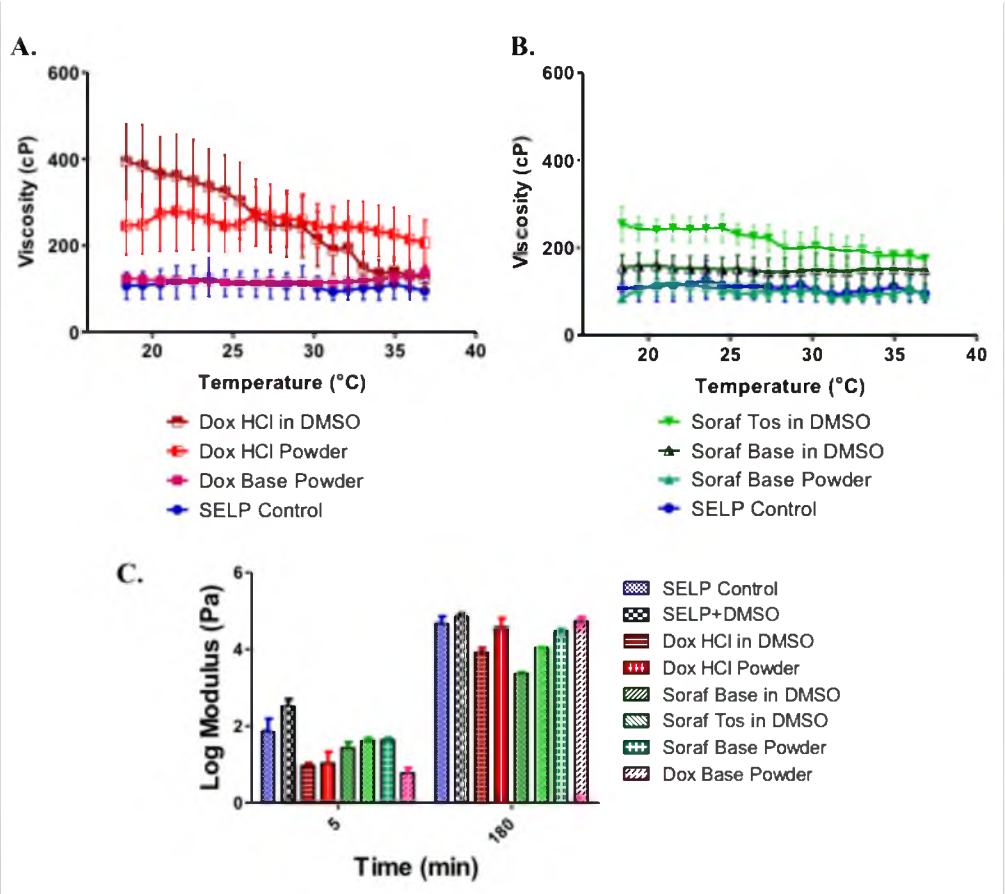

Figure 4.1. Rheological evaluation of 9% SELP-815K loaded with 25 mg/mL doxorubicin and/or sorafenib in both salt and base forms, incorporated into the polymer solution either dissolved in DMSO or in powder form. Panels A and B) Viscosity traces of SELP incorporating the various forms of doxorubicin or sorafenib. C) Storage modulus, G', values for the SELP hydrogels formed with and without drug incorporation at 5 minutes and 3 hrs at 37 °C. Data represent the mean±standard deviation, N=3.

temperature thinning, although to a lesser degree than SELP with Dox HCl. Sorafenib base in DMSO also displayed an increased viscosity, but not temperature thinning.

While the increase in viscosity of the SELP solution with the salt forms of the drugs added in DMSO could be due to the drugs or the DMSO, the temperature thinning effect is due to the salt forms of the drugs, not the DMSO, since the effect was not seen with sorafenib base in DMSO. Since the viscosity of a polymer solution is dependent on the chemical and physical interactions of the polymer chains, it follows that the salt forms of the drugs in DMSO affect these interactions. The incorporation of doxorubicin HCl and sorafenib tosylate or base as solutions in DMSO increased the viscosity of the SELP solution to levels that exceeded the acceptable injectable viscosity of <150 cP at room temperature, making them unsuitable SELP liquid embolic formulations. On the other hand, the incorporation of either drug in base form as a powder did not change the viscosity nor the viscosity behavior as a function of temperature compared to the SELP control (Figures 4.1A and B). These formulations were deemed to meet the injectability criterion for a SELP liquid embolic.

The SELP drug formulations were further tested to determine their gel stiffness at 37 °C. Figure 4.1C shows the storage modulus, G', at 5 and 180 minutes. G' is a measure of the material stiffness and an indicator of gel network crosslinking. To allow for the addition of drug, the SELP concentration of the tested formulations was decreased to 9% w/w, rather than the 12% w/w previously defined for the SELP liquid embolic [18]. Thus, the modulus was expected to be less than the target $\geq 1 \times 10^5$ Pa specified in Table 4.1. Therefore, the change in modulus as a function of drug incorporation relative to the SELP control was used to assess the effect of drug addition and the relative suitability of the

formulations as liquid embolics. The results indicate that the storage modulus of the gels at 5 minutes decreased when drug was added in any form, more so with doxorubicin than sorafenib. At 180 minutes, however, only the formulations with drug added in DMSO showed reduced moduli. Interestingly, SELP with DMSO only showed no reduction in modulus. Doxorubicin and sorafenib added as powders had moduli comparable to the SELP control. However, none of these observed differences were statistically significant and they were not used to exclude formulations from further study. Therefore, injection viscosity was the primary criterion used to move chemoembolic drug candidates forward and the base forms of the drugs were selected to continue in the remaining characterization and release studies. Both methods of drug incorporation were studied.

4.3.2 SEM analysis of drug loaded SELP-815K gels

Scanning electron micrographs were examined to assess the extent and uniformity of drug dispersion throughout the SELP matrix. Representative images of the dual drug loaded gel shown in Figure 4.2A confirm the higher level of drug homogeneity throughout the matrix when the drug is incorporated in DMSO versus the powder. In the gel incorporating the two drugs in DMSO (Figure 4.2A) distinct crystalline structures of doxorubicin base (star polyhedron formations) and sorafenib base (cubic polyhedrons) (determined from SEM images of single drug loaded gels), which were possibly induced during the flash freezing and dehydration process, are visible in the inset images. The distinct crystals uniformly coat the entire surface of the polymer matrix. The same level of homogeneity was not present in the gel samples incorporating the powdered drugs (Figure 4.2B). As expected, the hydrophobic drugs formed clusters that were interspersed

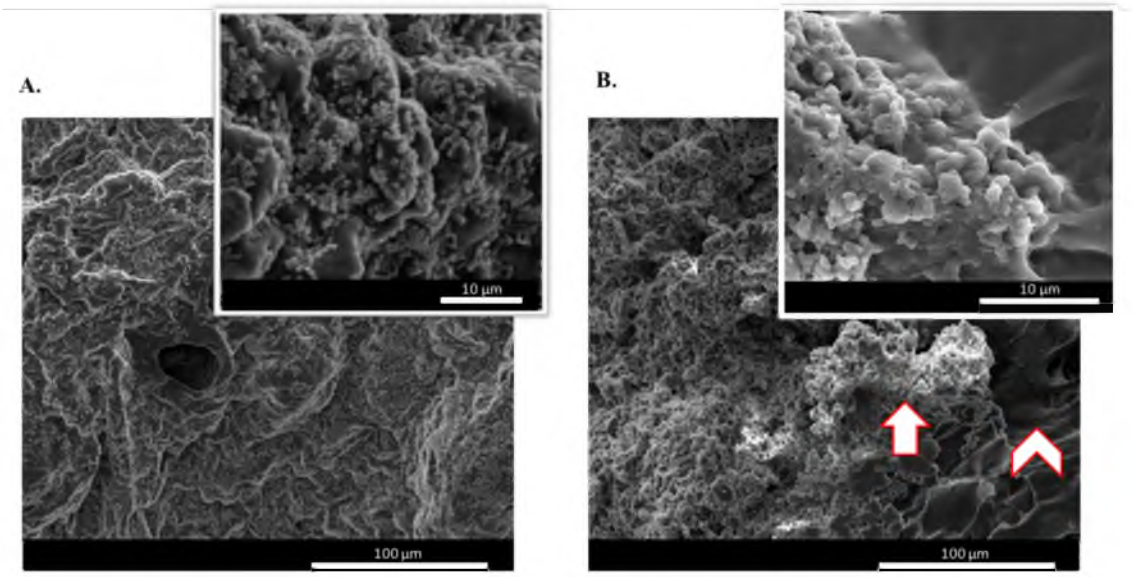

Figure 4.2. Scanning electron micrographs of 9% SELP-815K gels loaded with base forms of both doxorubicin and sorafenib. A) Representative scan of a gel sample with the drugs incorporated dissolved in DMSO. Star polyhedron crystals are doxorubicin and the cubic polyhedron crystals are sorafenib, which coat the polymer matrix in a consistent layer. B) Representative scan of a gel sample with powdered drugs mixed into the liquid SELP. During the gelation process, the polymer indicated by the arrowhead entraps the drug clusters indicated by the arrow.

throughout the matrix. The SELP polymer matrix is indicated by the arrowhead and drug cluster by the arrow. Often, projections of the polymer were observed caging the drug clusters.

4.3.3 Drug release from 9% SELP-815K gels

Based on the rheological data, the base forms of each drug were selected for further evaluation. Appropriate drug release is a key component of a chemoembolic system. *In vitro* release studies were conducted with 9% SELP-815K gels to measure the relative cumulative release of each drug individually and compare the modes of incorporation for single and concurrent drug loadings. Doxorubicin release in the first 24 hrs was significantly greater from the gels with drug in DMSO versus drug powder (Figure 4.3A). However, no difference was observed after Day 1. More than 50% of the loaded doxorubicin was released in the first day, followed by a decline in release rate and a subsequent plateau on days 7 to 14, with the majority of the loaded drug released by Day 14. The relative release difference was highly significant between the sorafenib groups at all time points. Interestingly, the relative release rates for sorafenib changed in the presence of doxorubicin (Dual). In Figure 4.3B, a significant difference was observed between the release of sorafenib from the dual drug loaded gel compared to single drug gel with both incorporation methods. It must be noted that the dual drug gels had a 12.5 mg/mL loading for each drug versus 25 mg/mL for single drug gels. Significant differences were observed between all groups. In the DMSO dissolved drug group, sorafenib released from the dual drug loaded gels reached 95% cumulative release, while from the single drug loaded gel less than 60% cumulative release was achieved. In the powder drug incorporated gels, the

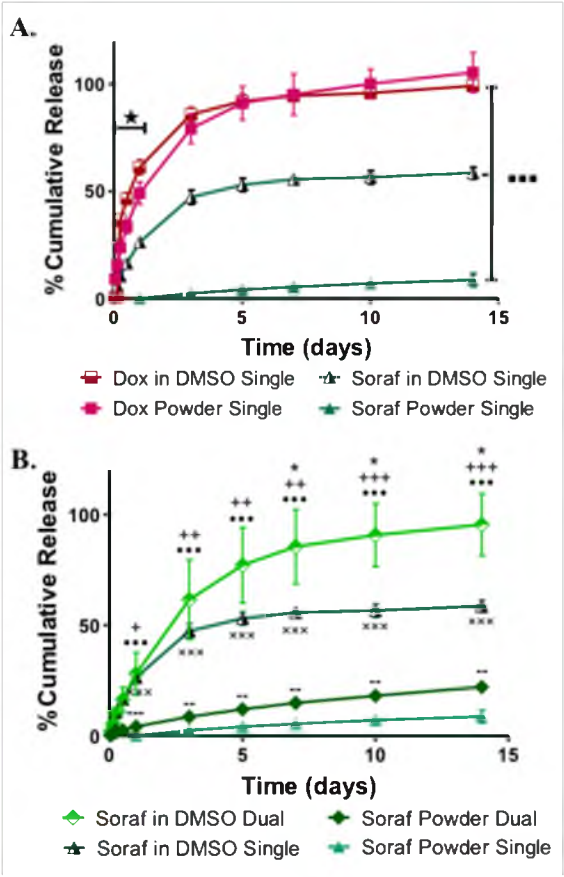

Figure 4.3. *In vitro* drug release from 9% SELP-815K gels loaded with base forms of doxorubicin and sorafenib. A) Comparison of the relative release rates of the single drug loaded gels of different incorporation methods. The star represents a statistically significant greater release ($p<0.05$) for all time points less than 1 day of release of doxorubicin base dissolved in DMSO versus powder. The three squares represent statistically significant differences ($p<0.001$) for release of doxorubicin gels as compared to release of sorafenib. B) Comparison of the four sorafenib loaded gels. * Shows statistical significance between the sorafenib dissolved in DMSO released from the dual drug loaded gel versus single drug loaded gel. + Shows statistical significance between the sorafenib dissolved in DMSO released from the dual drug loaded gel versus sorafenib powder released from the dual drug loaded gel. • Shows statistical significance between the sorafenib dissolved in DMSO released from the dual drug loaded gel versus sorafenib powder released from the single drug loaded gel. x Shows statistical significance between the sorafenib dissolved in DMSO released from the single drug loaded gel versus sorafenib powder released from both the single and the dual drug loaded gels. - Shows statistical significance between the sorafenib powder groups. Presence of doxorubicin significantly increases the cumulative release of sorafenib. Data are represented as the mean±standard deviation, N=3.

Table 4.3. Drug concentration released *in vitro* at specific time points from the 9% SELP-815K gels.

Experimental Group	Average Concentration (μM)		
9% SELP Gels	Day Time Point		
	1	**7**	**14**
Doxorubicin DMSO	32.4	1.3	1.8
Doxorubicin powder	23.9	1.9	1.0
Doxorubicin DMSO (Dual)	11.9	0.8	0.3
Doxorubicin powder (Dual)	16.8	2.2	1.1
Sorafenib DMSO	16.0	1.6	1.2
Sorafenib powder	0.0	0.7	1.0
Sorafenib DMSO (Dual)	7.6	2.3	1.3
Sorafenib powder (Dual)	1.3	0.9	1.2

dual drug loaded gel resulted in 22% cumulative release versus 8.7% in the single drug loaded gel.

Table 4.3 provides the average drug concentrations in the release media at given time points. For comparison, the cytotoxicity IC_{50} values of the drugs determined in these studies for human HCC HepG2 cells were 1.72 ± 0.7 μM for sorafenib and 0.62 ± 0.41 μM for doxorubicin (see Table 4.2), which substantially agree with the values reported in the literature [27, 28].

4.3.4 Swelling analysis of gels post-release

We examined whether the significant differences in the observed relative release of the two drugs in the different SELP drug formulations was associated with different gel structures by determining the swelling ratio of the gel specimens following drug release (Figure 4.4). Hydrogel swelling is affected by the degree of solvation of the gel composition and by the network crosslinking density. Both of these factors could affect drug release rates. The swelling coefficient, q, of the gel disks was measured after 14-day release. The gels loaded with sorafenib had lower swelling ratios than the doxorubicin-loaded gels (although not statistically significant), consistent with sorafenib's slower drug release profile. All drug loaded gels had lower swelling ratios than the SELP control, but again not statistically significant. These differences could indicate minor differences in the gel structure caused by the drugs during gelation or they could be due simply to the presence of drug in the gels. The fact that there were no statistically significant differences in the swelling ratios after 14 days of release and there was no significant difference in the gel stiffness immediately upon gelation indicates that drug incorporation, at least for the base form of the drugs as powders, did not significantly alter the gel structure either

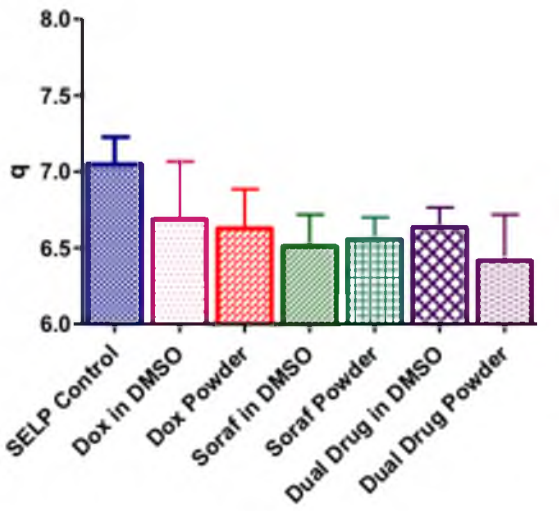

Figure 4.4. The swelling coefficient, q, was calculated for 9% SELP-815K gels loaded with base forms of doxorubicin and sorafenib after 14-day release. No statistically significant differences were determined between any groups.

immediately or after 14 days of release.

4.3.5 ATR-FTIR analysis of drug loaded gels

Drug-loaded 9% SELP-815K gels were analyzed by ATR-FTIR to detect the possible changes in protein secondary structure in the presence and absence of the two individual drugs and when incorporated together in the SELP matrix. Further FTIR analyses were also done on the two groups of the drug-loaded SELP wherein the drugs were either dissolved in DMSO before incorporation or were mechanically mixed in powder form into the SELP solution. The Amide I band (1595-1705 cm^{-1}) in the absorption spectrum arises from the C=O stretching vibrations in the protein backbone and is indicative and most sensitive to the secondary structures in the protein backbone [29]. In particular, the region between 1614 and 1640 cm^{-1} is assigned to beta-sheets, 1640 and 1660 cm^{-1} to random/unordered coils, and alpha helices and the region between 1660 and 1690 cm^{-1} to beta-turn secondary structures. Smaller peaks between 1690 and 1705 cm^{-1} can arise from additional beta-sheet structures. The Amide II region arises from the N-H bending and the C-N stretching vibrational modes [30-34].

Absorbance spectra of the amide I region are shown in Figure 4.5. Panel A consists of spectra for gels with drug dissolved in DMSO and incorporated into SELP. Panel B shows the spectra for gels incorporating powder drug. These spectra were subjected to Fourier self-deconvolution (FSD) with Guassian bands to quantify the fraction of different secondary structures of the protein matrix in the absence or presence of drug. The second derivative of each spectrum was calculated to determine the locations of the secondary structure peaks, which were confirmed with assignments in the literature [30, 33, 34].

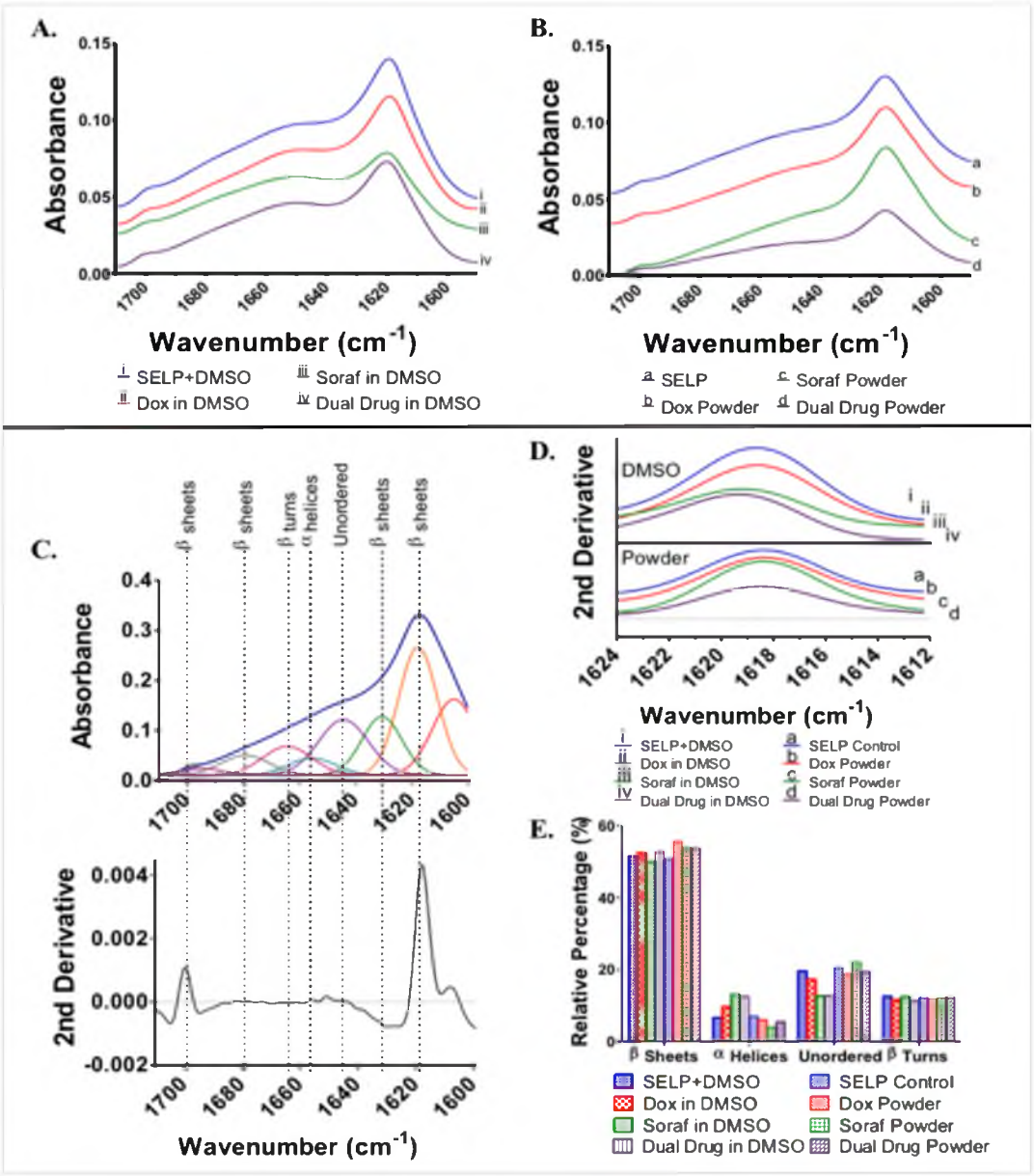

Figure 4.5. ATR-FTIR absorbance spectra of 9% SELP-815K gels loaded with base forms of doxorubicin, sorafenib, or both drugs (Dual). A) Comparison of spectra of the Amide I region for SELP gels loaded with dissolved drug in DMSO. B) Comparison of spectra of the Amide I region for SELP gels loaded with powder drug. C) Representative absorbance spectrum of 9% SELP-815K with no mechanical mixing deconvolved using the Voigt model. The composite spectrum, shown in blue, appropriately fits the original curve, shown in black. The second derivative of the original scan is shown below and used to identify peak assignments for secondary structures. D) Comparison of the second derivative traces for original spectra of each gel sample at the primary beta-sheet peak assignment. Upshifting of gels loaded with sorafenib dissolved in DMSO is evident. E) Comparison of relative percent of secondary structures present in each gel.

Figure 4.5C displays the deconvoluted spectra of a control 9% SELP-815K sample. Peaks associated with the following secondary structure were identified: beta-sheets (1618, 1630, 1679, and 1694 cm^{-1}), random/unordered coils (1644 cm^{-1}), alpha helices (1656 cm^{-1}), and beta-turns (1664 cm^{-1}). The beta-sheets are the dominant structural component of the SELP matrix. Therefore, changes in relative amount of beta-sheet would be indicative of ultrastructural changes in the gel network. Peak shifts were examined in the primary beta-sheet absorbance peak at 1618 cm^{-1}, identified in the second derivative traces (Figure 4.5D). An upshift of the peak, indicative of increased energy required for vibrational motion, was seen for gels loaded with sorafenib dissolved in DMSO (single drug and dual drug). No other gels showed obvious peak shifts.

The relative percentage of secondary structures for each test group is shown in Figure 4.5E. In the gels incorporating powder drug, an increase in total percentage of beta-sheets was observed. The Dox powder incorporated gel showed the greatest increase when compared to the SELP control. Additionally, this gel showed a decrease in the amount of unordered coils. Gels with drug dissolved in DMSO displayed changes in content of alpha helices and unordered coils. Percentage of alpha helices increased compared to the control, with increasing content as follows: Dox in DMSO < dual drug in DMSO < Soraf in DMSO. Soraf in DMSO had a 1.97-fold increase over the control. In this same group, the relative amount of unordered coils decreased compared to the control. Soraf in DMSO had the greatest decrease of 1.5-fold. The dual drug in DMSO-loaded samples showed trends more similar to sorafenib alone versus doxorubicin alone, indicating that the presence of sorafenib had a greater effect on the protein secondary structures. Interestingly, the method of sorafenib incorporation resulted in opposite trends

in the two groups. When dissolved in DMSO, the relative percent of alpha helices increased and unordered coils decreased while with the powder there was a decrease in the alpha helix content and increase in unordered coils. The presence of doxorubicin in the SELP gels increased the beta-sheet content for both methods of incorporation. No change in beta-turns was determined for any gels when compared to their respective controls.

4.3.6 Rheological characterization and drug release from 12% SELP-815K gels

The information gained from the drug-loaded 9% SELP-815K gels indicated that drug release of doxorubicin, sorafenib, or both drugs was sufficient to provide therapeutically effective local concentrations of the drugs for 14 days. While incorporation into SELP solution of either or both drugs dissolved in DMSO yielded a more uniform dispersion than incorporation of the powder drugs as indicated by SEM, it resulted in at least a 2-fold increase in viscosity of the SELP solution, exceeding the maximum viscosity for injectability through a microcatheter, whereas incorporation of either or both drugs as powders caused no change in viscosity. However, the 9% concentration of SELP used in these evaluations yielded gel stiffness that was below the targeted specification of $1x10^5$ Pa. Therefore, we repeated the drug incorporation and release studies with 12% SELP-815K, the liquid embolic formulation that was shown previously to occlude branches of the hepatic artery *in vivo* [18].

Based on the results of the 9% SELP-815K gels, the incorporation of the base forms of each drug as powder in the 12% SELP-815K formulation were tested. In these studies, the dual drug group had a loading of 25 mg/mL of each drug, therefore a total drug loading

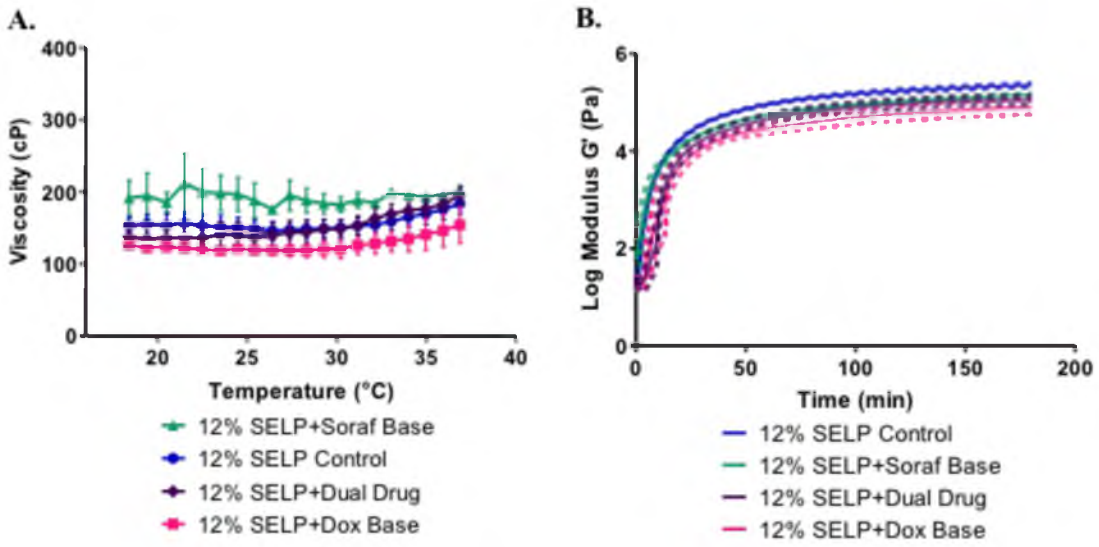

Figure 4.6. Rheological characterization of 12% SELP-815K loaded with base forms of doxorubicin and/or sorafenib as powders at 25 mg/mL. In the dual drug gels, each drug was loaded at 25 mg/mL with final total drug loading of 50 mg/mL. A) Viscosity curves for each experimental group. B) The storage modulus, G', is representative of the material stiffness. No significant difference was determined between groups as compared to the control in both viscosity and stiffness. Data are represented as the mean±standard deviation, N=3. Standard deviation is presented as the dotted lines above and below the solid traces in panel B.

of 50 mg/mL (twice the amount used in the 9% gels). Rheological characterization was conducted. Figure 4.6A shows the viscosity curves for the 12% SELP-815K samples. When compared to the control with no drug, no significant differences in viscosity were observed at any temperature. Therefore, loading of the base forms of each drug up to 25 mg/mL or both drugs up to a combined 50 mg/mL total drug content had no effect on the injectability of the formulation. The storage modulus, G', (Figure 4.6B) shows that while drug incorporation reduced the storage modulus compared to the control, the differences were not statistically significant and all gels resulted in an average 180 minute modulus of $\geq 1x10^5$ Pa. The test formulations including single drug loaded gels at 50 mg/mL were evaluated in 30-day *in vitro* relative release studies. Release profiles were similar to those of the 9% SELP-815K loaded gels (Figure 4.7). Between the 25 mg/mL single drug loaded and dual drug loaded gels, doxorubicin had higher release from the single drug loaded gel during the first 24 hrs. After day 1, however, no significant difference was observed. At the end of the experiment, Day 30, 30% of the total drug content of doxorubicin was released. Both of these groups showed significant increase in cumulative release over the 50 mg/mL single drug loaded gel, which resulted in only 15% cumulative release. The release profiles all similarly plateaued at 1 week. Conversely, the sorafenib loaded gels showed more linear release, though less than the doxorubicin. As seen with the 9% SELP-815K gels, sorafenib release was significantly greater from the dual drug loaded gel than the single drug loaded gels. The drug concentrations for days 1, 7, 15, and 30 are presented in Table 4.4. Concentrations of released drug determined for this group of 12% SELP gels were lower than concentrations released from the 9% gels, although the gels loaded at 50 mg/mL showed concentrations of released doxorubicin in the micromolar range up to 30 days.

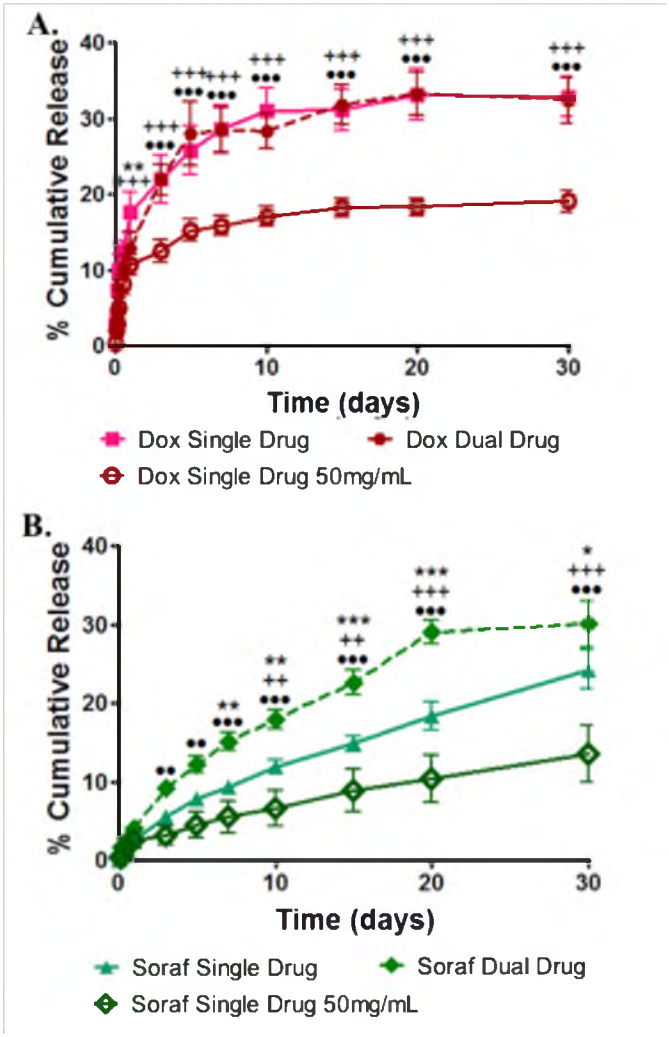

Figure 4.7. *In vitro* drug release profiles from 12% SELP-815K loaded with base forms of doxorubicin and sorafenib powders. A) Comparison of the relative release rates of doxorubicin from single drug loaded gels at either 25 mg/mL or 50 mg/mL, and from the dual drug loaded gel, 25 mg/mL loading per drug. * Shows statistical significance between the doxorubicin single drug loaded versus dual drug loaded gels, + Shows statistical significance between single drug loaded 25 mg/mL versus single drug loaded 50 mg/mL gels, and • Shows significance between the dual drug loaded gels and the single drug loaded 50 mg/mL gels. The same symbolic scheme applies to the sorafenib results in panel B). Data are represented as the mean±standard deviation, N=5.

Table 4.4. Drug concentration released *in vitro* at specific time points from the 12% SELP-815K gels.

Experimental Group 12% SELP Gels	Average Concentration (μM) Day Time Point			
	1	**7**	**15**	**30**
Doxorubicin powder (25 mg/mL)	1.2	0.9	0.9	-
Doxorubicin powder (Dual)	4.7	0.8	1.5	-
Doxorubicin powder (50 mg/mL)	6.0	0.5	0.8	0.6
Sorafenib powder (25 mg/mL)	1.1	0.7	1.2	2.7
Sorafenib powder (Dual)	1.29	2.1	2.7	0.8
Sorafenib powder (50 mg/mL)	1.6	0.9	2.1	3.0

4.3.7 SEM analysis of 12% SELP-815K drug loaded gels

The prerelease SEM images presented in Figure 4.8 illustrate the clustering effect of the hydrophobic drugs as well as their entrapment by the SELP matrix. In comparison to the 9% SELP-815K drug loaded samples, the drug clusters in the 12% gels tended to be smaller and more distinct. In the postrelease samples, large clusters were not visible. Rather, wisp-like layers with crystalline features were spread on the polymer foundation (more clear in the inset images). A difference between the doxorubicin and sorafenib groups could not be distinguished. Compared to the 9% gels, the lack of large drug clusters in the 12% gels and the greater dispersion of drug could have been responsible for the lesser drug release rates, although the increased SELP-815K concentration could also have contributed.

4.4 Discussion

Treatment of intermediate stage HCC by transarterial chemoembolization (TACE) using drug eluting beads is currently limited by the types and the amount of drug that can be loaded. The direct incorporation of drugs, such as doxorubicin and sorafenib either individually or in combination, into *in situ* gelling SELP liquid embolic presents the potential to overcome this limitation. Thus, we incorporated these drugs into SELP-815K embolic formulations and determined their effect on the gelation of SELP solutions, the gel properties and the release rates of the drugs from the SELP gels *in vitro*. Release profiles of incorporated agents from SELP polymeric networks are controlled by the physical and chemical properties of both the gel and the drug including the degree of swelling of the three-dimensional network, the cross-linking density of the polymer matrix,

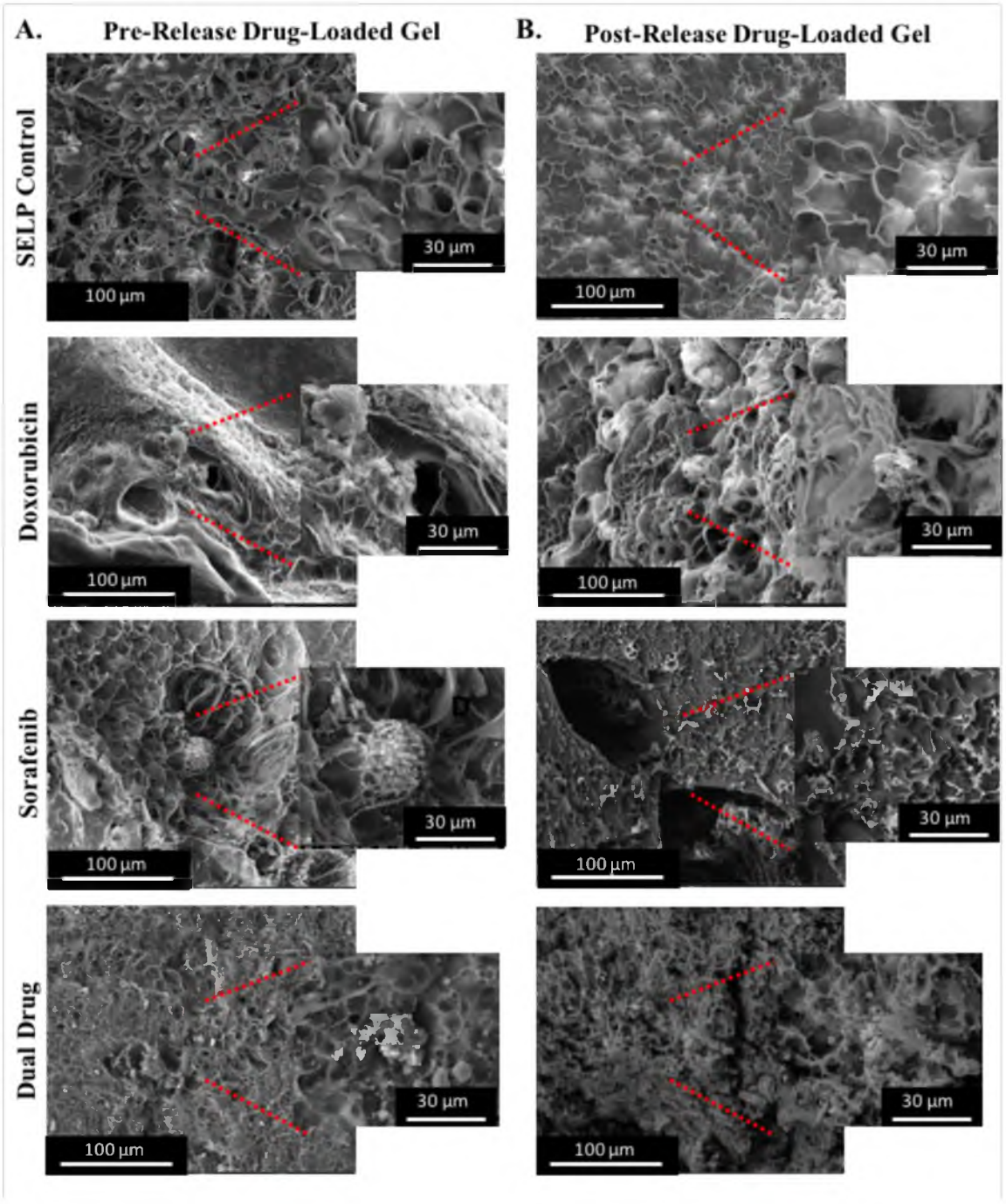

Figure 4.8. Scanning electron micrographs of 12% SELP-815K gel loaded with base forms of both doxorubicin and sorafenib powders. A) Representative images of prerelease gels. Drug clusters are clearly visible dispersed throughout the loaded gels. B) Representative images of postrelease gels. The bulk drug clusters are not readily observed but thin layers of crystalline drug are visible.

drug-polymer interactions, drug solubility and drug-drug interactions [35]. Low molecular weight, hydrophilic drug transport is dictated by Fickian diffusion in the regions of bulk water, a consequence of a highly porous hydrogel network. However, sparingly soluble agents, like doxorubicin and sorafenib, will display different release behavior, particularly from a protein polymer matrix that consists of large regions with hydrophobic residues. Hydrogen bonding, hydrophobic interactions, and ionic interactions may serve significant roles in transport behavior [36]. In the first series of studies, the salt forms of each drug were tested: doxorubicin hydrochloride and sorafenib tosylate. The salt forms are clinically used because of their relatively higher aqueous solubility compared to the base forms. Nonetheless, the aqueous solubility of doxorubicin HCl and of sorafenib tosylate are 10 mg/mL and 6-12 μg/mL, respectively. Both the literature referenced and the manufacturer's recommended drug loading level of DC Beads™ with doxorubicin is 25-40 mg/mL, which provides good handling properties for the drug-device combination and delivers a clinically effective local therapeutic dose [37, 38]. DC Beads™ cannot deliver sorafenib because the drug is not sufficiently soluble and is not positively charged. Thus, we investigated the incorporation of doxorubicin or sorafenib at 25 and 50 mg/mL drug loading levels and the combination of both drugs (Dual) at 12.5 and 25 mg/mL each in the SELP-815K liquid embolic. We incorporated the drugs into the SELP solution by direct dispersion of the drug powders, either the salt forms of the drugs or the free base, or by predissolving the drugs in DMSO. Because incorporation of predissolved drug was tested, addition of volume to the original 12% SELP-815K liquid embolic previously described [18], resulted in dilution of the protein content to 9%. Therefore, to understand the initial effects of drug incorporation on mechanical properties and subsequent relative release, all

solutions were diluted to 9% for comparison of the different test groups.

An immediate increase in the viscosity of the SELP solution occurred when drug was incorporated in either the salt form or if dissolved in DMSO. When doxorubicin HCl (Dox HCl) was mixed into 9% SELP solution (either as a powder but more so when dissolved in DMSO), the viscosity increased more than 2-fold compared to the SELP control. Similarly, the viscosity of the 9% SELP solution increased when doxorubicin base was dissolved in DMSO. On the other hand, incorporation of Dox base powder did not result in a change in viscosity. Similar results were observed although to a lesser extent with sorafenib tosylate (Soraf Tos) and sorafenib base. Incorporation of these drugs at 25 mg/mL, especially in the salt form, adds considerable ionic strength to the SELP formulation. For example, the concentration of potential solute introduced by addition of Dox HCl at 25 mg/mL is 96 mM. Depending on the extent of solubilization of the additive, a "salting out" effect of the SELP could occur. Temperature thinning was observed with 9% SELP solution containing the salt forms, Dox HCL and Soraf Tos, dissolved in DMSO. This may be due to reorganization of the drugs at higher temperature. Doxorubicin is known to self-associate in water and intercalate DNA as a function of hydrophobic forces induced through the electronic properties of its planar and aromatic doxomycinone portions [39–42]. Higher temperatures may cause self-association of the dissolved drug, especially for Dox HCl, decreasing the total effective solute concentration and resulting in less "salting out" of the SELP and reduced viscosity of the solution. However, even with the observed temperature thinning, the viscosity at room temperature of the SELP solutions containing the salt forms of the drugs were greater than the maximum viscosity required for injectability through a microcatheter (150 cP), and precluded these formulations from

proceeding to further testing.

While the addition of the salt forms of the drugs, especially dissolved in DMSO, affected viscosity, the final gel strength was not significantly affected. Differences in the storage moduli at 180 minutes were not significantly different between SELP incorporating the two drugs, but at 5 minutes doxorubicin loaded into the SELP solution in any form resulted in lower modulus. Again, this may be specific to doxorubicin; its planar and aromatic portions allow electronic interaction with a broad range of low and high molecular weight compounds that also contain planar aromatic ring systems [40]. SELP-815K does not have aromatic residues in the polymer backbone containing the repeating silk-like and elastin-like domains. However, there are aromatic residues in the head and tail sequences of the polymer. It is possible that drug-polymer interactions with these residues early in the gelation process may slow gelation, but as the silk-like blocks form long-range inter-polymer interactions resulting in beta-sheet crosslinks, the drug interactions with the tail sequences become inconsequential to the final gel network strength.

Drug-drug and drug-polymer interactions as a result of hydrophobic effects were hypothesized to contribute to extended release from the SELP matrices. In designing hydrogel networks for drug delivery, inclusion of hydrophobic blocks is commonly utilized to provide binding sites for hydrophobic drugs and reduce the average pore size to allow for slower diffusion-limited release [43]. The low cumulative release of sorafenib clearly demonstrates the effectiveness of the SELP hydrophobic domains to shield the drug from bulk water. Furthermore, during network formation, as the SELP solution loaded with drug begins to gel, and its hydrophobic domains aggregate, the drug clusters are immobilized (evidenced by the SEM micrographs). The entrapment augments the hydrophobic effect as

the hydrophobic regions of the polymer shield the drug clusters from water.

Although the hydrophobic interactions provided a means for entrapment and longer release rates, they also contributed to the limitations of the incorporation methods and release kinetics tested. It must be clarified how the cumulative release was determined and the sources of error that contributed to the limitations of this study. The cumulative release was calculated based on the expected drug loading of the gels, which was calculated based on weight with the assumption of even drug distribution when the gels were prepared. However, as the rheology data had indicated, specifically the 9% samples, the initial starting viscosity was low and the drug clusters would start to settle during preparation before the SELP solution started to gel (this concern was less evident in preparation of the 12% gels, since increase in viscosity occurred at a faster rate, trapping the clusters). Although the syringes were continuously rotated to minimize this effect, the drug cluster distribution was not fully homogenous. Furthermore, although the clusters were mechanically broken up in the samples with powder drug incorporation, larger clusters would re-form during preparation of the syringes, again contributing to the variability in drug distribution. Therefore, the actual drug loading may have been greater than the theoretical loading, resulting in higher calculated release. Thus, the release kinetics are considered as relative, and attention was given to the overall trends and the order of magnitude of the calculated concentrations.

The FTIR spectra and deconvoluted peak areas revealed each drug and its incorporation method caused changes in the protein secondary structures. First, sorafenib dissolved in DMSO and incorporated into the SELP solution alone or in combination with doxorubicin subsequently upshifted the primary beta-sheet peak to a higher wavenumber.

An upshift indicates an increased energy requirement to induce the C=O stretching vibrations in the protein backbone. This upshift does not necessarily indicate that the drug is interacting with the SELP backbone. Rather, the presence of the drug could be changing the chemical energy of the solution in the SELP network consequently affecting the configuration and bond energy of the hydrogen bonds in the beta-sheets, similar to the "salting out" effect hypothesized to be responsible for the increased viscosity of the SELP solution containing drug. Similarly, the presence of sorafenib resulted in higher alpha helix content and lower unordered coil content. This could be due either to drug: SELP interactions or simply to changes in backbone configuration due to the drug's influence on the solution in the SELP network. Both sorafenib and doxorubicin incorporated in powder form resulted in protein networks with higher beta-sheet content than the unloaded gel. Increased beta-sheet content is consistent with a less permeable network and the slower observed release profiles from these gels in addition to the lower swelling ratios.

The *in vitro* release profile of doxorubicin from 12% SELP gels was similar to published release from DC Beads™ of the same loading into a saline sink. In fact, the release plateau for the DC Bead™ started at 5 hrs, versus 7 days in the 12% SELP system, and cumulative release remained below 30% [45]. In the presence of plasma, doxorubicin release from DEBs is greater and more linear compared to release into saline [46]. Consequently, we expect that the release of doxorubicin and sorafenib may increase when release occurs in plasma or *in vivo*.

From a clinical standpoint, the released concentrations of drug from 12% SELP are in a range to produce therapeutic efficacy. *In vivo* testing in nontumor bearing pigs of 25 mg/mL doxorubicin loaded DC Beads™ revealed mean tissue concentration of

doxorubicin ranged between 0.75 and 2.05 μM [28]. In our study, even though release was into a PBS sink, doxorubicin was released at concentrations at or above the lower range of *in vivo* tissue concentrations for 2 weeks by both the 9% and 12% gels, in nearly all experimental groups. A study investigating the pharmacokinetics of sorafenib delivered as an emulsion in Lipiodol by TACE in rabbit livers, measured concentrations 1.7 μM and 0.14 μM in the liver tissue 24 hrs and 72 hrs after treatment, respectively [47]. SELP gels incorporated with sorafenib achieved similar concentrations in a sustained manner in the *in vitro* release tests. Therefore, based on *in vitro* results, the SELP embolic system has the capability of achieving therapeutically effective drug concentrations with the current design.

The base forms of each drug as a powder incorporated alone or in combination into 12% SELP-815K solution resulted in appropriate injection viscosity and gelation kinetics for a liquid chemoembolic. Although the doxorubicin showed a burst release from all groups, release continued over a period of at least 2 weeks, achieving 30% cumulative release, very similar to *in vitro* release from DC Beads™ that are now clinically used. Moreover, sorafenib, which cannot be delivered via DC Beads™, was incorporated and released from 12% SELP gels with greater linearity than doxorubicin. Although less than 30% cumulative release of sorafenib was achieved, the concentrations of drug released were in the micromolar range, adequate for therapeutic effects. An interesting finding in this study was the significant difference in release rate of sorafenib from dual drug loaded gels versus single drug loaded. The presence of doxorubicin with its greater relative hydrophilicity than sorafenib may facilitate water channeling into the combination drug clusters as doxorubicin is dissolved and released, increasing sorafenib's exposure to the

media. Investigation of different ratios of doxorubicin to sorafenib in dual drug loaded gels may provide insight into how the release of sorafenib may be tailored. Moving forward, the release kinetics of doxorubicin and sorafenib, alone and in combination, from SELP 815K liquid chemoembolic will be evaluated *in vivo* and based on the results, drug loading levels may be adjusted for clinical use.

4.5 Conclusion

Clinically established chemotherapeutics for the treatment of intermediate stage hepatocellular carcinoma, doxorubicin and sorafenib, were incorporated into SELP-815K solution developed for use as a liquid chemoembolic. The *in situ* gelling system resulted in drug release capable of locally sustained co-delivery of doxorubicin and sorafenib suggesting that the combination therapy may be utilized in TACE for the treatment of HCC. The results warrant the testing of the system *in vivo* to determine its chemoembolic performance and efficacy for treatment of HCC.

4.6 References

[1] El-Serag HB, Kanwal F. Epidemiology of hepatocellular carcinoma in the United States: where are we? Where do we go? Hepatology 2014;60:1767–75. doi:10.1002/hep.27222.

[2] El-Serag HB. Hepatocellular carcinoma. N Engl J Med 2011;365:1118–27. doi:10.1056/NEJMra1001683.

[3] Bruix J, Sherman M. Management of hepatocellular carcinoma: an update. Hepatology 2011;53:1020–2. doi:10.1002/hep.24199.

[4] Kan Z, Madoff DC. Liver anatomy: microcirculation of the liver. Semin Intervent Radiol 2008;25:77–85. doi:10.1055/s-2008-1076685.

[5] Lencioni R. Loco-regional treatment of hepatocellular carcinoma. Hepatology 2010;52:762–73. doi:10.1002/hep.23725.

[6] National Center for Biotechnology Information. Doxorubicin n.d. https://pubchem.ncbi.nlm.nih.gov/compound/31703 (accessed March 17, 2016).

[7] NCI. Doxorubicin hydrochloride. NCI Drug Dict 2015. www.cancer.gov.

[8] NCI. Sorafenib tosylate. NCI Drug Dict 2015. www.cancer.gov.

[9] Abou-Alfa GK, Johnson P, Knox JJ, Davidenko I, Lacava J, Leung T. Doxorubicin vs doxorubicin alone in patients with advanced hepatocellular carcinoma. JAMA 2010;304:2154–60. doi:10.1001/jama.2010.1672.

[10] Kudo M, Imanaka K, Chida N, Nakachi K, Tak WY, Takayama T, et al. Phase III study of sorafenib after transarterial chemoembolisation in Japanese and Korean patients with unresectable hepatocellular carcinoma. Eur J Cancer 2011;47:2117–27. doi:10.1016/j.ejca.2011.05.007.

[11] Pawlik TM, Reyes DK, Cosgrove D, Kamel IR, Bhagat N, Geschwind JFH. Phase II trial of sorafenib combined with concurrent transarterial chemoembolization with drug-eluting beads for hepatocellular carcinoma. J Clin Oncol 2011;29:3960–7. doi:10.1200/JCO.2011.37.1021.

[12] Cosgrove DP, Reyes DK, Pawlik TM, Feng AL, Kamel IR, Geschwind J-FH. Open-label single-arm phase II trial of sorafenib therapy with drug-eluting bead transarterial chemoembolization in patients with unresectable hepatocellular carcinoma: clinical results. Radiology 2015;277:594–603. doi:10.1148/radiol.2015142481.

[13] Zhang L, Hu P, Chen X, Bie P. Transarterial chemoembolization (TACE) plus sorafenib versus TACE for intermediate or advanced stage hepatocellular carcinoma: a meta-analysis. PLoS One 2014;9. doi:10.1371/journal.pone.0100305.

[14] Lewis AL, Dreher MR. Locoregional drug delivery using image-guided intra-arterial drug eluting bead therapy. J Control Release 2012;161:338–50. doi:10.1016/j.jconrel.2012.01.018.

[15] Poursaid A, Jensen MM, Huo E, Ghandehari H. Polymeric materials for embolic and chemoembolic applications. J Control Release 2016. doi:10.1016/j.jconrel.2016.02.033.

[16] Giunchedi P, Maestri M, Gavini E, Dionigi P, Rassu G. Transarterial chemoembolization of hepatocellular carcinoma- agents and drugs: an overview part 2.

Expert Opin Drug Deliv 2013;10:799–810. doi:10.1517/17425247.2013.796359.

[17] Arifin DY, Lee LY, Wang CH. Mathematical modeling and simulation of drug release from microspheres: implications to drug delivery systems. Adv Drug Deliv Rev 2006;58:1274–325. doi:10.1016/j.addr.2006.09.007.

[18] Poursaid A, Price R, Tiede A, Olson E, Huo E, McGill L, et al. In situ gelling silk-elastinlike protein polymer for transarterial chemoembolization. Biomaterials 2015;57:142–52. doi:10.1016/j.biomaterials.2015.04.015.

[19] Cappello J, Crissman JW, Crissman M, Ferrari F a., Textor G, Wallis O, et al. In-situ self-assembling protein polymer gel systems for administration, delivery, and release of drugs. J Control Release 1998;53:105–17. doi:10.1016/S0168-3659(97)00243-5.

[20] Cappello J, Crissman J, Dorman M, Mikolajczak M, Textor G, Marquet M, et al. Genetic engineering of structural protein polymers. Biotechnol Prog 1990;6:198–202.

[21] Megeed Z, Cappello J, Ghandehari H. Genetically engineered silk-elastinlike protein polymers for controlled drug delivery. Adv Drug Deliv Rev 2002;54:1075–91. doi:10.1016/S0169-409X(02)00063-7.

[22] National Center for Biotechnology Information. Sorafenib n.d. https://pubchem.ncbi.nlm.nih.gov/compound/216239 (accessed March 17, 2016).

[23] Dinerman A a, Cappello J, Ghandehari H, Hoag SW. Solute diffusion in genetically engineered silk– elastinlike protein polymer hydrogels. J Contr Rel 2002;82:277–87.

[24] Dandu R, Cresce A Von, Briber R, Dowell P, Cappello J, Ghandehari H. Silk-elastinlike protein polymer hydrogels: Influence of monomer sequence on physicochemical properties. Polymer (Guildf) 2009;50:366–74. doi:10.1016/j.polymer.2008.11.047.

[25] Biocompatibles. Instructions for use: DC Bead^{TM} drug delivery embolisation system n.d. http://bead.btg-im.com/products/.

[26] Blanchet B, Billemont B, Cramard J, Benichou a. S, Chhun S, Harcouet L, et al. Validation of an HPLC-UV method for sorafenib determination in human plasma and application to cancer patients in routine clinical practice. J Pharm Biomed Anal 2009;49:1109–14. doi:10.1016/j.jpba.2009.02.008.

[27] Pascale F, Bedouet L, Baylatry M, Namur J, Laurent A. Comparative chemosensitivity of VX2 and HCC cell lines to drugs used in TACE. Anticancer Res 2015;35:6497–503.

[28] Namur J, Wassef M, Millot JM, Lewis AL, Manfait M, Laurent A. Drug-eluting beads for liver embolization: concentration of doxorubicin in tissue and in beads in a pig model. J Vasc Interv Radiol 2010;21:259–67. doi:10.1016/j.jvir.2009.10.026.

[29] Barth A. Infrared spectroscopy of proteins. Biochim Biophys Acta - Bioenerg 2007;1767:1073–101. doi:10.1016/j.bbabio.2007.06.004.

[30] Fu T, Guerette PA, Tan RYT, Zhao H, Schefer L, Mezzenga R, et al. Biomimetic self-assembly of recombinant marine snail egg capsule proteins into structural coiled-coil units. J Mater Chem B 2015;3:2671–84. doi:10.1039/C4TB01434K.

[31] Teng W, Cappello J, Wu X. Physical crosslinking modulates sustained drug release from recombinant silk-elastinlike protein polymer for ophthalmic applications. J Control Release 2011;156:186–94. doi:10.1016/j.jconrel.2011.07.036.

[32] Hu X, Wang X, Rnjak J, Weiss AS, Kaplan DL. Biomaterials derived from silk-tropoelastin protein systems. Biomaterials 2010;31:8121–31. doi:10.1016/j.biomaterials.2010.07.044.

[33] Hu X, Kaplan D, Cebe P. Determining beta-sheet crystallinity in fibrous proteins by thermal analysis and infrared spectroscopy. Macromolecules 2006;39:6161–70. doi:10.1021/ma0610109.

[34] Bradley MS, Nishikida K. Infrared measurements of proteins: theory and applications. Madison: Thermo Electron Corporation; 2005.

[35] Haider M, Leung V, Ferrari F, Crissman J, Powell J, Cappello J, et al. Molecular engineering of silk-elastinlike polymers for matrix-mediated gene delivery: biosynthesis and characterization. Mol Pharm 2005;2:139–50. doi:10.1021/mp049906s.

[36] Dinerman A, Cappello J, El-Sayed M, Hoag SW, Ghandehari H. Influence of solute charge and hydrophobicity on partitioning and diffusion in a genetically engineered silk-elastin-like protein polymer hydrogel. Macromol Biosci 2010;10:1235–47. doi:10.1002/mabi.201000061.

[37] Lewis AL, Gonzalez MV, Lloyd AW, Hall B, Tang Y, Willis SL, et al. DC bead: in vitro characterization of a drug-delivery device for transarterial chemoembolization. J Vasc Interv Radiol 2006;17:335–42. doi:10.1097/01.RVI.0000195323.46152.B3.

[38] Lewis AL, Gonzalez MV, Leppard SW, Brown JE, Stratford PW, Phillips GJ, et al. Doxorubicin eluting beads - 1: Effects of drug loading on bead characteristics and drug distribution. J Mater Sci Mater Med 2007;18:1691–9. doi:10.1007/s10856-007-3068-8.

[39] Dalmark M, Storm HH. A Fickian diffusion transport process with features of transport catalysis. Doxorubicin transport in human red blood cells. J Gen Physiol 1981;78:349–64.

[40] Dalmark M, Johansen P. Molecular association between doxorubicin (adriamycin) and DNA-derived bases, nucleosides, nucleotides, other aromatic compounds, and proteins in aqueous solution. Mol Pharmacol 1982;22:158–65.

[41] Fülöp Z, Gref R, Loftsson T. A permeation method for detection of self-aggregation of doxorubicin in aqueous environment. Int J Pharm 2013;454:559–61. doi:10.1016/j.ijpharm.2013.06.058.

[42] Agrawal P, Barthwal SK, Barthwal R. Studies on self-aggregation of anthracycline drugs by restrained molecular dynamics approach using nuclear magnetic resonance spectroscopy supported by absorption, fluorescence, diffusion ordered spectroscopy and mass spectrometry. Eur J Med Chem 2009;44:1437–51. doi:10.1016/j.ejmech.2008.09.037.

[43] Hoare TR, Kohane DS. Hydrogels in drug delivery: Progress and challenges. Polymer (Guildf) 2008;49:1993–2007. doi:10.1016/j.polymer.2008.01.027.

[44] Hotha KK, Reddy SPK, Raju K, Ravindranath LK. Forced degradation studies: practical approach- overview of regulatory guidance and literature for the drug products and drug substances. Int J Pharm 2013;4:78–85.

[45] Jordan O, Denys A, De Baere T, Boulens N, Doelker E. Comparative study of chemoembolization loadable beads: in vitro drug release and physical properties of DC Bead and Hepasphere loaded with doxorubicin and irinotecan. J Vasc Interv Radiol 2010;21:1084–90. doi:10.1016/j.jvir.2010.02.042.

[46] Gonzalez MV, Tang Y, Phillips GJ, Lloyd AW, Hall B, Stratford PW, et al. Doxorubicin eluting beads - 2: Methods for evaluating drug elution and in-vitro:in-vivo correlation. J Mater Sci Mater Med 2008;19:767–75. doi:10.1007/s10856-006-0040-y.

[47] Chatziioannou AN, Siskos AP, Loxas D, Kavatzas N, Agrogiannis G, Fokas D, et al. Transarterial embolization with sorafenib in animal livers: A pharmacokinetics study. J Vasc Interv Radiol 2013;24:1657–63. doi:10.1016/j.jvir.2013.08.007.

CHAPTER 5

CONCLUSIONS AND FUTURE DIRECTIONS

5.1 Conclusions

In this dissertation, the potential to exploit unique material properties of recombinant silk-elastinlike protein (SELP) polymers for development to a novel liquid chemoembolic in treatment of hepatocellular carcinoma (HCC) was demonstrated. HCC remains a substantial global disease and transarterial chemoembolization (TACE) offers a palliative treatment with significant clinical outcome for patients ineligible for surgery.[1]. The embolic materials and chemotherapeutics used in this procedure, however, are not standardized [2]. Reasons for this are the multitude of advantages and disadvantages of the currently available materials illustrated in Chapter 2 [3]. The oil-drug emulsion system used with degradable gelatin particles provides high tumor penetration and a non-permanent option while drug eluting beads (DEBs) allow for a permanent blockage and extended controlled release of drug locally. The goal of this work was to combine and refine the advantages of the liquid emulsion system and the controlled release of the embolizing DEBs using a SELP platform.

In Chapter 3, a series of design criteria were established that qualified the SELP embolic including injectability through a commercially available microcatheter and occlusion of an *in vitro* arterio-capillary network simulating an HCC tumor under flow

conditions [4]. Formulation development began with testing two different SELP compositions at different weight percentages. The importance of the structure-function relationship was demonstrated in this these studies. Higher silk content of the SELP-815K provided a more robust construct as compared to the SELP-47K in creation of an embolic required to withstand physiologic blood pressure. The crystalline beta-sheet formations afforded by long range interpolymer hydrogen bonding of the silk-like units is essential for appropriate gelation and stiffness parameters. This was shown when measuring the rheological properties of SELP formulations made up by resuspending lyophilized powder into aqueous solutions versus shear processing the solution first. Shearing subjects the formulation to high shear stress that strips low strength intrapolymer hydrogen interactions, allowing for the long range hydrogen bonding between polymer strands [5]. Disruption of these secondary structures by drug incorporation was a potential design element to consider, which was analyzed in Chapter 4 when hydrophobic drugs were loaded into the SELP solution. The work in Chapter 3 resulted in identification of a specific SELP composition and concentration, SELP-815K 12% by weight, that required shear processing, which met the design criteria for a bland liquid embolic. This formulation tested *in vivo* TACE procedures in a rabbit model demonstrated easy injectability followed by increase in resistance during the saline flush and clinical stasis in the target vessel. Hepatic and pulmonary tissues from the sacrificed animals were analyzed for evidence of the liquid embolic and potential nontarget embolization. The SELP material was located within the arterioles of portal triads, which was the expected target. The liquid embolic filled the entirety of the lumen, an advantage over microspheres. Therefore, the ability of a SELP solution to function as a bland embolic was verified.

These studies, however, did not test a series of injection methods that may take place clinically. In the rabbit studies, the microcatheter was maneuvered as distally into the target vessel as possible, nearly matching the diameter of the vessel before the SELP liquid embolic was injected. The position of the catheter created a temporary embolus, blocking blood from flowing past the catheter tip. This allowed the SELP embolic to gel in the target smaller vessels without any dilution by blood. Clinically, though, there may be situations where the catheter has to be positioned more proximally, meaning more upstream from the target location of embolization. This would require the SELP liquid embolic to travel farther as a liquid before physically cross-linking into a gel. Therefore, several questions remain: will the liquid embolic reach its target? Will it gel along the way? Or will it dilute in blood and not gel at all if the injection site is in a larger artery? While the SELP solution is being injected and subjected to shear force, the material will continue to flow, even when already warmed to physiological temperature. However, once the force stops, the increase in viscosity is logarithmic. But, the gel remains pliable for several minutes as was shown in the rheological studies and from empirical evidence. Therefore, a follow-up injection of more SELP solution or saline will push the soft gel and lodge it in the downstream target location. But, if a partially or fully gelled embolus is lodged to create an obstruction, blood flow is blocked and the gel embolus essentially acts like the DEBs; the advantage of permeation into the small arteriole branches is lost. Larger scale *in vitro* models using three-dimensionally printed, anatomically correct vessels may provide a fast testing system to be able to answer some of these questions.

Chapter 4 built upon the work accomplished in Chapter 3 to broaden the bland SELP-815K liquid embolic into a drug loadable system [6]. The drugs investigated were

doxorubicin, the most commonly used and literature referenced chemotherapeutic in TACE, and sorafenib, the only FDA approved drug with antiangiogenic properties for intermediate and advanced HCC. The goal was to show incorporation of more than one therapeutic to address the single drug limitation of DEBs. The high lipophilicity of these drugs was hypothesized to allow for extended release from the SELP matrix, which also has high hydrophobic character. The incorporation method of these drugs was well deliberated. For a clinically relevant material, the ability to mix in drugs just prior to use with a range of possible loadings to fit the patient's needs, was part of the design. But, level of drug homogeneity when suspended in the SELP solution and subsequent gelation had to be considered. Therefore, both predissolved drugs in dimethyl sulfoxide (DMSO) (DMSO solvent is used in clinically approved market liquid embolics) mixed into the SELP solution and drug powders mechanically mixed in were tested. Although the incorporation of pre-dissolved drug showed better dispersion throughout the resulting gel network, the overall release rate of doxorubicin was similar. A significant difference was evident only in the first 24 hours, with higher release from the predissolved group. Incorporation method showed a more pronounced effect for sorafenib, with more cumulative release from the predissolved drug mixed into the SELP solution. The presence of doxorubicin improved the release kinetics of sorafenib. Powder drug mixed into the 12% SELP solution was studied for extended release. Therapeutic concentrations were achieved from these gels for up to 2 weeks for doxorubicin and up to 30 days for sorafenib. The drug loaded SELP solutions and resulting gels were carefully characterized to determine the effects of drug loading on rheological properties and protein secondary structures, namely the solution viscosity, the gelation kinetics, and the final gel strength. The 12% SELP-815K loaded

with single and dual drug powders continued to meet the original liquid embolic specifications.

It must be emphasized, however, the incorporation methods and subsequent release studies described had limitations. The primary design goal for the SELP liquid embolic had been use of a straight-forward, *ex vivo* mix-in method for the drugs. This approach is available owing to the aqueous formulation, which is one of the described advantages of the SELP liquid embolic over the clinically available counterparts. It would allow the physician control over which drug and what concentration to use based on the needs of the patient. However, the high concentration of the chosen drugs and their hydrophobic character resulted in a pharmaceutical dispersion at best, which was further complicated by settling of the drug particulates unevenly. The latter is one of the sources of error when calculating the cumulative release, which was based on the assumption of a homogenous drug dispersion.

Several methods to determine the actual drug content from drug loaded gel samples pre- and postrelease were investigated by attempting to break down the SELP matrix to liberate the drug. The SELP matrix, once gelled, however, is insoluble in most solvents. Only high molarity acids or bases may be used to completely hydrolyze the matrix. First, 26 M formic acid was used to try and dissolve the gel in a short period of time, 30 minutes, by breaking the hydrogen bonds that create the physical network. Unless the gel is mechanically broken up into small pieces first, <1mm pieces, the entire gel does not go into solution. Drug standards made up in DMSO were subjected to the same conditions, then neutralized and analyzed via HPLC. For both drugs, no peaks could be resolved, indicating stress induced degradation. But, clear degradation product peaks could not be

determined. Mass spectrometry approaches may provide an alternative analysis technique. Next, base hydrolysis was investigated. However, when the gel was subjected to 0.1M NaOH at 37° C for a week, the gel remained intact. Higher molarity base, up to 12 M, and higher temperatures will have to be investigated and the same conditions will have to be used on drug standards to determine if any degradation products can be detected or if the molecules are completely hydrolyzed. Nonetheless, the drug release studies provided important understanding regarding relative release kinetics of hydrophobic drugs from the SELP matrix. Future directions will involve improving the method of drug incorporation to result in a homogenous drug dispersion.

The *in vitro* release results from the drug loaded gels were determined to be in therapeutic ranges. However, release into a saline sink does not diametrically translate *in vivo*. A rat hepatoma model was used for preliminary testing of therapeutic efficacy of the drug loaded 12% SELP-815K chemoembolic formulations, presented in Appendix A. The hepatoma model used provides a clinically relevant syngeneic HCC tumor. Two parallel treatment administration avenues were pursued, both requiring the animals to undergo multiple abdominal surgeries. The first, which was more successful, was comprised of direct intratumoral treatment administration. In these studies, complication rates resulted in low power and therefore no significance could be reported. However, trends revealed that location of the injected SELP solution and subsequent gel are imperative for therapeutic outcome. When centrally located, drug loaded SELP gels showed higher tumor regression than SELP alone and treatments consisting of drug simply suspended in saline. Location of the gel addresses the diffusion driven release of the drugs. When the gels were located at the tumor perimeter on the liver edge, neoplastic tissue expanded away from the

gel and into the liver lobe. These results provide motive to expand the *in vivo* studies in the future. The second administration route, which is homologous to the TACE procedure, required arterial catheterization to access the hepatic vasculature. The microsurgical finesse required did not allow for successful number of procedures to test the SELP chemoembolic. However, this second method provides the more appropriate animal model for future testing.

5.2 Challenges and future directions

The culmination of this work indicates clinical translation of the SELP chemoembolic may result in an improved treatment system for HCC patients. However, before advancing towards translation, several details of the described system must be further addressed. Although *in vitro* release showed micromolar concentrations may be reached and the preliminary intratumoral efficacy studies suggested *in vivo* translation, several more encompassing animal studies are required. Intraarterial treatment would provide a stronger model. The rat hepatoma model or the rabbit VX2 model should be investigated. The rat hepatoma model provides a more clinically relevant syngeneic tumor but requires a highly skilled microvascular surgeon while the rabbit provides larger and more convenient vessels for intraarterial access and subsequent intrahepatic treatment administration. The rabbit model can be used to assess long-term biocompatibility of the SELP chemoembolic. The longevity of the SELP embolus in the vessels must be determined as well as the type of physiological response the body initiates. Since SELP is a protein, the embolus can be degraded. However, the SELP-815K composition in previous work has shown very slow degradation rates and high level of fibrotic encapsulation, but

these studies were of SELPs injected into squamous cell carcinoma tumors with highly dynamic physiologic milieu [7]. A natural progression is investigating SELP compositions with added matrix-metalloproteinase (MMP) degradable sequences [5,8]. HCC patients often require multiple TACE treatments as secondary tumors grow or the residual tumor is revascularized and begins to progress. Therefore, a degradable SELP system with a predictable degradation rate may address this need. MMP-2 and MMP-9 are both highly expressed by HCC neoplasms [9]. Location of the MMP responsive unit is imperative to the mechanical integrity of the liquid embolic. If the MMP responsive unit is placed in the silk block, the SELP solution does not readily transition into a gel nor does the eventual gel have high enough mechanical stability since the silklike units provide the primary mechanical support of the physically cross-linked gel. Three MMP-responsive SELP analogs that have been synthesized and characterized show clear evidence of how location affects mechanical properties [5]. The MMP responsive analog with the responsive unit placed at the juncture between the silk block and elastin block had similar mechanical characteristics as the native SELP-815K postshear processing. Therefore, this analog may be investigated in future studies as a degradable option. Another approach in design would be to incorporate a responsive sequence that would activate a component of the natural fibrinolysis cascade such as plasminogen [10].

Next, the method of drug incorporation should be expanded and improved. For a clinically useful system, the chemoembolic must be designed with the end users in mind—the clinician and the patient. In the operating room, physicians prefer tools with minimal preparation time and low number of components. That is the motivation behind the direct mix in method for drug incorporation. But, the hydrophobicity of the selected drugs, a

characteristic common to many chemotherapeutics, posed the problem of drugs clustering upon mixing with the aqueous based SELP solution, particularly in powder form. The level of clustering cannot be satisfactorily controlled in the current method, which as described earlier poses a risk of inaccurate release rates. One direction for improvement is to create preloaded SELP syringes, with several options for concentration, as well as to increase the drug and drug combination options. To develop the SELP liquid embolic into a generic drug carrier, model drugs that encompass the range of different molecules available would have to be tested. Parameters to modulate may include molecular weight, molecular architecture, overall charge, and partition coefficient in addition to expansion from small molecule drugs to biologics like monoclonal antibodies. The drugs could be incorporated into the SELP solution just prior to shearing at the appropriate concentration, which would not lead to dilution of the SELP content. Furthermore, the shearing would aid in maintaining drug distribution and break down precipitating crystals. However, precipitation of highly hydrophobic drugs out of solution postshearing may remain a limitation of the current formulation. Extensive characterization studies similar to those presented in this work would be conducted. Mathematical modeling using the acquired data may then provide predictive models for similar drugs. If the preloaded solutions result in a chemoembolic solution meeting the established design criteria, an even simpler product can be provided to the clinician. This would, though, require the clinician to pre-determine the appropriate drug/drug combination and dosing for the patient being treated.

Next, larger animal studies will be required to study the distribution of drug within the tissue surrounding the drug loaded SELP embolic as well as the systemic drug levels. Since there is a level of interaction between the drug and SELP backbone, it must be

determined how much drug diffuses out of the matrix and into the tissue. Measuring systemic levels will also help understand the release kinetics and provide guidance to the maximum drug loading that can be tolerated. Swine, including Yucatan pigs, provide a relevant model, particularly since they have vessels comparable in size to humans [11]. At designated time points, blood and tissue samples must be taken and extraction methods implemented to determine drug content [12]. Successful completion of these studies on the developed generic SELP liquid embolic would allow progression to scaling up production for clinical translation. Work with the larger animal models would continue to conduct preclinical toxicology and performance testing, which if shown safe and effective would pave a way towards clinical trials.

Finally, as Chapter 2 had elucidated, an "imageable" embolic provides the clinician better prediction methods of therapeutic outcome having the ability to track the injected embolus and in turn location of drug delivery over time. The SELP-815K composition has lysine residues that provide access points for chemical linkage of an MRI or CT detectable agent like gadolinium. Furthermore, during the formulation development study (Chapter 3), direct incorporation of iso-osmolar contrast dye (iodixanol) at 20% by weight revealed no significant change to the SELP physical properties. However, the amount of contrast was not high enough for visualization once injected *in vivo*. Higher content of radiopaque dye should be investigated. Another future direction would be to incorporate magnetothermally-responsive nanomaterials into the SELP embolic. These nanostructures would serve as imaging agents and provide trigger controlled drug delivery [13]. The imaging component would allow for detection of the embolic. If for example drug release is desired after a period when necrosis begins, then using an alternating current magnetic

field, the drug carrier would be triggered to release its payload via localized heating [13]. The carrier systems currently described in the literature have a lower critical solution temperature between 40-45 °C, which would not destroy the encompassing SELP embolic. Along the lines of trigger release systems, ultrasound-triggered drug release nanoparticulate systems are also an avenue for investigation. Polymeric polylactic acid particle systems have been described in the literature that can incorporate model drugs and release the drug load with a pressure trigger via ultrasound [14,15]. Developing a combination embolic systems adds another level of complexity, but a multifunctional, controllable system has clinical relevance.

While treatment of HCC was the intended application explored in this work, the application for the SELP liquid embolic can be expanded to several other disease models, including but not limited to arteriovenous malformations and leiomyomas. To expand even further, bioactive agent or stem cell delivery to cardiac tissue postmyocardial infarction for muscle regeneration or muscle support with a gel-like matrix is another possible investigative avenue. Less invasive, endovascular techniques are increasing overall and a liquid biomaterial composed of a highly tunable composition, capable of drug or biologic delivery, and *in situ* gelling provides a very unique material platform to continue innovating.

5.3 References

[1] Ferri F. Hepatocellular carcinoma. Ferri's Clin. Advis. 2016. 2nd ed., Elsevier; 2016, p. 605–7.

[2] Lencioni R. Management of hepatocellular carcinoma with transarterial chemoembolization in the era of systemic targeted therapy. Crit Rev Oncol Hematol 2012;83:216–24. doi:10.1016/j.critrevonc.2011.10.008.

[3] Talenfeld AD, Sista AK, Madoff DC. Transarterial therapies for primary liver tumors. Surg Oncol Clin N Am 2014;23:323–51. doi:10.1016/j.soc.2013.11.002.

[4] Poursaid A, Price R, Tiede A, Olson E, Huo E, McGill L, et al. In situ gelling silk-elastinlike protein polymer for transarterial chemoembolization. Biomaterials 2015;57:142–52. doi:10.1016/j.biomaterials.2015.04.015.

[5] Price R, Poursaid A, Cappello J, Ghandehari H. Effect of shear on physicochemical properties of matrix metalloproteinase responsive silk-elastinlike hydrogels. J Control Release 2014.

[6] Poursaid A, Jensen MM, Nourbakhsh I, Weisenberger M, Cappello J, Ghandehari H. Silk-elastinlike protein polymer liquid chemoembolic for localized release of doxorubicin and sorafenib. Mol Pharm 2016:Submitted.

[7] Price R, Gustafson J, Greish K, Cappello J, McGill L, Ghandehari H. Comparison of silk-elastinlike protein polymer hydrogel and poloxamer in matrix-mediated gene delivery. Int J Pharm 2012;427:97–104. doi:10.1016/j.ijpharm.2011.09.037.

[8] Gustafson JA, Price RA, Frandsen J, Henak CR, Cappello J, Ghandehari H. Synthesis and characterization of a matrix-metalloproteinase responsive silk-elastinlike protein polymer. Biomacromolecules 2013;14:618–25. doi:10.1021/bm3013692.

[9] Arii S, Mise M, Harada T, Furutani M, Ishigami SI, Niwano M, et al. Overexpression of matrix metalloproteinase 9 gene in hepatocellular carcinoma with invasive potential. Hepatology 1996;24:316–22. doi:10.1053/jhep.1996.v24.pm0008690399.

[10] Leytus SP, Bowles LK, Konisky J, Mangel WF. Activation of plasminogen to plasmin by a protease associated with the outer membrane of Escherichia coli. Proc Natl Acad Sci 1981;78:1485–9.

[11] Namur J, Wassef M, Millot JM, Lewis AL, Manfait M, Laurent A. Drug-eluting beads for liver embolization: concentration of doxorubicin in tissue and in beads in a pig model. J Vasc Interv Radiol 2010;21:259–67. doi:10.1016/j.jvir.2009.10.026.

[12] Dharmalingam SR, Nadaraju S. A simple HPLC bioanalytical method for the determination of doxorubicin hydrochloride in rat plasma: application to pharmacokinetic studies. Trop J Pharm Res 2014;13:409–15.

[13] Brazel CS. Magnetothermally-responsive nanomaterials: combining magnetic nanostructures and thermally-sensitive polymers for triggered drug release. Pharm Res 2009;26:644–56.

[14] Böhmer MR, Chlon CHT, Raju BI, Chin CT, Shevchenko T, Klibanov AL. Focused ultrasound and microbubbles for enhanced extravasation. J Control Release 2010;148:18–

24.

[15] Lensen D, Gelderblom EC, Vriezema DM, Marmottant P, Verdonschot N, Versluis M, et al. Biodegradable polymeric microcapsules for selective ultrasound-triggered drug release. Soft Matter 2011;7:5417–22.

APPENDIX A

PRELIMINARY *IN VIVO* EVALUATION OF SELP CHEMOEMBOLIC IN A RAT HEPATOMA MODEL

A.1 Introduction

Investigation of new pharmaceuticals, drug delivery vehicles, combination medical devices, etc. requires use of appropriate animal models to translate *in vitro* results in the complex physiological milieu. In cancer models, syngeneic orthotopic tumors are considered more clinically relevant than subcutaneous xenograft models for testing therapy efficacy [1]. The intended microenvironment and specific pathophysiological features are mimicked at the molecular and cellular level, the levels at which most treatments target [2]. The disease being investigated in this work is hepatocellular carcinoma (HCC). Treatments for HCC often involve a host of therapeutic materials and treatment modalities. This disease presents a significant global clinical burden whose long-term survival remains elusive [3]. One palliative treatment method for nonsurgical candidates is transarterial chemoembolization (TACE), which involves intravascular access of tumor vessels and delivery of chemoembolic materials to induce necrosis via hypoxic and cytotoxic mechanisms. A new aqueous based liquid chemoembolic is currently under investigation. Silk-elastinlike protein (SELP) polymers provide the embolic material platform [4,5].

SELPs are recombinant block co-polymers whose structure directly affects their

function based on sequence composition. The developed SELP-815K consisting of 8 silk-like units and 15 elastin-like units per monomer was designed into a liquid embolic that gels *in situ* at physiological temperature. It was shown to maintain low viscosity for injection via microcatheter, gel within the arterio-capillary network *in vivo* and achieve clinical stasis in a nontumor bearing rabbit model, and incorporate the drugs doxorubicin and sorafenib for localized dug delivery [4,5]. These determined features present a competitive chemoembolic system to the materials currently available for HCC treatment. The purpose of this study was to investigate the therapeutic efficacy of the drug loaded SELP chemoembolic in a tumor bearing animal model. *In vitro* release studies indicated therapeutic concentrations may be achieved. However, this must be confirmed *in vivo* [4].

The rabbit VX2 model is often used in HCC studies investigating image-guided interventions for its convenience of size for vascular catheterizations. However, the VX2 cell line is of squamous cell carcinoma origin and does not offer an appropriate HCC likeliness [2]. Therefore, rat hepatoma models were explored. The McA-RH7777 hepatoma cell line derived from the Morris 7777 line provides a syngeneic HCC model in immune competent animals. When implanted into Sprague Dawley rats, isolated tumors grow with minimal metastatic spread. Furthermore, this animal model can be used for preclinical investigation of intravascular delivered therapeutics [6].

Herein we assessed the therapeutic efficacy of the drug loaded SELP-815K liquid embolic intratumorally in the McA-RH7777 rat hepatoma model in a preliminary study. SELP solutions either loaded with doxorubicin alone or jointly with sorafenib were tested in comparison to unloaded SELP-815K and injections of suspended drug in phosphate buffered saline (PBS). Additionally, the occlusive ability of the SELP-815K liquid embolic

was also tested in the rat via catheterization of the gastroduodenal artery (GDA) that feeds into the proper hepatic artery.

A.2 Materials and methods

A.2.1 Materials

SELP-815K was synthesized and characterized as previously described [7,5]. Sorafenib base was purchased from LC Laboratories (Woburn, MA) and doxorubicin base was purchased from MedKoo Biosciences (Chapel Hill, NC). Adult, male Sprague Dawley (SD) rats were purchased from Charles River Laboratories (Wilmington, MA). The McA-RH7777 cell line was generously donated by the Larson Lab, Northwestern University (Chicago, IL).

A.2.2 Cell culture

McA-RH7777 rat hepatoma cells were cultured in Dulbecco's Modified Eagle Medium (DMEM) (ATCC) supplemented with 10% fetal bovine serum (FBS) and 1% penicillin-streptomycin antibiotic. The cells were grown at 37°C in a humidified atmosphere of 5% CO_2.

A.2.3 Tumor induction

Animal studies were approved by our institutional animal care and use committee (IACUC). Orthotopic tumor induction required a laparotomy and direct hepatic injection. Briefly, animals were prepped under sterile surgical conditions. Isoflurane at 5% was used to induce anesthesia and animals were maintained at 2% for the duration of the procedure.

A longitudinal subxiphoid incision of approximately 4 cm was made to expose the liver lobes. The left lobe was isolated and $1x10^6$ cells suspended in 200 μL of nonsupplemented DMEM was injected beneath the liver capsule using a 0.5 cc insulin syringe equipped with a 28-gauge needle. Upon retraction of the needle, hemostatic gauze was immediately placed over the wound with gentle compression to prevent bleeding. After confirmation of a successful injection and no bleeding, the abdominal wall was closed using 4-0 monocryl suture with a simple interrupted stitch followed by subcuticular suturing of the skin layer. Skin adhesive was applied along the incision line. Animals were closely monitored post-operatively. Pain level was managed with buprenorphine and nonsteroidal anti-inflammatory drugs. To prevent self-mutilation, rats were either wrapped in bandages or fitted with a cone collar or a combination of both. Tumors were allowed to grow for 1 week prior to imaging and subsequent treatment surgery.

A.2.4 MRI imaging

Tumor growth was monitored using an MR-compatible physiological monitoring system with body temperature controlled via warm air fan system (SA Instruments, Stony Brook, NY, USA). Imaging experiments were performed on a 7T Bruker Biospec MRI scanner (Bruker Biospin Inc, Ettlingen, Germany) interfaced with 12-cm actively shielded gradient insert capable of producing magnetic field gradient up to 600 mT/m. Rats were placed in a 72-mm volume coil for signal transmission, and a 4-channel phased array coil for signal reception. To visualize and estimate tumor volume, respiration-gated T2-weighted rapid acquisition with relaxation enhancement (RARE) was used to image 15-20 short-axis slices covering the left liver lobe with the following parameters: repetition time

(TR) of 800-1200 ms depending on breathing rate, echo time (TE) of 14 ms, echo train length 2, signal excitations 2, slice thickness 1mm, field of view 3 cm × 3 cm, and an in-plane resolution of 234 μm × 234 μm. Acquired DICOM files were analyzed in OsiriX 7.0 image processing software to identify and calculate tumor dimensions and volumes.

A.2.5 Intratumoral treatment surgery

Intratumoral treatment surgery was conducted 8 days post-tumor induction. Animals were imaged as previously described to ensure solitary tumors of approximately 4mm x 4mm were present. Similar to the first surgery, the rats were anesthetized and a laparotomy was performed to isolate the tumor bearing liver lobe. Identified treatment was prepared in a sterile hood just prior to use. Briefly, treatment groups with SELP required thawing pre-measured volumes of SELP (stored frozen) and kept chilled on ice. Preweighed, milled drug powders were next transferred to the SELP solution and mechanically mixed using a custom built overhead mixer equipped with a 1/16" diameter spiral impeller for 10 seconds at 5400 RPM, resulting in a 25 mg/mL/dug concentration. The drug-SELP mixture was loaded into a sterile 1 mL syringe and capped with a 25-gauge needle. Treatment groups without SELP underwent the same mixing procedure where the SELP solution was replaced with phosphate buffered saline. Next, the tumor was palpated and the center was approximated. Gently, the needle was inserted into the center of the mass and 20 μL of treatment solution was slowly injected. The treatment volume was determined based on the typical TACE human dosing of 1-1.5 mg/kg. The rats in this study averaged 400 g, resulting in a similar dose. Due to the delicate surface of the expanded liver capsule covering the tumor, hemostatic gauze was placed on top of the injection site

with minimal compression to prevent tumor rupture. Once lack of bleeding was ensured, the rat was closed up as previously described. Overall health and weight were monitored along with tumor growth via MRI. Imaging was conducted on days 3, 7, and 14 for all treatment groups and up to 21 and 30 days for subsets of SELP injected animals following treatment administration.

A.2.6 Intraarterial embolization surgery

The intraarterial catheterization procedure was adapted from Sheu *et al.* [6]. This surgery provides an analogous treatment procedure to TACE in humans. The goal was to catheterize the animal and access the hepatic artery for injection of chemoembolic material into the liver vascular supply. Briefly, the procedure consisted of performing a laparotomy as previously described followed by careful dissection of the portal triad structures and the gastroduodenal artery, which branches from the common hepatic artery. Use of a dissecting microscope aided in the dissection process. A 2-0 silk suture was used to anchor the GDA and create a ligation point as well as provide traction on the common hepatic artery. The introducer of a 24-gauge SurFlash polyurethane catheter (Terumo Medical Co., Somerset, NJ) was inserted into the GDA proximal to the ligation site but as distally to the branch point of the GDA from the common hepatic artery. Carefully, the catheter was advanced into the GDA past the common hepatic artery and into the proper hepatic artery. Another silk suture was placed beneath the catheterized vessel and tied to anchor the catheter. Contrast dye diluted 50:50 with saline was injected and the vessels were visualized using an OEC/GE Series 9800 Mobile C-arm (GE Healthcare, Little Chalfont, UK). Next, 0.6 mL of SELP-815K solution was injected until resistance was detected. Saline was followed

to flush the catheter (0.1 mL). Following a 5-minute wait time, more contrast was injected to visualize change in flow with in the hepatic vasculature. The GDA was ligated and the procedure was ended.

A.2.7 Histological analysis of tissues

Livers of each animal were harvested at designated time points and fixed in 10% buffered formalin for 48 hrs and then transferred to 70% ethanol. Sections from the left liver lobe were cut in 5 mm slices and analyzed. Tissue samples were stained using hematoxylin and eosin (H&E) stain. Pieces of pregelled SELP with and without drug were fixed, sliced, mounted onto a slide, and stained as positive controls. Slides were imaged using a Nikon DXM 1200C Digital Camera affixed to an Olympus BH2 microscope and analyzed in ACT-1C for DXM1200C software.

A.3 Results

A.3.1 Tumor induction

Tumors were successfully induced in 90% of rat livers, confirmed via MRI. Two rats out of 20 grew extrahepatic secondary tumors in the body wall and in the omentum just outside of the liver, respectively. These tumors remained contained and the overall health of the animals was not affected. During tumor induction surgery of these two animals, reflux of cells from the injection site had been noted. They were in earlier surgical groups, and the practice of dabbing the tissue with 70% ethanol followed by saline rinse and immediate pressure on the wound was ensued to prevent extraneous tumors in subsequent animals. Location of the hepatic tumors was consistent, growing on the lower

left lobe just distal to the liver edge. Figure A.1 shows an image of a tumor just prior to treatment injection.

A.3.2 Intratumoral treatment and MRI tumor growth analyses

The average pretreatment (pre-tx) tumor volume was determined to be 48 mm^3 of spheroid tumors with 4.5 mm average diameters. The pretreatment tumors were imaged 7 days posttumor induction. Treatment surgery was performed the following day. A representative MRI slice showing the solitary tumor is shown in Figure A.2. The three-dimensional tumor model is also shown, depicting how tumor volume was calculated. In this preliminary study, one of the following treatments was administered: SELP alone, doxorubicin mixed into SELP (SELP+Dox), doxorubicin and sorafenib mixed into SELP (SELP+Dual), doxorubicin suspended in PBS (Dox Sol), or doxorubicin and sorafenib suspended in PBS (Dual Sol). Three rats were randomly assigned to each treatment group. However, due to surgical or postoperative complications, only SELP+Dox and SELP+Dual groups had all three animals reach designated time points. Therefore, significance in results cannot be reported. Change in tumor volume, the measure of treatment efficacy, is presented in Figure A.3. The treatment groups consisting of drug suspended in saline had the greatest increase in tumor volume over time, more so in the Dual Sol group; though as evident by the error bars, the growth behavior was not consistent between rats. Treatment groups with SELP had similar changes in tumor volume. A subset of animals consisting of one rat from each SELP treatment group was followed up to 30 days. By day 21 and up to day 30, no tumor was evident in either rat treated with SELP and drug, either doxorubicin or the dual combination. In general, the animal with the dual drug treatment

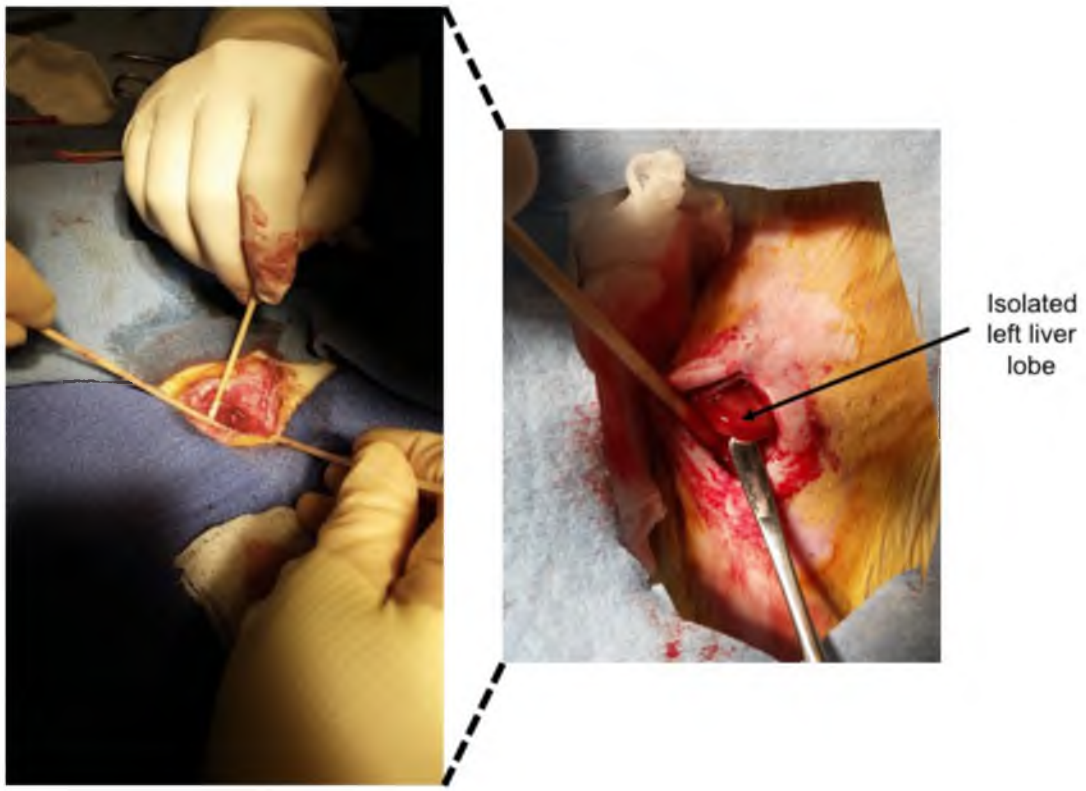

Figure A.1. Images from rat laparotomy. This procedure was performed to isolate the left liver lobe for tumor induction followed by a second similar surgery for treatment.

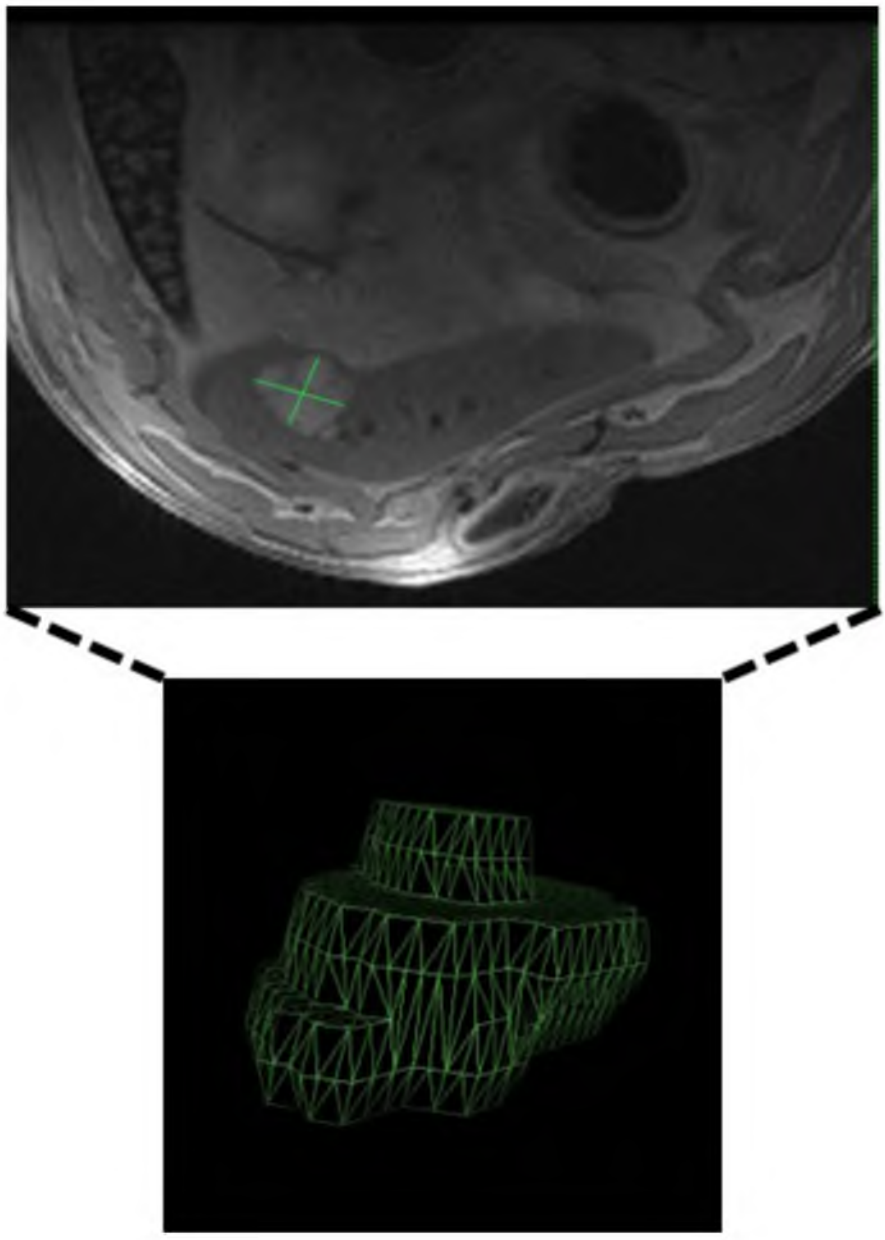

Figure A.2. MRI slice of rat liver 7 days post tumor induction. A solitary hepatoma tumor is clearly visible in the MRI scan. The drawn dimensions measure 4.43 mm x 3.54 mm. The three-dimensional tumor rendering has a calculated volume of 21.6 mm^3.

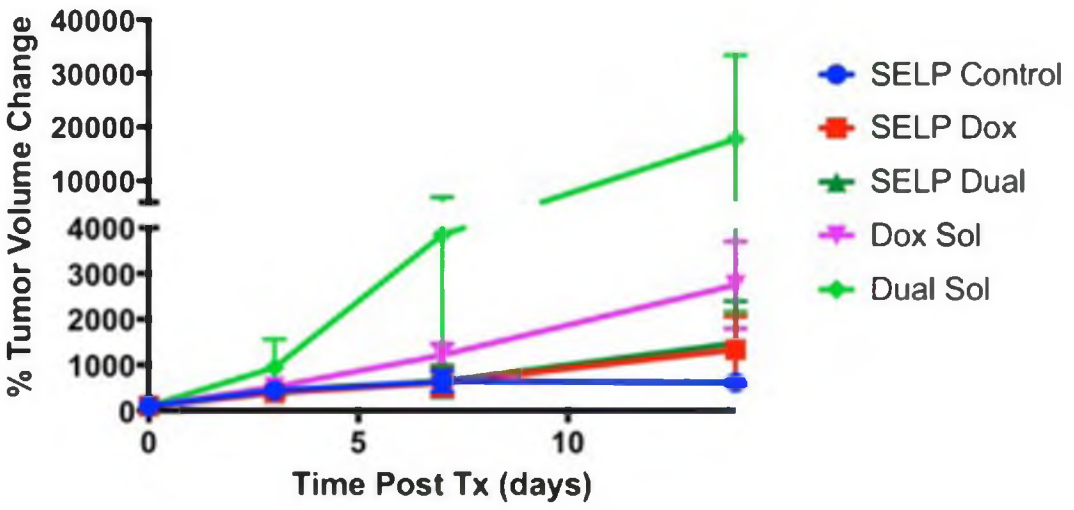

Figure A.3. Change in tumor volume post intratumoral treatment administration. Percent change in tumor volume is presented as mean ± standard error of the mean. Significance cannot be reported.

had lower change in tumor volume. The SELP control showed tumor regression, but the neoplasm was still present by day 30.

A.3.3 Histological analysis of intratumorally treated tissues

Although change in tumor volume showed high variability in between groups, histological analysis provided some insight into the observed trends. Tumor regression was only apparent in animals treated with either SELP or SELP loaded with single or dual drug. In animals where tumor regression was not observed, lower change in tumor volume was determined again in animals treated with SELP+drug as compared to drug suspended in PBS. Tissue samples from the animals with observed regression revealed the SELP gel in the center of the tumor. In Figure A.4, images from three rats all treated with SELP+Dual drug are presented. The first animal showed tumor regression over time while the other two did not. The treatment injection in the first animal was in the center of the tumor. The SELP is clearly visible, demarcated by neoplastic tissue and fibrosis. Clusters of red doxorubicin are visible throughout the SELP matrix. In the second animal, no SELP gel was identified in any slices taken from the entirety of the mass, indicating the possibility of improper injection or reflux of the SELP solution postinjection before it gelled. In the third animal, a small amount of gel was identified surrounded by cancerous tissue, residing on the edge of the tumor rather than near the center. Tissue samples from the SELP only and SELP+Dox are presented in Figure A.5. Animal 1 in the SELP control group showed tumor regression. As evidenced in the histological section, the gel is central to the neoplasm. Based on the original tumor volume of 27.5 μL, the 20 μL SELP injection may have mechanically disrupted the tumor, and therefore growth. In the adjacent

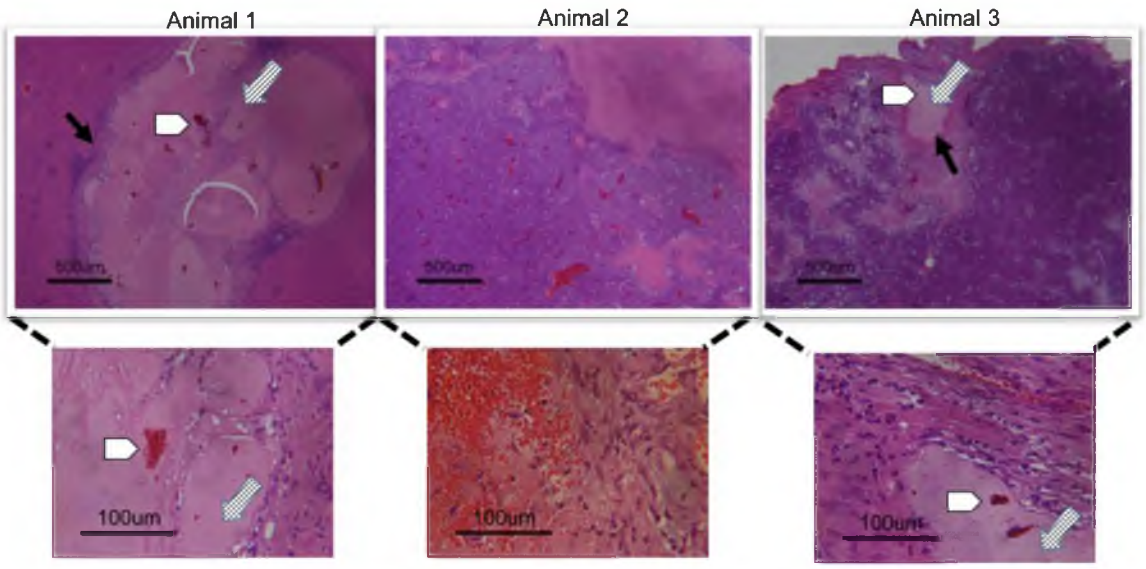

Figure A.4. Histological sections from three animals treated with SELP+Dual drug. The striped arrow indicates the SELP gel, that shows up on H&E as a pink, amorphous material (confirmed with histological samples of control gels). The white arrowheads indicate clusters of red doxorubicin. Sorafenib clusters are only visible under high magnification due to relative transparency. Animal 1 had tumor regression and neoplastic tissue is not evident as with the samples from animals 2 and 3. All images taken at 70x total magnification.

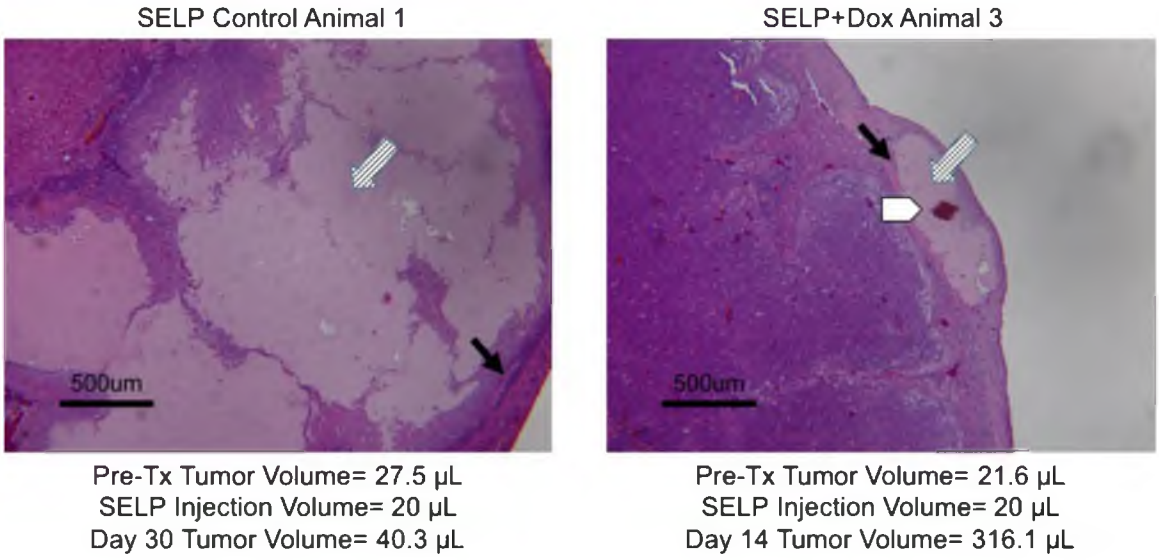

Figure A.5. Histological analysis of tumors injected with only SELP or SELP+Dox. The control animal that displayed tumor regression may have had mechanical disruption by the gel, which is shown surrounded by fibrotic tissue. The animal treated with SELP+Dox shows the gel residing on the tumor edge. Neoplastic tissue is seen growing away from the treatment material. Striped arrows indicate the SELP matrix, black arrows point out fibrotic tissue, and the white arrowhead indicates drug crystals. All images taken at 70x total magnification.

panel, the SELP gel (loaded with doxorubicin) is visible at the tumor edge. Neoplastic tissue extends away from the treatment material. In this particular animal, tumor regression was not observed. Based on these results, location of the initial SELP injection affects tumor response to the treatment.

A.3.4 Intraarterial embolization

In parallel to the intratumoral studies, intraarterial catheterization of the hepatic artery was tested. This procedure provides the most relevant model to TACE treatment of HCC. Out of four separate surgeries, one resulted in artery catheterization. The angiogram showing contrast filling the hepatic arterial tree is shown in Figure A.6A. As the injection continued, however, the vessel was over pressurized or movement of the catheter resulted in a vessel tear. Figure A.6B provides evidence for this as contrast dye is seen flowing along the diaphragm and outlining the liver lobes (indicated by the black arrows).

A.4 Discussion

With the conclusion of this preliminary *in vivo* study, several key findings were demonstrated. First, drug loaded into SELP and delivered intratumorally results in lower rate of tumor size increase than administration of drug in a saline solution. Second, the injection location of the SELP solution is essential for satisfactory intratumoral response. When the SELP gel was located on the perimeter of the tumor, no tumor regression was observed. However, the animals treated with SELP loaded with drug and who had gels detected within tumor borders (indicated by a fibrotic border interlaced with residual neoplastic cells), regression was clearly indicated. In fact, no mass was detected

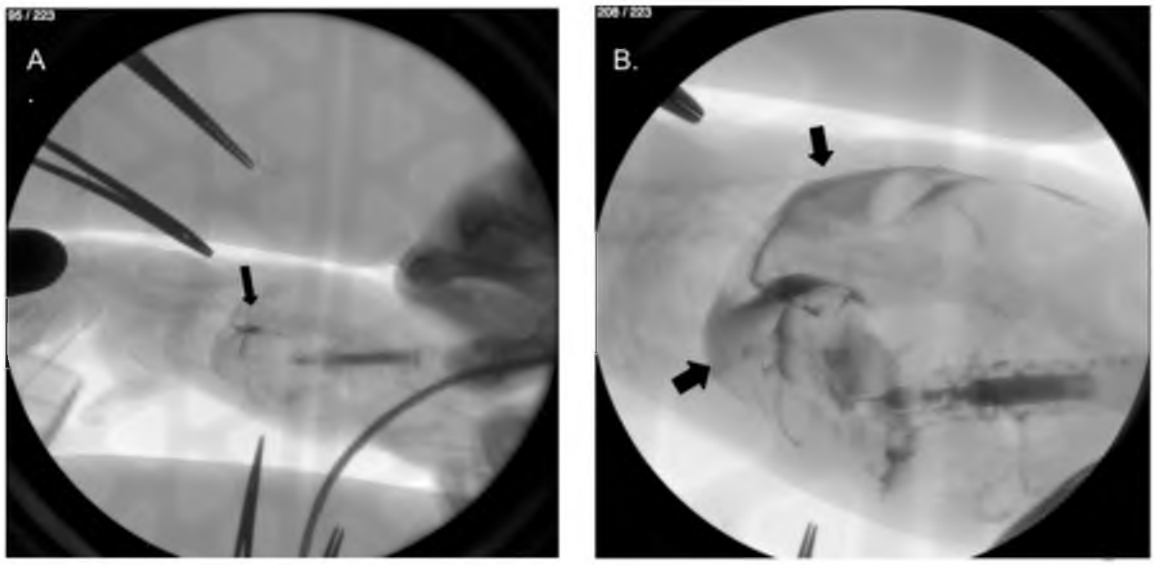

Figure A.6. Angiograms showing contrast dye being injected in the rat hepatic arterial tree. A) The small arrow indicates the contrast filling the hepatic vasculature. B) Contrast is seen outlining the liver lobes, indication that during the remainder of the injection, the vessel was over pressurized and damaged, leading to subsequent contrast leaking extra hepatically.

on MRI for these animals after day 21 post treatment. Although definitive outcomes cannot be declared, tumors centrally injected with drug loaded SELP showed better therapeutic response, more so the dual drug treated animal, than tumors injected with only SELP or drugs suspended in saline. Although mechanical disruption by the gel mass caused tumor damage and subsequent necrosis seen with the SELP control animal, the same level of regression was not observed as the animals treated with the drug loaded SELP (30-day subset group).

As the results indicate, the intratumoral administration does not provide the most ideal treatment route, especially when trying to test the therapeutic effect of a therapy intended for intraarterial delivery. Nonetheless, useful observations were made. The intraarterial catheterization procedure conducted in parallel is the more appropriate model. However, as described, the procedure requires precise microsurgical technique.

A.5 Conclusions

The rat model using the McA-RH7777 cancer line in the Sprague Dawley rat provides a useful syngeneic orthotopic tumor to study new treatments for HCC. In this study, solitary hepatoma tumors were successfully induced and treated intratumorally. Improved surgical technique and larger animal numbers are required for future studies to determine significance between treatment groups. Perfecting the intraarterial procedure will provide the most pertinent model to study the therapeutic efficacy of the SELP chemoembolic as a whole— realizing the embolic effects as well as the therapy resulting from localized drug release.

A.6 References

[1] Bibby MC. Orthotopic models of cancer for preclinical drug evaluation: advantages and disadvantages. Eur J Cancer 2004;40:852–7. doi:10.1016/j.ejca.2003.11.021.

[2] Hwang GL, van den Bosch MA, Kim YI, Katzenberg R, Willmann JK, Paulmurugan R, et al. Development of a high-throughput molecular imaging-based orthotopic hepatocellular carcinoma model. Cureus 2015;7:e281. doi:10.7759/cureus.281.

[3] Ferri F. Hepatocellular carcinoma. Ferri's Clin. Advis. 2016. 2nd ed., Elsevier; 2016, p. 605–7.

[4] Poursaid A, Jensen MM, Nourbakhsh I, Weisenberger M, Cappello J, Ghandehari H. Silk-elastinlike protein polymer liquid chemoembolic for localized release of doxorubicin and sorafenib. Mol Pharm 2016:Submitted.

[5] Poursaid A, Price R, Tiede A, Olson E, Huo E, McGill L, et al. In situ gelling silk-elastinlike protein polymer for transarterial chemoembolization. Biomaterials 2015;57:142–52. doi:10.1016/j.biomaterials.2015.04.015.

[6] Sheu AY, Zhang Z, Omary R a, Larson AC. Invasive catheterization of the hepatic artery for preclinical investigation of liver-directed therapies in rodent models of liver cancer. Am J Transl Res 2013;5:269–78.

[7] Dandu R, Cresce A Von, Briber R, Dowell P, Cappello J, Ghandehari H. Silk-elastinlike protein polymer hydrogels: influence of monomer sequence on physicochemical properties. Polymer (Guildf) 2009;50:366–74. doi:10.1016/j.polymer.2008.11.047.

APPENDIX B

ATR-FTIR EVALUATION OF DRUG LOADED SELP-815K GELS

B.1 Introduction

Identifying the structure of proteins at the atomic level has been part of proteomic research since the late 1950s beginning with X-ray crystallography techniques [1]. More recently, advances with nuclear magnetic resonance (NMR) spectroscopy allow for two-dimensional (2D) analysis of tertiary protein structure also with atomic resolution. Although these analytical methods provide detailed information about a protein's structure including absolute conformations, they have limitations and do not provide insight into protein function [2]. To perform X-ray crystallography, the protein must be crystallized and in a dry state, which is difficult and in the case of a recombinant protein with many repeating units like silk-elastinlike protein polymers (SELP), not possible [3]. To perform 2D NMR, the protein must be suspended and maintained at a low concentration. Furthermore, proteins greater than 30-40 kDa in size reach the NMR spectra limit and are difficult to analyze [4]. Although the same atomic resolution is not available, infrared (IR) spectroscopy is a nondestructive analytical tool that can be used to understand the secondary structure of proteins, which in turn also provides information about protein function in a short period of time [2]. Infrared energy can be used to probe and identify the

secondary structural elements including α-helices, β-sheets, β-turns, and random coils [3]. Infrared spectroscopy allows investigation of protein composition and architecture in its natural state, and changes to the protein's structure including folding, unfolding, and misfolding in the presence or absence of a stimulus or external factors may be determined [5]. Protein folding is influenced by hydrophobic and hydrophilic forces, hydrogen bonding, and ionic and dipolar interactions, which are affected by changes to the environment [3]. Therefore, IR spectroscopy provides a useful tool to understand the change in protein structure and function in changing environments. Moreover, this technique is not limited to the protein size, and low amount of sample may be analyzed, as low as 10 μg [5].

Briefly, IR spectroscopy employs the vibrational states of organic molecules, which follow a spring and ball model. When the proteins are subjected to IR energy, the absorption of the infrared radiation excites the vibrational bonds. The position of an infrared absorption band is determined by the vibrating masses and type of bond, in addition to intra- and intermolecular effects [5]. Proteins have characteristic bands in the infrared spectra that are a coalescence of individual vibrational peaks including the Amide I and Amide II peaks. These bands are resultant of the stretching vibrations of the C=O bond of the amide bond of the protein backbone and the bending vibrations of the N—H bond, respectively [2]. Both of these elements are involved in the hydrogen bond formations leading to the different secondary structures. Therefore the spectra correlating to these regions, and particularly the Amide I region, are used to systematically correlate the shape to secondary structure content [2]. The Amide I region is a summation of the different secondary structures. However, the contribution from each type of structure is

proportional to the amount present and mathematical Fourier self-deconvolution (FSD) and curve fitting techniques have been developed to break down the primary band into individual peaks [3]. The theory behind FSD is based on the assumption that a spectrum of single bands correlating to a secondary structure is broadened in the liquid or solid state [6]. FSD mathematically reduces the bandwidths so that overlapped bands can be resolved from one another. The deconvoluted band is then fitted with Gaussian and/or Lorentzian band shapes using an iterative curve fitting process. Over the years, compilation of fitted data confirmed with X-ray crystallography has resulted in resolved peaks correlated to the specific secondary structures [3].

Fourier transform infrared (FTIR) spectrometers are now the most common instrument for protein IR spectroscopy, where an interference method is used to simultaneously collect high spectral resolution data over a wide spectral range. On an FTIR, data can be collected from liquid samples using a transmission detection method or from solids and/or liquids without further preparation using an attenuated total reflectance (ATR) attachment. In the former method, the environment of the sample may be systematically changed in the holding cuvette to observe changes in protein structure. The latter method, and the method used in this work, allows for direct examination. ATR-FTIR consists of placing the sample on a crystal, typically germanium or diamond, and IR light is coupled into the crystal and towards the sample. The angle of incidence is totally reflected at the interface and this reflection forms an evanescent wave which extends into the sample and then exits and is picked up by the detector and results in the output spectra [5].

The ability to understand the structure-function relationship of proteins, particularly

in a solid form, using ATR-FTIR was applied to our study of developing a recombinant silk-elastinlike protein polymer as a liquid chemoembolic to understand the effect of drug incorporation. The mechanical properties of the SELP liquid embolic are inherent to its function, which are dictated by the secondary structures of the protein strands when interacting to form an insoluble, physical hydrogel network. Samples of the SELP embolic loaded with the drugs doxorubicin and sorafenib and in combination were tested as solid gels. The drugs were either incorporated directly mixed in as a powder, followed by a period of gelation, or predissolved in dimethyl sulfoxide (DMSO) and mixed in, again followed by a period of gelation. The solid gels tested via ATR-FTIR provided insight into changes in the content of secondary structures of the SELP proteins.

In this appendix, the complete data from the tests of the chemoembolic gels described in Chapter 4 are presented to elucidate how the final Figure 4.5 was compiled showing the relative percentages of the secondary structures in the drug loaded SELP gels.

B.2 Materials and methods

B.2.1 Materials

SELP-815K was synthesized and characterized as previously described [7,8]. Sorafenib base was purchased from LC Laboratories (Woburn, MA) and doxorubicin base was purchased from MedKoo Biosciences (Chapel Hill, NC). Hydrated 9% SELP-815K gels fully loaded with drug incorporated as a DMSO solution or milled powder were tested as described in Chapter 4. Absorbance spectra of powdered drug, PBS, and DMSO were measured as references.

B.2.2 ATR-FTIR analysis

FTIR analysis were performed on a Nicolet 6700 spectrometer (Thermo Scientific) equipped with a mercury cadmium telluride (McT-A) detector and a SmartiTX attenuated total reflectance (ATR) accessory, which was fitted with a single element diamond crystal. Individual spectra were acquired with 512 co-added scans ratioed to a background of 512 scans from the diamond itself. Scans were performed over the range of 850 to 4000 cm^{-1} with a resolution of 4 cm^{-1}. Data were analyzed with OMNIC 9.2 software loaded with Proteus Protein Analysis Kit from Thermo Scientific. The background spectrum of the buffer was subtracted, as was DMSO, if applicable, and the baseline was corrected. The amide I region (1700 cm^{-1} to 1600 cm^{-1}) was deconvoluted and curve fitted using Gaussian curves by the Voigt model. The second derivative of spectra was used to identify locations of the secondary structure peaks and confirmed using literature references. The percentages of secondary structures in each sample were calculated from peak integration.

B.3 Results

B.3.1 Absorbance spectra of samples

The full spectra followed by the focused Amide I region are presented first for the samples with powder drug mechanically mixed in, Figure B.1. The peaks correlating to water or DMSO were subtracted out. The Amide I peak was subjected to FSD and curve fitting using the OMNIC Peak Resolve software resulting in the curves presented in Figure B.2. Figures B.3 and B.4 present the data for the gels incorporated with predissolved drugs.

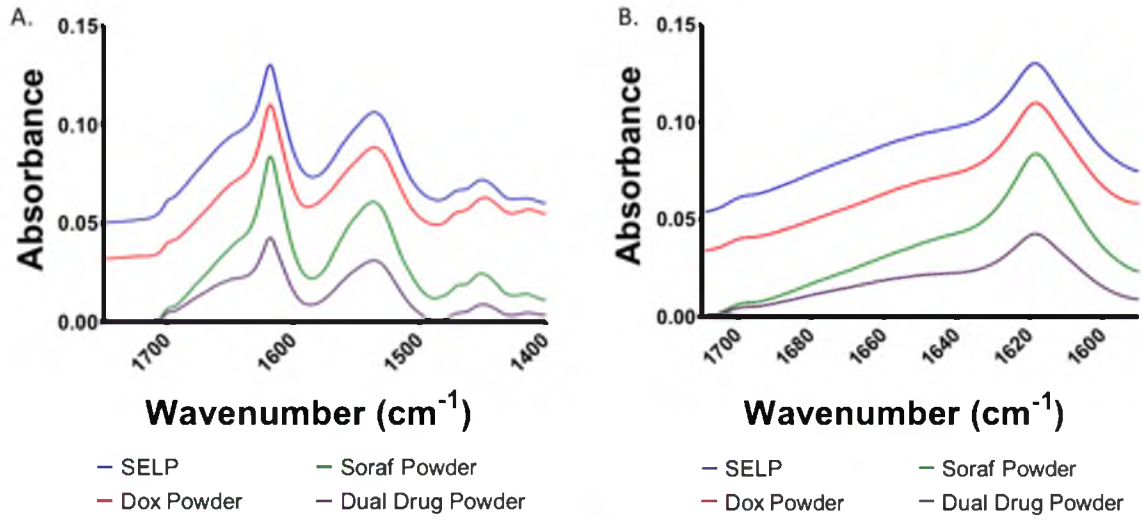

Figure B.1. Absorbance spectra of gels incorporated with powder drugs. A) Full spectra B) Spectra of the Amide I region.

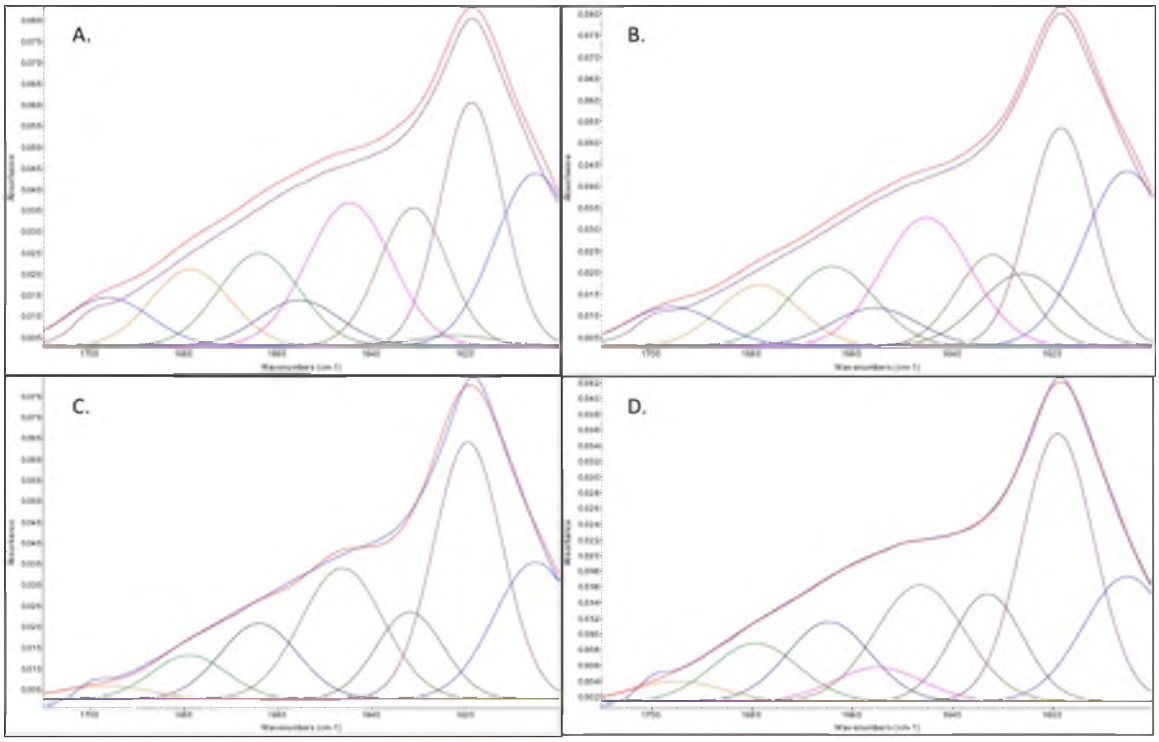

Figure B.2. Deconvoluted spectra of powder drug incorporated gels. The comprehensive FSD curve is represented by the red curve. A) Control B) Doxorubicin C) Sorafenib D) Dual drug.

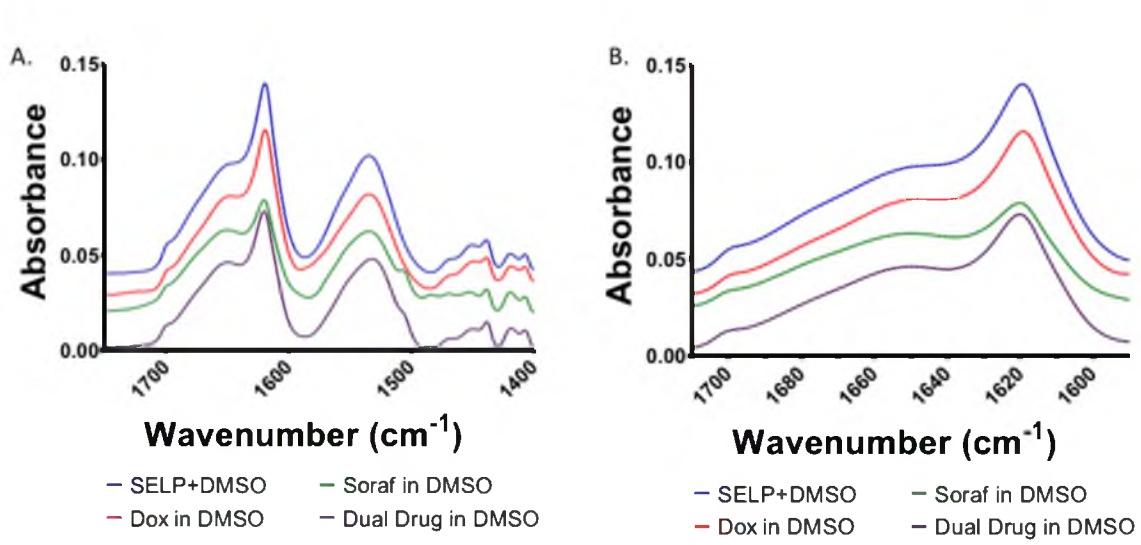

Figure B.3. Absorbance spectra of gels incorporated with predissolved drugs. A) Full spectra B) Spectra of the Amide I region.

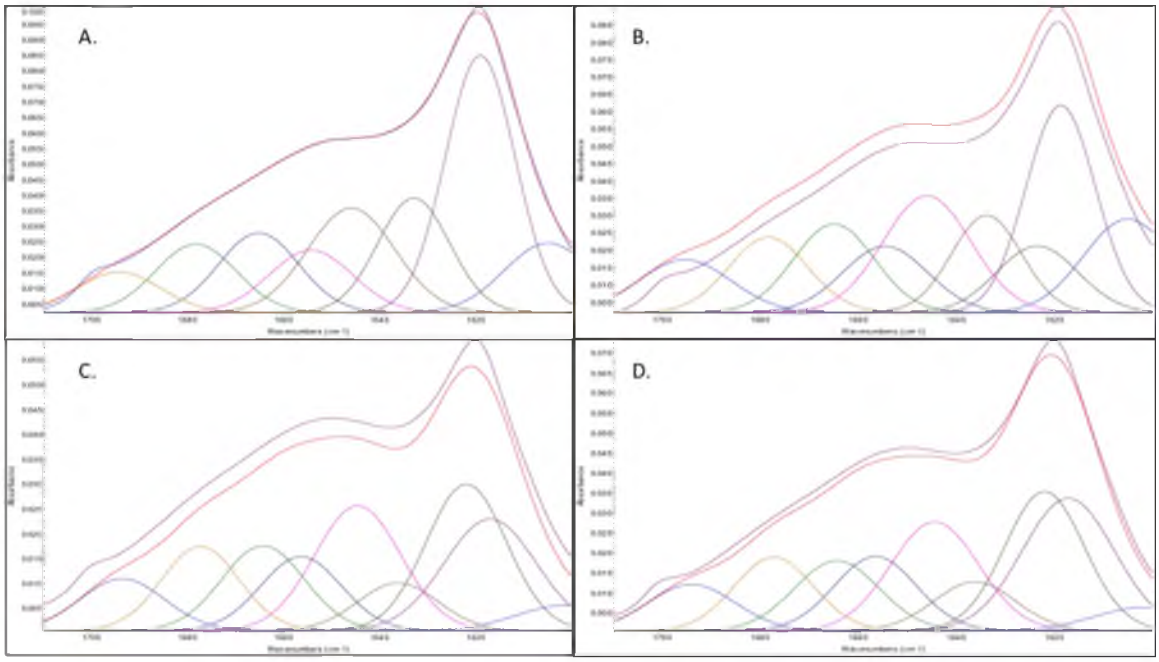

Figure B.4. Deconvoluted spectra of predissolved drug incorporated gels. The comprehensive FSD curve is represented by the red curve. A) Control B) Doxorubicin C) Sorafenib D) Dual drug.

B.4 Discussion and conclusions

Each of the peaks resulting from the curve fitting algorithm was assigned to specific secondary structures based on known literature references and presented in Figure 4.5C. The area under each peak was tabulated, each representing the relative amount of the identified secondary structure. The relative percent of each secondary structure was calculated based on the total area of the entire Amide I region and presented in Figure 4.5E. This analysis provided insight into changes in the secondary structures of the gelled SELP chemoembolic in the presence of the drugs doxorubicin and sorafenib and in combination.

The results from these studies as discussed in Chapter 4 were consistent with other observations, particularly the final stiffness of the gels. It would be interesting to expand these studies to measure the secondary structures as they are forming during the sol-gel transition. The unique ability to test a solution or solid sample using the ATR-FTIR is a clear advantage of this technique, particularly when trying to understand the change in secondary structure formation in the presence of the drugs. Determining any changes during the sol-gel transition may provide insight into how the drugs may be interacting with the protein backbone.

Since X-ray crystallography and 2D NMR cannot be applied to look for possible interactions between the drugs and the protein on the atomic scale at relevant concentrations, small-angle scattering (SAS) techniques may provide alternative investigative tools that would provide atomic resolution of sample structures including shape and orientation that FTIR cannot [9]. Samples can be tested as an aqueous solution, a solid, a powder, or a crystal. Similar to ATR-FTIR, a sample can be tested in different environments to study responses to different external stimuli. SAS encompasses both small

angle neutron scattering and small angle X-ray scattering. Briefly, SAS involves directing a beam of radiation into the sample and detecting the deflection of the collimated radiation away from the straight trajectory after interacting with the sample [10]. Since the structures in the samples are larger than the radiation wavelength, deflections are small, which allows for attainment of the high information content regarding structural size, shape, and orientation within a sample. The disadvantage of these techniques boils down to access and cost. Particle accelerator equipment are required, *i.e.*, a cyclotron, which are not readily accessible— most are available at national laboratories. Nonetheless, all of the analytical techniques presented have clear advantages when they can be used to provide insight into sample, and particularly protein, structure which ultimately dictates function. For recombinant protein polymers, clear understanding of function allows for improved design of future polymers for a given application.

B.6 References

[1] Kendrew JC, Bodo G, Dintzis HM, Parrish RG, Wyckoff H, Phillips DC. A three-dimensional model of the myoglobin molecule obtained by x-ray analysis. Nature 1958;181:662–6.

[2] Gallagher W. FTIR analysis of protein structure. Biochemistry 1997:662–6.

[3] Bradley MS, Nishikida K. Infrared measurements of proteins: theory and applications. Madison: Thermo Electron Corporation; 2005.

[4] Wüthrich K. Protein structure determination in solution by NMR spectroscopy. J Biol Chem 1990;265:22059–62.

[5] Barth A. Infrared spectroscopy of proteins. Biochim Biophys Acta - Bioenerg 2007;1767:1073–101. doi:10.1016/j.bbabio.2007.06.004.

[6] Tooke PB. Fourier self-deconvolution in IR spectroscopy. TrAC Trends Anal Chem 1988;7:130–6.

[7] Dandu R, Cresce A Von, Briber R, Dowell P, Cappello J, Ghandehari H. Silk-elastinlike protein polymer hydrogels: Influence of monomer sequence on physicochemical properties. Polymer (Guildf) 2009;50:366–74. doi:10.1016/j.polymer.2008.11.047.

[8] Poursaid A, Price R, Tiede A, Olson E, Huo E, McGill L, et al. In situ gelling silk-elastinlike protein polymer for transarterial chemoembolization. Biomaterials 2015;57:142–52. doi:10.1016/j.biomaterials.2015.04.015.

[9] Svergun DI, Koch MHJ. Small-angle scattering studies of biological macromolecules in solution. Reports Prog Phys 2003;66:1735.

[10] Feigin LA, Svergun DI. Structure Analysis by Small-Angle X-Ray and Neutron Scattering. New York: Plenum Press; 1987.